SOLUTION OF INVERSE ELECTROCARDIOGRAPHY PROBLEM USING MINIMUM RELATIVE ENTROPY METHOD

A THESIS SUBMITTED TO
THE GRADUATE SCHOOL OF NATURAL AND APPLIED SCIENCES
OF
MIDDLE EAST TECHNICAL UNIVERSITY

BY

ALİ BİRCAN

IN PARTIAL FULFILLMENT OF THE REQUIREMENTS
FOR
THE DEGREE OF MASTER OF SCIENCE
IN
ELECTRICAL AND ELECTRONICS ENGINEERING

SEPTEMBER 2010

Approval of the thesis:

SOLUTION OF INVERSE ELECTROCARDIOGRAPHY PROBLEM USING MINIMUM RELATIVE ENTROPY METHOD

submitted by **ALİ BİRCAN** in partial fulfillment of the requirements for the degree of **Master of Science in Electrical and Electronics Engineering Department, Middle East Technical University** by,

Prof. Dr. Canan Özgen _____
Dean, Graduate School of **Natural and Applied Sciences**

Prof. Dr. İsmet Erkmen _____
Head of Department, **Electrical and Electronics Engineering**

Asst. Prof. Dr. Yeşim Serinağaoğlu Doğrusöz _____
Supervisor, **Electrical and Electronics Engineering Dept, METU**

Examining Committee Members:

Prof. Dr. Murat Eyüboğlu
Electrical and Electronics Engineering, METU _____

Assist. Prof. Dr. Yeşim Serinağaoğlu Doğrusöz
Electrical and Electronics Engineering, METU _____

Prof. Dr. Nevzat Güneri Gençer
Electrical and Electronics Engineering, METU _____

Assoc. Prof. Dr. Uğur Baysal
Electrical and Electronics Engineering, Hacettepe University _____

Assist. Prof. Dr. İlkay Ulusoy
Electrical and Electronics Engineering, METU _____

Date: _____

I hereby declare that all information in this document has been obtained and presented in accordance with academic rules and ethical conduct. I also declare that, as required by these rules and conduct, I have fully cited and referenced all material and results that are not original to this work.

Name, Last Name: ALİ BİRCAN

Signature :

ABSTRACT

SOLUTION OF INVERSE ELECTROCARDIOGRAPHY PROBLEM USING MINIMUM RELATIVE ENTROPY METHOD

Bircan, Ali

M.S., Department of Electrical and Electronics Engineering

Supervisor : Asst. Prof. Dr. Yeşim Serinağaoğlu Doğrusöz

September 2010, 118 pages

Coronary problems -such as heart attacks, stroke and arrhythmia- are the leading cause of death in the world. Thus, understanding the functioning of the heart is crucial. The interpretation of heart's electrical activity is very important in clinical medicine since contraction of cardiac muscles is initiated by the electrical activity of the heart. In other words, the electrical activity of the heart reflects its mechanical activity. The electrocardiogram (ECG) is a diagnostic tool that measures and records the electrical activity of the heart. The conventional 12 lead electrocardiogram (ECG) is a clinical tool that provides information about the heart status. However, it has limited information about functionality of heart due to limited number of recordings. In addition, classical ECG is not based on a biophysical model of body; it rather depends on a heuristic match of waveforms and disease state. A better alternative approach for understanding cardiac electrical activity is the incorporation of body surface potential measurements with torso geometry and the estimation of the equivalent cardiac sources. The problem of the estimating the cardiac sources from the torso potentials and the body geometry is called the inverse problem of electrocardiography. In this study, epicardial potentials are used as equivalent cardiac sources in modeling the electrical activity of the heart. The aim of this thesis is reconstructing accurate high resolution maps of epicardial potential representing

the electrical activity of the heart from the body surface measurements. However, accurate estimation of the epicardial potentials is not an easy problem due to ill-posed nature of the inverse problem. In order to obtain correct result, the inverse problem should be solved by imposing constraints depending on the prior information about the true epicardial potential. In this thesis, the linear inverse ECG problem is solved using different optimization techniques such as Conic Quadratic Programming, multiple constrained convex optimization, Linearly Constrained Tikhonov Regularization and Minimum Relative Entropy (MRE) method. The MRE method treats the elements of epicardial potentials as random variables and estimates the epicardial potentials (m) as the expected value of the posterior distribution using some prior information. The prior information used in MRE method is the lower and upper bounds of m and a prior expected value of m. The results are compared with Tikhonov Regularization and with the true potentials. The performance of each method studied in the thesis is tested at different level of measurement noise and geometric noise in order to investigate the effects of different errors.

Keywords: Inverse electrocardiography, MRE, Minimum Relative Entropy, Entropy Optimization, Iterative Optimization

ÖZ

ELEKTROKARDİYOGRAFİ GERİ PROBLEMİNİN MİNİMUM BAĞIL ENTROPİ YÖNTEMİ KULLANILARAK ÇÖZÜMÜ

Bircan, Ali
Yüksek Lisans, Elektrik ve Elektronik Mühendisliği Bölümü
Tez Yöneticisi : Yrd. Doç. Dr. Yeşim Serinağaoğlu Doğrusöz

Eylül 2010, 118 sayfa

Kalp krizi, felç ve aritmi gibi koroner sorunlar ölüme sebep olan önde gelen nedenidir. Bu nedenle, kalbin işleyişini anlamak çok önemlidir. Kalp kaslarının kasılması kalbin elektriksel aktivitesinin tarafından oluşturulduğu için kalbin elektriksel aktivitesinin yorumlanması çok klinik tıp alanında oldukça önemlidir. Başka bir deyişle, kalbin elektriksel aktivitesi mekanik işleyişini yansıtır. Elektrokardiyogram (EKG) kalbin elektriksel aktivitesinin ölçülmesi ve kaydedilmesinde kullanılan bir tanı aracıdır. Klasik 12 kanallı elektrokardiyogram(EKG) kalp durumu hakkında bilgi sağlayan bir klinik araçtır. Ancak, kayıt sayısının azlığı nedeniyle kalbil işlevselliği hakkında sınırlı bilgi sağlar. Ayrıca, klasik EKG vücudun bir biyofiziksel modeline bağlı değil, daha çok elde edilen dalga şekilleri ile hastalık durmunun sezgisel olarak eşleştirilmesi dayalıdır. Kalbin elektriksel aktivitesinin anlaşılması için daha iyi bir alternatif yaklaşım, vücut yüzeyinden alınan ölçümler ile gövde geometrisi birleştirilip eşdeğer kalp kaynakların tahmin edilmesidir. Torso potansiye ölçümleri ve vücut geometri kullanarak kardiyak kaynaklarının tahmin edilmesi ters elektrokardiyografi problemi olarak tanımlanır. Bu çalışmada, epikardiyal potansiyelleri kalp aktivitesinin modellemesinde eşdeğer kalp kaynağı olarak kullanılmaktadır. Bu tezin amacı, vücut yüzey ölçümlerinden kalbin elektriksel aktivitesini temsil eden, doğru ve yüksek çözünürlüklü epikardiyal potansiyel haritaları elde

etmektir. Ancak, problemin kötü konumlandırılmış doağasından dolayı doğru epikardiyal potansiyellerinin hesaplanması kolay bir problem değildir. Doğru sonuçlar elde etmek için, gerçek epikardiyal potansiyeli hakkında önceden bilinen bilgilere bağlı bazı kısıtlar probleme dahil edilerek ters problemin çözülmesi gerekilidir. Bu tezde, goğrusal ters EKG problemi; Konik Karesel Programlama, birden çok kısıtlı dışbükey optimizasyonu doğrusal Kısıtlı Tikhonov düzenlileştirmesi ve Minimum Bağıl Entropi (MBE) yöntemi gibi farklı optimizasyon teknikleri kullanılarak çözülmüştür. MBE yöntemi epikardiyal potansiyellerinin elemanları rassal birer değişken olarak ele alır ve epikardiyal potansiyellerini (m) bazı ön bilgileri kullanarak sonsal dağılımının ortalama değeri şeklinde hesaplar. MBE yönteminde önsel bilgi olarak m rassal değişkeninin alt ve üst sınırları değerleri ile beklenen ortalama değer kullanılmaktadır. Sonuçların uygunluğu gerçek potansiyellerini kullanarak Tikhonov düzenlileştirmesi ile karşılaştırılır. Değişik hatalar karşısındaki performanlarını incelemek amacıyla tezde çalışılan herbir yöntem, farklı düzeyde ölçüm gürültüsü ve geometrik hataların bulunduğu problemler ile test edilmiştir.

Anahtar Kelimeler: Geri elektrokardiyografi, MGE, Minimum Bağıl Entropi,Entopi Optimizasyonu, İteratif Optimizasyon

ACKNOWLEDGMENTS

I would like to thank my thesis supervisor Assist. Prof. Dr. Yeşim Serinağaoğlu Doğrusöz for her invaluable support, encouragement, supervision and useful suggestions throughout this work. Her moral support and continuous guidance from the initial to the final level enabled me to develop an understanding of the subject and complete my work.

I would like to thank all my firends Ümit Aydın, Ceren Bora and Alireza Mazloumi at ECG laboratory for their comments and technical supports.

I am indebted to Esma Koca and Ahmet Melik Koca for accepting to read and review this thesis and their suggestions.

I am most thankful to my family for their love, support and encouregement. Their belief in me let this thesis come to an end.

TABLE OF CONTENTS

LIST OF TABLES

TABLES

LIST OF FIGURES

FIGURES

CHAPTER 1

INTRODUCTION

1.1 Motivation

Proper functioning of heart is crucial for human body. Coronary problems -such as heart attacks, stroke and arrhythmia- are the leading cause of death. Thus, interpretation of heart's electrical activity is very important in clinical medicine. Electrocardiography (ECG) is the most widely used noninvasive tool for diagnosing and monitoring heart diseases [1].

ECG is a representation of the heart's electrical activity recorded from electrodes on the body surface [2]. It records the difference of electrical potentials on the body surface. This obtained electrical signal's shape, rate and rhythm are used to determine the activity of the heart by cardiologists. Thus, ECG reflects the electrical activity of the heart.

The conventional ECG consists of 12 different electrical signals recorded from 6 electrodes simultaneously. Six of these signals are vertical and use frontal leads I, II, and III and limb leads aVR, aVL, and aVF, and six of them are horizontal and use precordial leads V1, V2, V3, V4, V5, and V6. This kind of ECG involves the low-resolution projections of heart's electrical activity on the body surface [3]. The 12-lead ECG is crucial for establishing many cardiac diagnoses, especially arrhythmias and myocardial ischemia. Although the conventional ECG provides information about the heart status, it has limited information about functionality of heart due to the limited number of recordings. However, it is possible to image cardiac electrical activity with high resolution using the body surface potentials recorded from a large number of electrodes. The Body Surface Potential Map (BSPM) method is an electrocardiographic method which records and displays the surface potentials from wide areas of chest in order to obtain the electrical activity of heart with the increased spatial resolution.

Body surface potential maps (BSPMs) allow the detection of significant physiological and diagnostic information by measurements from large number of electrodes on body surface. By this increased spatial resolution, these maps provide a comprehensive three-dimensional image of cardiac electrical activity that is not possible with the conventional 12-lead ECG [4]. Thus, the BSPM is considered more appropriate to diagnose certain heart disease, compared with the conventional 12-lead electrocardiogram [5, 6, 7]. The two main advantages of the body surface potential maps over the 12-lead ECG are providing all information available in the cardiac electrical field on the surface of the body and being more sensitive in detection of the local electrical events in the heart [6].

Although BSPMs are useful tools to visualize the heart's electrical activity on the body surface, relating measurements with the cardiac activity and understanding it remains still a problem. BSPM has limited ability in localization of cardiac electric events since the potential distribution at each point on torso is determined by the electric activity in the entire heart. Moreover, it has also limited ability in resolving multiple electric events due to the smoothing effects of the volume conductor [8, 9, 10]. A better alternative approach for understanding cardiac electrical activity is the incorporation of BSPMs with torso geometry from magnetic resonance imaging (MRI) or computed tomography (CT) scans and the estimation of the equivalent cardic sources [10, 3, 4]. This is called inverse problem of ECG and enables a better qualitative and quantitative understanding of heart's electrical activity. By this kind of approach, the estimation of cardiac sources from BSPMs yields to obtain more meaningful and useful results for realization the events in heart.

Electrocardiography problem, which aims to gain a better understanding of cardiac electrical activity, can be modeled in two major ways. In the first type, body surface potentials (effect) is computed using a given cardiac sources distribution (cause). This problem is called forward problem of electrocardiography. On the other hand, inverse problem of electrocardiography can be defined as reconstruction of cardiac electrophysiological activity (cause) from remotely measured torso ECG recordings (effect) [11, 12]. The objective of inverse electrocardiography is improving traditional ECG recordings and gaining a better qualitative and quantitative understanding of the cardiac electrical ectivity in order to detect diseases and malfunctions of heart [13]. In solving the inverse ECG problem, the cardiac sources are represented by the simplified models, such as fixed dipole, moving dipole, multiple dipoles, multipoles, the epicardial potential distribution and the heart-surface activation isochrones on the surface of the

heart [14, 13]. The details about these cardiac source models are represented in Background section.

Epicardial potential distribution is one of the equivalent source models of heart that is used in inverse ECG problem, since the potential distribution on epicardium reflects underlying local electrical activity of myocardium. In the present work inverse problem of electrocardiography, given a potential distribution on body surface and forward transfer matrix, is studied in order to find epicardial potential distribution on heart surface.

1.2 Contribution of the Thesis

The inverse problem of electrocardiography is ill-posed which means that even small perturbations lead to serious errors in the solutions. Due to this ill-posedness, it needs a regularization process in order to estimate the desired solution. There are many different regularization and statistical methods in literature in order to reconstruct the desired epicardial potential distribution in solution of inverse problem of electrocardiography. Some of these methods are Tikhonov Regularization [15, 11], Truncated Singular Value Decomposition (TSVD) [16], Convex Optimization with multiple constraints [17, 18, 19], Bayesian Maximum A Posteriori Estimation (Bayes MAP) [20], State-Space Models [21, 22] (see Background section for details). There are also modified and combined forms of these regularization methods [23, 24, 25, 15] in order to improve the solutions. Methods based on Tikhonov and TSVD are able to robustly reconstruct epicardial potentials without any prior information. However, these methods suffer from smoothing in edges of the solution i.e. reconstructed epicardial potentials have limited relevance to real potential distribution especially at the edges. Bayes MAP and state-space models are statistical methods that enable to incorporate prior information to solve inverse problem. However, success of these methods is strongly dependent on relevance of epicardial potentials to prior data. Thus, obtaining a good prior is problem in these methods. Moreover, these methods assume that the random variables are normally distributed, which is not true for all cases.

Due to these deficiencies of the methods in literature, in this thesis it is aimed to investigate and study some novel methods in order to solve inverse electrocardiography problem. For this purpose following studies are performed:

(i) Different least square optimization methods, similar to Tikhonov Regularization, are studied. L2-norm constraint is modified in zero-order Tikhonov regularization in order to add prior information to formulation, which is also known as Twomey Regularization. Conic Quadratic Programming is another studied method that is used for least square minimization. Results of each method are compared.

(ii) The inverse ECG problem is reformulated as convex optimization problem in order to improve the solution by addition of energy regularization and total variation regularization constraints into the problem. This technique enables to regularize the problem with both spatial and temporal constraints.

(iii) The minimum relative entropy (MRE) method, a statistical inference method, is used for estimation of the *a posteriori* probability density function (pdf) using prior information. This method is more flexible than other statistical inference methods in use of prior information. Prior information does not have to be in a standard form of distribution. The MRE method is studied with different types of priori and its performance is examined. The state transition matrix, which is originally used in state space models, is also used to create the a priori pdf for the MRE method.

1.3 Structure of Thesis

In this thesis the second chapter contains the background information about the electrocardiography and the studied methods in the thesis. In this chapter, first anatomy and physiology of the heart is given. Then, the forward and inverse problems of ECG are defined along with a literature survey on these topics. Next, the background information about the entropy optimization and the mathematical optimization is represented.

The third chapter we represent the problem definition of the inverse problem of ECG.Then the theory of the methods studied methods are represented. These methods are Conic Quadratic Programming, linearly constrained Tikhonov regularization, admissible solution approach (convex optimization with multiple constraints) and MRE Method.

In the fourth chapter, the application details of the methos given in theory section are provided. The results of the reconstructed solutions are represented. In the last chapter, conclusions of

this study are given.

CHAPTER 2

BACKGROUND

2.1 Anatomy and Electrophysiology of the Heart

2.1.1 Anatomy of the Heart

Heart is the pumping organ of circulatory system located in the thorax between the lungs and abdomen behind the sternum, which is also called mediastinum. The heart works like a pump that pushes blood through the blood vessels. It has four chambers as shown in Figure 2.1: left and right atria and left and right ventricles. The two atria act as collecting reservoirs receiving blood from the body and lungs, while the two ventricles act as pumping chambers to push blood through the body tissues and lungs. The atria on the right and left sides of the heart are separated by a thin wall referred to as the atrial septum. Similarly, the ventricular septum separates the two ventricles on the right and left side of the heart.

The heart has four valves to prevent backflow of blood as in any pumping system. Each atrium and ventricle is connected with an atrio-ventricular valve on two side of heart. The tricuspid valve is located on the right side of the heart and mitral valve is located on the left side. These valves prevent blood moving back from the ventricles into atria. The right ventricle is connected to the pulmonary artery through the pulmonary valve, while the left ventricle is connected to the aorta through the aortic valve.

In the circulation system, the flow of blood through the heart is as follows: Unoxygenated blood returns from the systemic circulation to the right atrium and then passes through the tricuspid valve to the right ventricle. The right ventricle forces blood through the pulmonary valve to the pulmonary artery and the lungs. Oxygenated blood returns from the lungs to the

left atrium, and then passes through the mitral valve to the left ventricle. Finally blood is pumped through the aortic valve to the aorta and the systemic circulation.

The wall of heart is composed of three layers. Epicardium, myocardium and endocardium are outer, middle and inner layers, respectively. Myocardium is relatively thick and consists mainly of cardiac muscle tissue responsible for forcing blood out of heart chambers.

2.1.2 Properties of Cardiac Cells

Mechanical and electrical activity of the heart are performed by two types of cardiac cells.The first type is the actual contractile units of the heart which are termed as myocardial cells, or myocytes [14, 26]. These cells are activated and begin to contract by electrical stimulus. The second type of cardiac cells involves special cells that form the heart's electrical conduction system. The cardiac cells have four specific properties that enable to carry out their function: automaticity, excitability, conductivity, and contractility [26].

Automaticity is the ability of of the cardiac cell to generate an impulse spontaneously without an external electrical stimulation. This property is attributed to the pacemaker cells, in which the concentration of potassium falls regularly during electrical diastole. The regular falls in the concentration of potassium cause to the self-initiated depolarization when the trans-membrane voltage reaches to the threshold. In a normal heart, the sinoatrial node acts as the primary pacemaker of the heart with the highest automaticity [26]. The increase or decrease in the automaticity can cause the arrhythmias [27]. Excitability refers to the ability of a cell to respond to an electrical stimulus that reaches to threshold. Conductivity is the ability of each cell in the cardiac conduction system to conduct electrical impulses from one cell to another. Cardiac muscle tissue differs from skeletal muscle that activation can propagate from one cell to another in any direction in heart muscle [14]. Thus, the propagation of impulse is more complex in cardiac tissues. Contractility is the mechanical response of cardiac muscle fibers in response to the electrical stimulation by shortening and contraction. The myocardial cells, or myocytes in myocardium have this property.

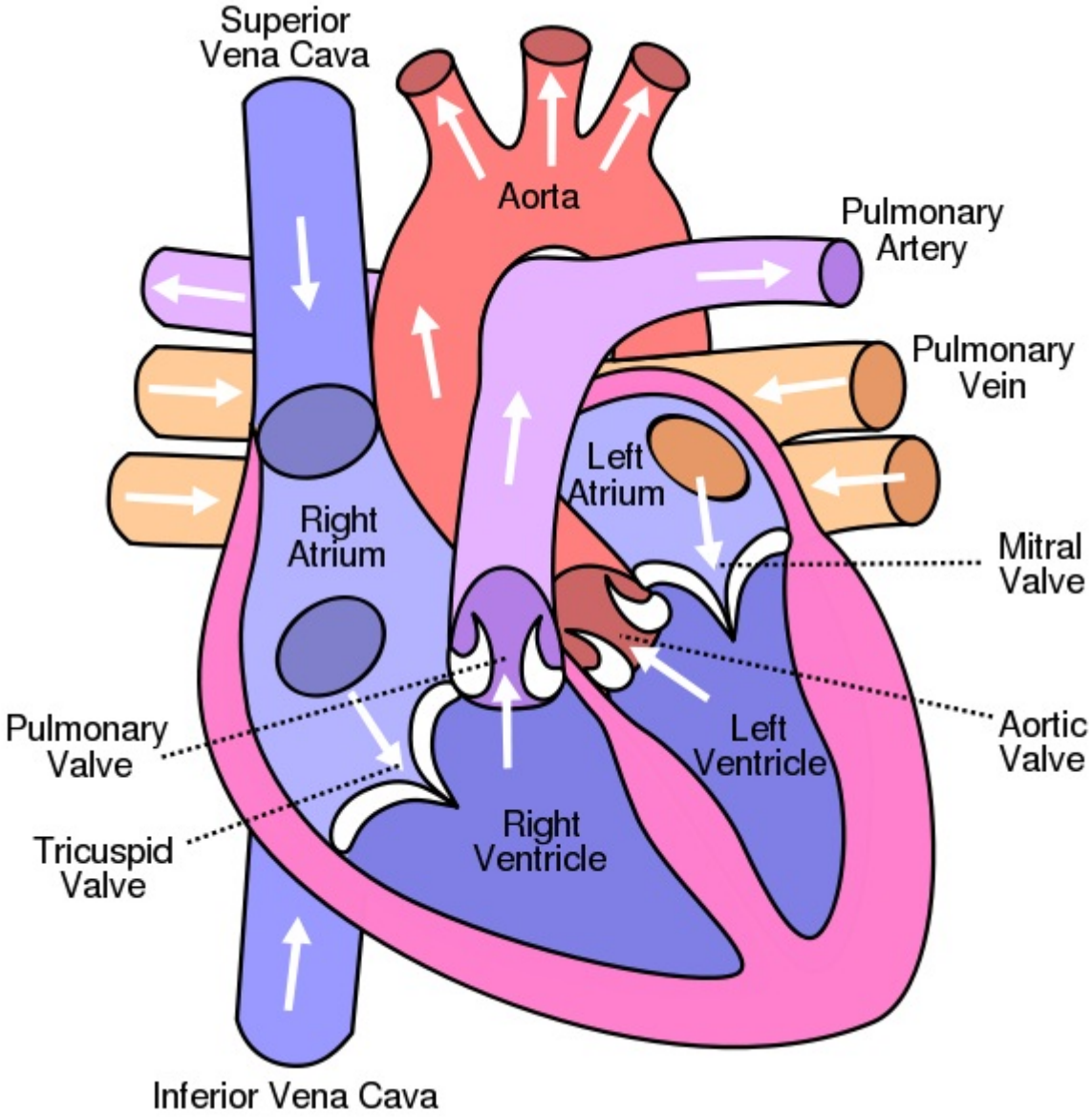

Figure 2.1: Anatomy of Heart [28]

2.1.3 Cardiac Action Potential

The mechanical contraction and relaxation of heart is a consequence of electrical activity of cardiac cells. The electrical activation of cardiac muscle cells occurs through the same mechanism as in the nerve cell. The electrical activities on cell membrane contain the depolarization and repolarization events. These events established by inflow and outflow some ions such as sodium, potassium and calcium. Due to the plateau phase between depolarization and repolarization, the pulse duration of the cardiac muscle is two times longer than that in nerve cells [14]. This change in membrane potential due to the movement of electric charges through the cell membrane, including depolarization and repolarization is termed as action potential.

The cardiac action potential consists of one depolarization phase and the four phases of repolarization. Action potential and electrolyte movements are illustrated in 2.2. The phases of action potential are [26, 29] :

Phase 4 Resting Membrane Potential and Diastolic Depolarization: This is the period that the cell remains in the resting membrane potential until stimulated by an external electrical stimulus. This external stimulus is typically from an adjacent cell. Certain cardiac cells (pacemaker cells) have the capacity to undergo spontaneous depolarization. In pacemaker cells, there is a time-dependent decrease of outward potassium current with a rapid influx of sodium, causing a self-initiated depolarization.

Phase 0 Rapid Depolarization: As the stimulus reaches to a threshold voltage, the permeability of cell membrane changes and sodium ions rush into the cell by activation of fast sodium channels. This makes the inside of the cell more positive and produces the upstroke in the action potential.

Phase 1 Initial Repolarization: In this phase, fast sodium channels are inactivated by the rapid influx of chloride.

Phase 2 The Plateau: During this phase, a slow inward flow of calcium balanced by the slow outward flow of potassium.

Phase 3 Final Rapid Repolarization: At this stage, a rapid repolarization occurs by the inactivation of slow calcium current and by the acceleration of the outflow of potassium.

The action potential has different shapes in pacemaker and non-pacemaker (working) cells

[26]. The difference between action potential in pacemaker and working cells is illustrated in Figure 2.3.

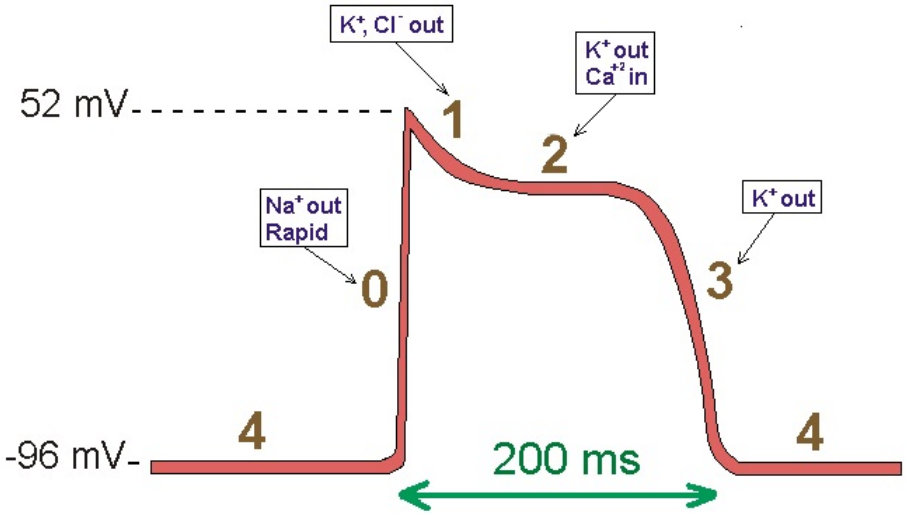

Figure 2.2: The cardiac action potential has five phases

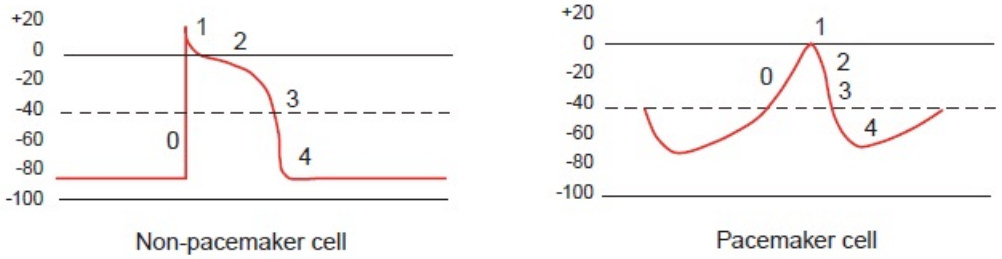

Figure 2.3: Schematic representation comparing action potential of pacemaker and non-pacemaker (working) myocardial cells [26].

2.1.4 The Electrical Stimulation and Conduction System of Heart

Heart has its own electrical system to stimulate contraction without any nerve supply. The specialized cardiac tissues generate and conduct the cardiac impulse all over the heart. Cardiac conduction system consists of following structures (see Figure 2.4):

Sinoatrial node (SA node): Sinoatrial node is located in the right atrium near opening of superior vena cava where the heart beat or contraction origins. It contains the primary pacemaker

cells of the heart [30, 26, 14]. The pacemaker cells, located SA node, generate an action potential at the rate of about 70 per minute [14].

Atrioventricular node (AV node) : It is is located at the boundary between the atria and ventricles. It provides the only conducting path from the atria to the ventricles [14]. Atrioventricular bundle (Bundle of His) AV node and Bundle of His comprise AV junction. The cardiac impulses from the AV node are conducted to the ventricles through the bundle of His.

Bundle branches (Left and right): These bundles branches distribute impulses from bundle of His to each ventricle.

Purkinje fibers: These fibers are also called Conduction myofibers. They are located in the ventricular myocardium. The cardiac stimulus spreads to the ventricular muscle cells through the Purkinje fibers.

The conduction speed of electrical impulses varies through conduction path of the heart. It is slowest through the AV node and fastest through the Purkinje fibers. This conduction speed difference has a functional importance. The relatively slow conduction speed through the AV node enables the ventricles enough time to fill with blood before the signal for cardiac contraction arrives [30].

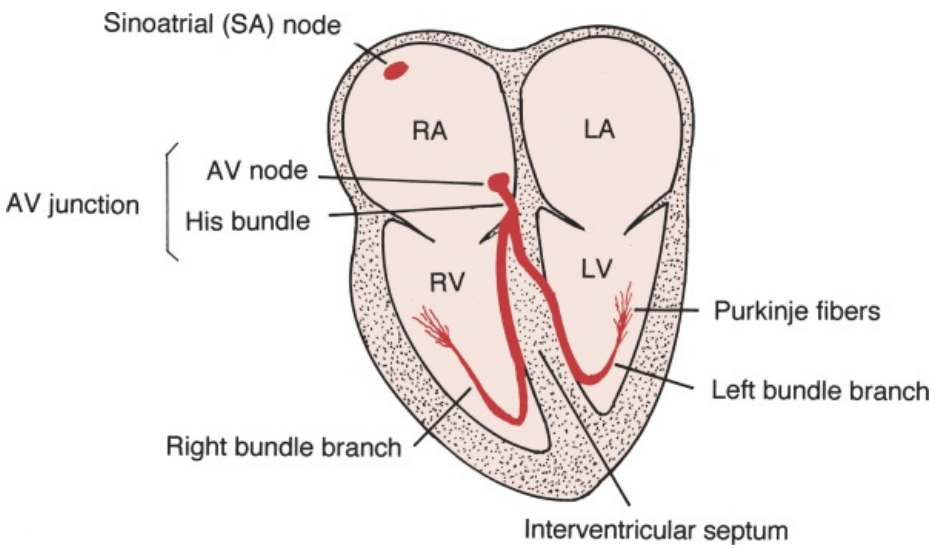

Figure 2.4: Cardiac Conduction System [30].

2.1.5 Electrocardiography of Heart

The cardiac electric events that are represented so far in this section occur on the intracellular level. The electric signals such as action potential may be recorded over a cardiac muscle cell. However, the electrocardiogram (ECG) is a picture of heart, generated by the electric activity of the heart, on the body surface. Thus, ECG records the electrical activity of a large mass of cardiac cells, not a single cardiac cell. The superposition of the electrical signals on the body surface forms the ECG wave. In Figure 2.5, pulses from different parts of heart and the resultant ECG waveform during a cardiac period are shown. A normal ECG waveform contains P wave, QRS complex, ST segment, T wave, and U wave that are generated by electrical activity of atrial and ventricular cells. P wave is caused by the atrial depolarization. QRS interval represents the ventricular depolarization. T and U wave are produced by ventricular repolarization.

2.2 Cardiac Source Models

A model is a simplified abstract representation of complex real subjects. Simplified models of cardiac sources are used to investigate and understand the functioning of the heart. Thus, a mathematical model of cardiac bioelectric sources enables to describe macroscopic cardiac electrical activity with the ECG measurements by estimating the parameter values of the model [31]. Equivalent cardiac current sources [32, 33, 34], cardiac activation isochrones [35] and pericard potential distributions [36, 37, 10] are three major equivalents cardiac models used in inverse electrocardiography problems. Equivalent cardiac current sources include the fixed-dipole, moving dipole, multi dipole and multipole models [14], while in the activation time based models, cardiac is represented by the uniform double layers and equivalent double layer source models.

2.2.1 Dipole

A dipole is a current source that consists of two monopoles of opposite sign, a source and a sink, separated by a very small distance [14]. The potentials tend to go to infinity near the source. Thus, this simple equivalent source model is used only for describing the potentials

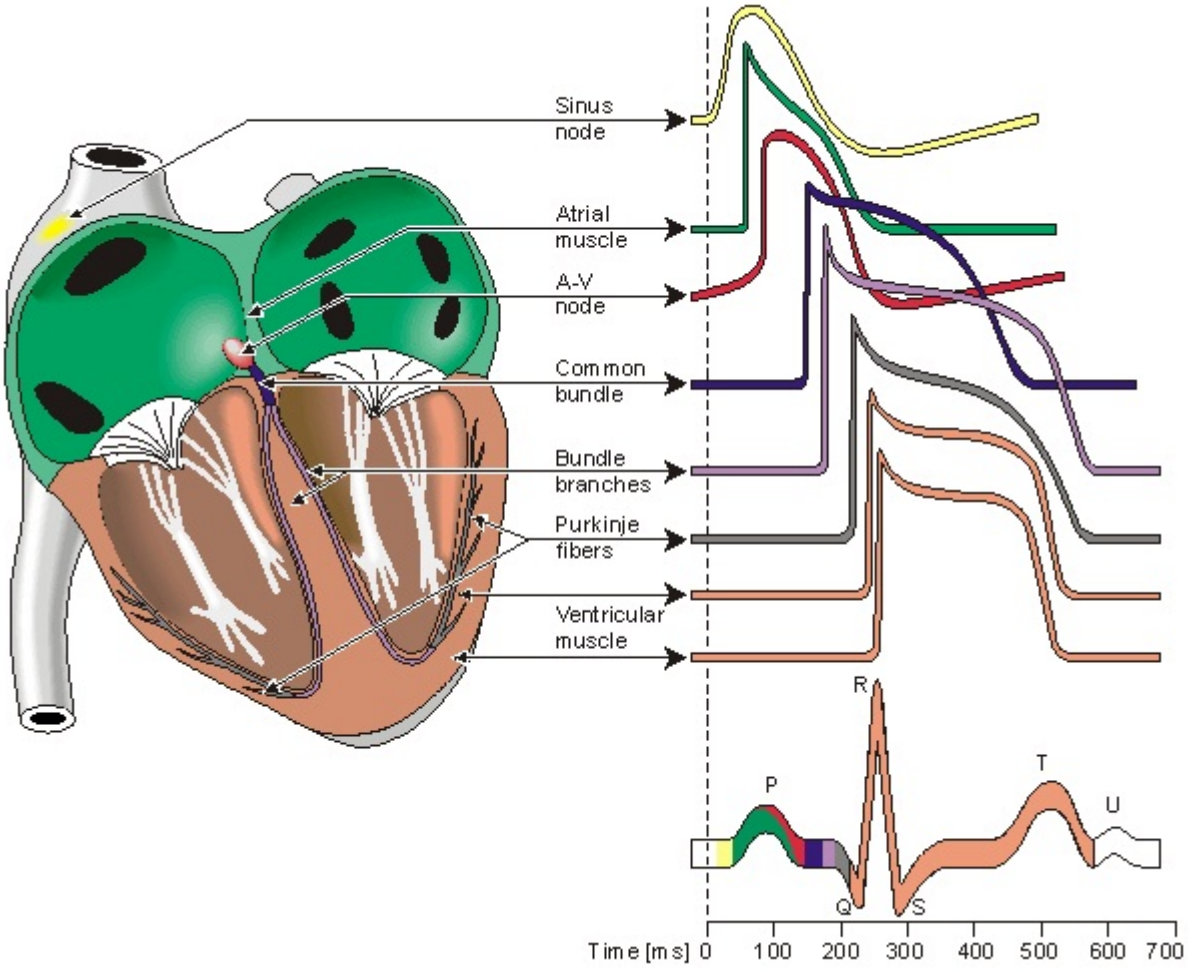

Figure 2.5: ECG Waveform [14].

at relatively large distances from the actual cardiac sources. Moreover, a dipole is limited equivalent source in reflecting the underlying electrical activity of myocardium. It is able to reflect the underlying electrophysiology when the electric activity is restricted to a small part of the myocardium [38].

A single dipole model can be a fixed-dipole or a moving-dipole model. The fixed dipole model has fixed origin location, its orientation and magnitude changes. This model expressed by three independent variables. The moving-dipole model is based on a single dipole that has varying location, magnitude and orientation, additionally variable. It has six independent variables [14].

A single dipole model produces a very robust, but not very specific estimate of the cardiac electrical activity. It is limited in ability to represent the entire electrical activity of the heart. Therefore, multiple dipole models are used to improve the link with the underlying electrophysiology. Multiple dipole models have more unstable solution in inverse problem solutions due to the increase in number of parameters in the models [38].

2.2.2 Multipoles

The multipole source models characterize the heart by a series of multipolar current generators such as dipole, quadrupole, octupole, hexadecapole, etc. A quadrupole sonsists of two equal and opposite dipoles that are close together. Higher order source configurations are obtained in similar way. The multipole representation of cardiac bioelectric sources is based on the approach that states the any given source configuration can be expressed as an infinite sum of multipoles of increasing order (i.e., dipole, quadrupole, octapole, etc.) all located at a fixed common origin [13, 14]. It provides a more suitable representation of cardiac source generators than the dipole model [38, 32].

2.2.3 Uniform Double Layers

The uniform double layer model (UDL) is a widely used model for representing cardiac sources. In this source model, it is assumed that the remote ECG wave forms during the depolarization phase of the ventricles are produced by a current dipole surface density (uniform double layer) lying along the activation wavefront and oriented in the normal direction

[31, 35]. In this model, the surfaces carrying elementary current dipoles are located in myocardium and represent depolarization wavefronts as they propagate through the myocardium. This source model is directly linked to the underlying electrophysiology [38]. However, the wavefronts in in this kind of UDL model is accessible only by the electrodes mounted within the heart tissue and therefore a more convenient equivalent source is needed [31]. This is achieved by equivalent double layer or surface double layer models.

2.2.4 Equivalent Double Layers

The equivalent double layer is a surface source model that is used to express the entire cardiac electrical activity by a source of double layer (dipole sheet) located on the closed surface of the epicardium and endocardium surrounding the myocardium [38]. In this source model, cardiac source is approximated as an equivalent uniform double layer on the pericardium instead of the actual current dipole surface density (equivalent uniform double layer) in myocardium [35, 39]. This equivalence is based on solid angle theorem [38, 35].

In this source model, equivalent surface is replaced with the the actual activation wavefront by any UDL that has the same solid angle. This equivalent double layer can be estimated from the external fields [39]. This equivalent UDL surface lies on the boundary of the heart and encloses all currently excited tissue [31]. The movement of the edge of this surface forms the activation time mapping during the depolarization.

The equivalent surface sources introduced by Geselowitz [40] by means of bidomain approach. Geselowitz claimed that in isotropic heart the volume distribution of cardiac sources can be replaced by a double layer on the heart surface and the local double layer strength is everywhere proportional to the transmembrane action potential.

In this model, the closed surface surrounding myocardium is digitized by dividing surface into the small surface source elements [35]. The strength of the each EDL source elements is zero until depolarization. By bidomain theory, during the depolarization for any point on the surface of heart the local surface strength is proportional to the transmembrane potential of the cells near surface. This leads to a uniform double layer with the assumption of the maximum strength is same at any point on heart surface during depolarization [38, 41].

The equivalent double layer method requires the assumption of the homogeneity of the anisotropy

ratio of intracellular and extracellular conductivities. Although this assumption may not always hold true, this cardiac model yields an accurate description of body surface potentials throughout the entire cardiac cycle during, i.e., including repolarization [41].

2.2.5 Transmembrane Voltages

The transmembrane voltage describes the electrical potential difference between the interior and exterior of the cell membrane. It is another type of cardiac source model that is used for representing cardiac activity. In this model, TMV distribution within myocardium and electrical potentials on body surface are related by bidomain model [42, 43]. The reconstruction of the transmembrane voltages defined around the whole active heart tissue gives a complete picture of cardiac activity [2].

The bidomain model provides a linear relation between transmembrane voltages and body surface potential, however, the inverse problem formulated in terms of TMVs as cardiac sources does not have a unique solution [42]. This problem can be overcome by imposing additional constraints to the solution.

2.2.6 Epicardial and Endocardial Potential Distribution

One of the reasons for using such surface potentials as cardiac sources is based on the unique one-to-one relationship between the potentials at the surface bounding a volume conductor in case that the surfaces are closed and that no primary sources are present in between the surfaces [38]. Aim of the inverse problems having epicardial potentials as cardiac source is to compute the epicardial potential distribution from the body surface potentials using the volume conductor model of the heart. In addition to its clinical importance, surface potentials provide a representation of cardiac sources that have the possibility of direct validation of the inverse solution using catheter measurements or sock electrodes [13, 42, 2]. Another advantage of using epicardial potentials as cardiac source is that the effects of inhomogenities inside the heart such as the intracardiac blood masses are avoided, since the epicardial potentials are outside of the heart.

The main disadvantage of the inverse problem for epicardial potentials is highly ill-posed due to the discretization and smoothing effects. Another weakness of this equivalent source

model is the difficult interpretation of reconstructed results since the potentials at each point is defined by the transmembrane voltages of the whole heart not just by the neighboring nodes[42].

Epicardial potential distribution is assumed as equivalent cardiac electric generator in this study. The relation between epicardial potential distribution and body surface measurements is linear. The detaila about the formulation of the inverse problem involving epicardial potentials as cardiac source are given in Chapter 3.1

2.3 Forward Problem of Electrocardiography

The forward problem of electrocardiography consists of the computation of the torso potentials from a given distribution of bioelectrical sources in the heart. Depending on the used model, these cardiac sources may be either equivalent current dipoles that represent the heart's electrical activity or epicard (heart's outer surface) potentials [13].

The forward problem of electrocardiography involves three basic steps [44]: (i) representation of bioelectrical sources in the heart, (ii)definition of electrophysiological properties (such as geometry, conductivity, inhomogeneity, etc) of the volume conductor, (iii) solving of model equations.

The major applications of the forward electrocardiography problem are [13, 2, 1, 44]: (i) studying the effects of geometry and electric properties of different tissues on the body surface potentials or epicardial potentials, (ii) validation of the cardiac cell models, (iii) optimization of the ECG measurement systems (e.g. electrode locations), (iv) obtaining the transfer matrix (volume-conductor relationships) for the inverse problem, (v) simulation (solution) of the inverse problem with the model-based optimization. (vi) the reciprocal problem of obtaining the currents traversing the heart due to current sources applied at the body surface (e.g. defibrillation)

Forward problem can be solved uniquely from a given cardiac sources distribution. Generally two different methods are used in forward problem, namely surface methods or volume methods. Surface methods require the numerical modeling of interfaces between various tissue regions. In surface methods, also termed boundary-element methods, torso is first discretized

to an approximately equivalent isotropic region. The discretized different torso regions are all assumed to be of isotropic conductivity. Only the interfaces between the different regions are represented and enter into consideration in computation of forward problem [13, 45].

On the other hand, three-dimensional torso model is represented numerically in volume methods. Volume methods include the finite-difference, finite-element, and finite-volume methods. In these methods, torso is represented by three-dimensional grid of discrete points or it is approximated by a combination of volume elements of simple geometrical shapes such as tetrahedra or hexahedra.

In surface methods, torso model represented with fewer elements. However, the potential at every element is combined with the potential at every other element. Consequently, the coefficient matrix that characterizes the set of equations is completely full. However, torso is modeled more complex with more elements in volume methods. Thus, the coefficient matrix is large. However, it is sparse since the potential at each point relates only to only the potentials at its nearest neighbors [13].

2.4 Inverse Problem of Electrocardiography

In the inverse problem of electrocardiography, a large number of body surface potentials are used to reconstruct the cardiac source and to understand the heart's electrical activity. In addition to measured ECG signal, information about the patient's anatomy and knowledge of the physical properties of the human body are also considered in solving the inverse problem. It is a great noninvasive technique, which provides practical information on the functionality of heart.

However, the inverse problem does not have a unique solution, i.e. different cardiac source distributions may result in the same body surface potentials. This non-uniqueness problem is overcome by the use of simplified models for cardiac sources. Fixed dipole, moving dipole, multiple dipoles, multipoles, the epicardial potential distribution, and the activation isochrones on the heart surface are examples of simplified models of heart. These models introduce implicit constraints that allow the model parameters to be uniquely calculated from torso potentials [13, 46].

Another difficulty encountered in the inverse problem of electrocardiography should be handled is ill-posed nature. Ill-posedness, i.e. ill-conditioned, is due to discretization and smoothing. And it means that the inverse solution is very sensitive to small perturbations in the measurement and to the errors in the model. In other words, solution is unstable and can oscillate wildly with small noise. This ill-posedness increases with the complexity of the assumed model. This ill-posed nature has to be stabilized through the use of some regularization methods [16] or computational statistical methods. These regularization methods stabilize solution usually by imposing additional explicit spatial and temporal constraints to the problem [13, 42, 46].

As mentioned earlier, the heart may be represented sources with simplified models, such as fixed dipole, moving dipole, multiple dipoles, multipoles, the epicardial potential distribution and the heart-surface activation isochrones on the surface of the heart. In the fixed dipole model, cardiac source is represented by a simple dipole with fixed location and variable orientation and magnitude. In the moving-dipole case, heart sources modeled by one or two dipoles having variable location as well as varying amplitude and orientation. In other words, cardiac dipole can move and/or rotate (six degrees of freedom) [47]. The multiple dipole models include several dipoles, each located at certain region of the heart. These dipoles have fixed location, varying magnitude and varying or fixed orientation [14].In the multipole representation, heart is modeled by a series of multipole current sources (dipole, quadrupole, octupole, hexadecapole, etc.). Each multipole component is located at a fixed common origin [13, 14].

One of the most widely used cardiac source model in the inverse problem of electrocardiography is epicardial potentials [48]. There is a relationship between epicardial and body surface potentials that depends on body geometry in this type of formulation. Epicardial potentials have proved to be a true reflection of the electrical activity of heart that occurs in the myocardium [37]. The main epicardial electrical activities such as the start of stimulus, excitation, repolarization and movement of stimulus can be easily observed from reconstructed inverse epicardial potential maps [36]. Due to the relation between epicardial potentials and electrical activities in the myocardium, heart surface potentials are used for representing the cardiac source in this thesis. Details of the model and the formulation of the inverse ECG problem are described in Chapter 3.

2.5 Mathematical Optimization

In one of the methods that is used in thesis, inverse ECG problem is formulated as convex optimization problem in order to regularize the problem with the spatio-temporal constraints. Because of this, this section introduces mathematical optimization. Certain types of optimization problems and their formulation and their general properties are represented.

Basically, optimization can be described as choosing best element from some set of alternatives. The desire to solve a problem in an optimal way is so common, as a result optimization arise in almost every area of application.

An optimization problem has the form:

$$\begin{aligned} &\underset{x}{\text{minimize}} \quad f_0(x) \\ &\text{subject to} \quad f_i(x) \leq b_i,\ i = 1, \ldots, m. \end{aligned} \tag{2.1}$$

where

$x = (x_1, \ldots, x_n)$: optimization variable vector,

$f_0(x) : R^n \rightarrow R$: objective function, the functions,

$f_i(x) : R^n \rightarrow R, i = 1, \ldots, m.$: constraint functions,

A vector x^* is called optimal solution, if it has the smallest objective value satisfying the constraints.

Solution procedure for a class of optimization problem is an algorithm that calculates the solution for the problem in a given accuracy. The effectiveness of these algorithms varies substantially. Specific forms of the objective and constraint functions, how many variables and constraints there are, and special structure, such as sparsity, are important factors that affect the effectiveness of the algorithms [49]. Even the objective and constraint functions are simple and well known, the general optimization problem may still be surprisingly difficult to solve. But, there are some important exceptions to the general rule that most optimization problems are difficult to find a solution.[49]. Certain problem classes such as least-squares problems, linear programs and convex optimization problems can be solved efficiently and reliably.

2.5.1 Least-squares problems

A least-squares problem is an optimization problem that has no constraints (i.e., $m = 0$) and it has an objective in the form of a sum of squares:

$$\text{minimize } f_0(x) = \|Ax - b\|_2^2 = \sum_{i=1}^{k} \left(a_i{}^T - b_i\right)^2$$

Here $A \in R^{k+n}$ (with $k \geq n$), $a_i{}^T$ are the rows of A and the vector $x \in R^n$is the optimization variable.

The solution of a least-squares problem can be reduced to solving a set of linear equations,

$$(A^T A)x = A^T b$$

so we have the analytical solution $x = (A^T A)^{-1} A^T b$.

2.5.2 Linear programming

Another impotant type of optimization problems is linear programming. In linear programming, the objective and constraint functions are all linear:

$$\begin{aligned} &\text{minimize} \quad c^T x \\ &\text{subject to} \quad a_i{}^T x \leq b_i, \ i = 1, \ldots, m. \end{aligned} \tag{2.2}$$

where the vectors $c, a_1, \ldots, a_m \in R_n$ and scalars $b_1, \ldots, b_m \in R$ are problem parameters that specify the objective and constraint functions.

There is no analytical solution or a formula to find a solution for a linear program. However, there are a lots of very effective methods to solve linear programming problems, such as Dantzig's simplex method and interior point method [49].

2.5.3 Convex optimization

A convex optimization problem has the following form

$$\begin{aligned} &\text{minimize} \quad f_0(x) \\ &\text{subject to} \quad f_i(x) \leq b_i,\ i = 1, \ldots, m. \end{aligned} \tag{2.3}$$

where functions $f_0, \ldots, f_m : R_n \rightarrow R$ are convex, i.e., satisfy

$$f_i(\alpha x + \beta y) \leq \alpha f_i(x) + \beta f_i(y)$$

for all $x, y \in R_n$ and all $\alpha, \beta \in R$ with $\alpha + \beta = 1, \alpha \geq 0, \beta \geq 0$. The least-squares problems and linear programming problems are special cases of the convex optimization problems [49].

There is no simple formula to find a solution for a convex optimization problems. However, there are very effective methods such as interior-point method to the convex optimization problems. Interior-point method works very well in practice [49].

2.5.4 Nonlinear optimization

If objective or constraint functions are not linear in an optimization problem it is called nonlinear optimization (or nonlinear programming). It is the most general form and there are no effective methods in solving a nonlinear programming problem. Even simple problems with a few variables can not be solved easily.The methods for solution of a general nonlinear programming problem therefore take several different approaches, each of which involves some compromise [49].

2.6 Entropy Optimization

Minimum Relative Entropy Method is one of the methods in solution of inverse ECG problem. Thus, in this section entropy optimization concepts and principles of maximum entropy and minimum relative entropy is explained shortly.

2.6.1 Entropy and Self Information Concepts

The word entropy is a widely used term in thermodynamics. It represents measure of energy in a thermodynamic system according to the temperature and the heat entering the system. [50].

Entropy is not a fundamentally intuitive subject, but it is something defined via equations. It describes the randomness and uncertainty in a system.

However, the information theory entropy is different from the entropy definition in thermodynamics [51]. The concept of entropy of random variables and processes is suggested by Claude E. Shannon [52, 53]. Entropy, uncertainty and related information measures provide useful tools in description of behavior of a random process [52].

The Shannon's entropy is a measure of information. It is used in a wide range of disciplines such as statistical mechanics, thermodynamics, statistical inference, business, finance, pattern recognition, queueing theory, information theory, parameter estimation and linear/nonlinear programming [50].

In information theory, entropy, self information and uncertainty are closely related terms. Self information is an information measure that is associated with the occurrence of an event. For a random experiment with probability mass function $p_x(i)$, the self information associated with the outcome $\{\underline{X} = x_i\}$ is denoted by

$$h(p_i) = log(\tfrac{1}{p_i}) = -log(p_i)$$

where $p_i = p_x(i) = P(\underline{X} = i)$.

By this definition, following properties of self information can be derived easily:

(i) Self Information has always a non-negative value: $h(p) \geq 0$

(ii) One can get no information from the occurrence of the event that has probability 1: $h(1) = 0$

(iii) The information that we get from observing the two independent events is the sum of the two information functions: $h(p_1 \times p_2) = h(p_1) + h(p_2)$

(iv) Self information, a measure of information, is a monotonic and continuous function of probability mass function.

By definition, the amount of information in a probabilistic event depends on only the probability of that event. It is clear that knowledge of the actual outcome of the random experiment eliminates the uncertainty and increases the information associated with it. It is also clear

that occurrence of an event with smaller probability gives more information, i.e. larger self-information.

Shannon entropy is a usable measure of the uncertainty or information associated with a random variable. It is closely related with the self information term. Shannon entropy is an expected value that quantifies the information contained in a message.

Entropy concept may be expressed more easily with an example. Suppose that we have a source that emits n symbols $\{a_1, a_2, ..., a_n\}$ with probabilities $\{p_1, p_2, ..., p_n\}$, respectively. And assume that these symbols are emitted independently. Then the average amount of information from each symbol in the stream can be calculated as follows:

The symbol a_i has $log(\frac{1}{p_i})$ information from a particular observation. In a stream with N observations, symbol a_i is seen approximately $N \times p_i$ times. Thus, in the N independent observations, we get total information h_{total} of

$$h_{total} = \sum_{i=1}^{n} (N \times p_i) \times log(\frac{1}{p_i})$$

where $\sum_{i=1}^{n} p_i = 1$.

Then, the average information that is get from the observed symbol will be

$$\begin{aligned} H(P) &= (1/N) \times h_{total} = (1/N) \times \sum_{i=1}^{n} (N \times p_i) \times log(\frac{1}{p_i}) \\ &= \sum_{i=1}^{n} p_i \times log(\frac{1}{p_i}) \end{aligned} \tag{2.4}$$

This result about average information, associated with a random variable with a probability distribution, leads to definition of Shannon's entropy. Entropy function $H(P)$ is the expected value of self-information $h(p)$ and it is defined as [50, 52, 54]:

For discrete case with a probability distribution $P = \{p_1, p_2, ..., p_n\}$ where $\sum_{i=1}^{n} p_i = 1$,

$$
\begin{aligned}
H(P) &= \sum_{i=1}^{n} p_i \times log(\frac{1}{p_i}) \\
&= -\sum_{i=1}^{n} p_i \times log(p_i) \\
&= E\left\{log\left[\frac{1}{p}\right]\right\} \\
&= E\left\{h(P)\right\}
\end{aligned}
\tag{2.5}
$$

and for continuous case with a probability distribution $P(x)$

$$H(P) = \int P(x) log\left[1/P(x)\right] d(x)$$

Given a probability distribution $P = \{p_1, p_2, \ldots, p_n\}$ where $\sum_{i=1}^{n} p_i = 1$, entropy function $H(P)$ has an important property, known as Gibbs inequality. This property is

$$0 \leq H(P) \leq log(n)$$

If entropy is zero, i.e. $H(P) = 0$, then one of the p_i's is one and all the rest are zero. That is, minimum entropy is zero and it is achieved by occurrence of an event that has probability 1 (no information).

Similarly, $H(P) = log(n)$is achieved only when all of the events have the same probability $1/n$. This means that the maximum of the entropy function is the logarithm of the number of possible events. And it occurs when all the events are equally likely.

2.6.2 Principle of Maximum Entropy

The principle of maximum entropy is a postulate that states that the most likely probability distribution satisfying a given set of constraints has the largest entropy. In other words, the probability distribution that best represents the current state of knowledge has the maximum entropy. The probability distribution that maximizes the entropy is the true probability distribution subject to known constraints.

The principle of maximum entropy is often used to obtain prior probability distributions of random variable with known constraints. Then, this obtained distribution may be used to select the prior distribution that is need by other methods such as Bayesian approach [55, 56]. Jaynes [57, 56, 58] claims that the maximum entropy method produces optimal solution for prior distribution subject to available constraints.

The method of maximum entropy is selecting a prior distribution that has the largest possible entropy subject to the limitations imposed by the known information. Formulation of maximum entropy method is for discrete case:

$$\begin{aligned} \text{maximize} \quad & H(P) = \sum_{i=1}^{n} p_i log\left[1/p_i\right] \\ \text{subject to} \quad & \sum_{i=1}^{n} p_i = 1 \\ & p_i \geq 0 \\ & \sum_{i=1}^{n} p_i f_i^k \leq f_k,\ k = 1, \ldots, m. \end{aligned} \tag{2.6}$$

The maximum entropy gives optimal solution for the available information. For example, if there is no information about distribution, i.e. the parameters have any value in a finite range, the entropy is maximized with uniform distribution. If there is prior information consisting of the mean value, upper and lower limit of random variable then entropy is maximized with a truncated exponential distribution [59, 60]. If there is prior information consisting of the mean value, and variance of random variable then entropy maximization leads to a normal distribution [60].

2.6.3 Principle of Minimum Relative Entropy

The principle of minimum relative entropy (MRE) is a method of statistical inference that was first introduced by Kullback [61]. Similar to the Bayesian MAP estimation, it is used to update the prior probability distribution to a new posterior probability distribution using the new data about random variable.

In information theory, relative entropy (or Kullback-Leibler divergence) is a measure of difference between two probability distributions P and Q. This divergence is a nonsymmetrical

measure i.e. Kullback-Leibler distance from P to Q is not necessarily equals to the Kullback-Leibler distance from Q to P. For two probability distributions q(x) and p(x) for a random variable X, the relative entropy of Q with respect to P is given as:

$$\begin{aligned} H(Q,P) &= E_q\{log\,[Q/P]\} \\ &= \sum_{i=1}^{n} q_i log\,[q_i/pi] \end{aligned} \tag{2.7}$$

Relative entropy function is a nonnegative function i.e. $H(Q,P) \geq 0$. And $H(Q,P) = 0$, when p(x) and q(x) are identical.

According to the principle of minimum relative entropy, also called principle of minimum discrimination information, we choose a probability distribution q(x) that minimizes relative entropy function subject to given constraints. This led to choose a new distribution q(x) that has minimum distance from p(x) and that satisfies the given constraints. By this way, a new probability distribution q(x), that is closest to the prior distribution p(x), is obtained using the new information in the forced constraints.

The principles of maximum entropy and minimum relative entropy are not completely different things. Actually, maximum entropy method is a special case of minimization of relative-entropy. They are equivalent to each other when the prior is a uniform distribution [62, 63, 64]. In other words, minimization of relative-entropy is identical to the maximization of Shannon entropy, if there is no specific prior information about the distribution of random variable and all prior probabilities are taken to be equal.

Minimum relative entropy method is a powerful tool in order to find an unknown posterior distribution when there exists a prior distribution and limitations about the random variable that are obtained from measurements[65]. The relative entropy minimization has application in various disciplines such as statistical physics, information theory, and financial mathematics [66]. It is also used for the solution of inverse problems [67, 61, 68, 69, 59].

CHAPTER 3

THEORY

3.1 Definition and Formulation of the Inverse ECG Problem

Forward problem of electrocardiography aims to estimate the body potential from the known electrical activity of heart using an equivalent cardiac source model. However in inverse problem, aim is reconstructing source using the electrical information available on the torso surface. In this thesis, inverse ECG problem that involves epicardium potentials as cardiac source is studied.

Epicardium potentials and body potential distribution is related with a discrete formulation in the forward equation. This relation is linear and formulated as follows:

$$d_k = Gm_k + n_k, k = 1, 2, 3, \ldots, T \tag{3.1}$$

where,

d_k is an Mx1 vector of recorded torso potentials from different electrodes on body surface at the time instant k,

m_k is the Nx1 vector of epicardial potentials from different points on heart surface at the time instant k,

G is the MxN matrix representing the forward transfer matrix,

n_k is the measurement noise of the same dimensions as the body surface vector,

and k and T are a discrete time index and the number of time samples, respectively.

Matrix G depends on body geometry and it is the forward transfer matrix. In inverse electrocardiography, the torso potentials d_k and transfer matrix G are known and the source, epicardial potential vector m_k , is unknown. The transfer matrix G shown in Equation 3.1 is estimated from the geometry and conductivities of the organs within the thorax using Boundary Element Method (BEM). An important issue is that observations (measurements) always contain some amount of noise.

One characteristic of the inverse problem is its ill-posed nature due to discretization and smoothing. It means that the reconstructed solution is unstable and can oscillate wildly with even a small noise. This property is also termed as ill-conditioning because the condition number of the transfer matrix G is very high. Due to this ill-conditioning, this problem can not be solved directly by estimating the inverse of the transfer matrix G. This ill-posed nature needs to be stabilized by using some regularization methods or statistical computational methods. The ill-conditioning of the inverse ECG problem will be analyzed in the later sections.

3.1.1 State Transition Matrix (STM)

When the epicardial potentials are recorded over a period of time, it can be observed that these potentials are continuous over that period, i.e. these potentials are temporally related. Thus it may be possible to represent the epicardial potentials in successive time instant as a function of previous time slot potentials on heart surface. This can be shown as:

$$m_k = f_k(m_{k-1}), k = 1, 2, 3, \ldots, T \tag{3.2}$$

Equation 3.2 represents the spatio-temporal relationship of epicardial potentials for two successive time instants. This equation can be linearized and approximated in the form:

$$m_k = Fm_{k-1} + w_k, k = 1, 2, 3, \ldots, T \tag{3.3}$$

where, F is the NxN state transition matrix (STM) which determines the relation between the epicardial potentials of two successive time instants

w_k is the Nx1 process noise vector

Inverse ECG problem takes the above form with the insertion of this equation into the formulation:

$$d_k = Gm_k + n_k, k = 1, 2, 3, \ldots, T$$
$$m_k = Fm_{k-1} + w_k, k = 1, 2, 3, \ldots, T \tag{3.4}$$

One possible choice for the state transition matrix is identity matrix. However, this is not enough for representing both spatial and temporal relations of the nodes. The determination of the state transition matrix is a problem for this kind of formulation. There are several methods for this such as using epicardial potentials. However, this is not an easy task since epicardial potentials are also unknown. In this thesis, various STMs are used and tested in solution of inverse ECG problem.

3.1.2 The Moore-Penrose (Generalized) Pseudo-inverse Matrix

The Moore-Penrose pseudo-inverse is a general way to find the solution to linear equations in the form of $d = Gm$. The pseudo-inverse of transfer matrix G is represented by G^+. The matrix G^+ is the unique matrix that satisfies the following properties:

i.$GG^+G = G$

ii.$G^+GG^+ = G^+$

iii.$(GG^+)^* = GG^+$(GG^+ is Hermitian)

iv.$(G^+G)^* = G^+G$(G^+G is Hermitian)

The pseudo-inverse matrix G^+ is estimated in the following way for the following different cases:

-If $M = N$ and G is full rank $G^+ = G^{-1}$.

-If $M > N$ and G is full rank i.e. it has a rank number N (in this case there are more constraining equations than there are free variables), the solution is the one that minimizes the

quantity $\|d - Gm\|_2$. In this case, it is not generally possible find a solution to the all equations. The pseudo-inverse of forward matrix G gives the solution such that G^+m^+ is closest to the measurements d in least-square sense. And G^+ is equal to $(G^TG)^{-1}G^T$.

-If $M < N$ and G is full rank i.e. it has a rank number N (in this case there are more free variables than there are constraining equations) then the solution minimizes the L2-norm of m. In this case, there are generally an infinite number of solutions, and the pseudo inverse solution is the particular solution whose L2-norm is minimal. And G^+ is equal to $G^T(GG^T)^{-1}$.

- If the rank of G is less than both M and N, the generalized pseudo-inverse solution encapsulates the behavior of both of the two previous cases, minimizing both of the quantities $\|d - Gm\|_2$ and $\|m\|_2$. In this case, the pseudo-inverse is can not be obtained directly from the transfer matrix G as in two previous cases. However, it can be computed using the methods such as Singular Value Decomposition.

In the next section, computation of generalized pseudo-inverse of a matrix and its properties will be discussed.

3.1.3 Singular Value Decomposition (SVD) and Pseudo-inverse Solution

Singular value decomposition (SVD) is a method of analyzing and solving ill-conditioned linear problems. In the SVD, MxN matrix G is factored into the following form [55].

$$G = USV^T \tag{3.5}$$

where

U is an MxM orthogonal matrix with columns that are unit basis vectors spanning the data space, R^M. V is an NxN orthogonal matrix with columns that are basis vectors spanning the model space, R^N. S is an MxN diagonal matrix with diagonal elements called singular values (eigenvalues).

The singular values along the diagonal of S are arranged in decreasing order, $s_1 \geq s_2 \geq \ldots \geq s_{min(M,N)} \geq 0$.Here some of the singular values may be zero. Then we represent the S in the following form where the p is the number of non-zere singular values. Here p is the rank of

transfer matrix G.

$$S = \begin{bmatrix} S_p & 0 \\ 0 & 0 \end{bmatrix} \tag{3.6}$$

Then the SVD representation of matrix G becomes the following forms:

$$\begin{aligned} G &= [U_{.,1}, U_{.,2}, \ldots, U_{.,m}] \begin{bmatrix} S_p & 0 \\ 0 & 0 \end{bmatrix} [V_{.,1}, V_{.,2}, \ldots, V_{.,m}]^T \\ &= [U_p, U_0] \begin{bmatrix} S_p & 0 \\ 0 & 0 \end{bmatrix} \left[V_p, V_0\right]^T \end{aligned} \tag{3.7}$$

where $U_{.,i}$ and $V_{.,j}$ are columns of matrices U and V. Then the Equation 3.7 can be simplified into [55]:

$$G = U_p S_p V_p^T \tag{3.8}$$

The columns of U_p form an orthonormal basis for $R(G)$ and the columns of V_p form an orthonormal basis for $R(G^T)$. In other words, columns of U_p represent a basis of measurement (data) space and the columns of V_p represent a basis of model space.

The SVD can be used to compute a generalized inverse of G. It satisfies the desirable inverse properties of Moore-Penrose pseudo-inverse described in previous section. The generalized inverse is [55]

$$G^+ = V_p S_p^{-1} U_p^T \tag{3.9}$$

Using the generalized inverse matrix G^+ one can estimate the pseudo inverse solution. It is defined as:

$$\begin{aligned} m^+ &= G^+ d \\ &= V_p S_p^{-1} U_p^T d \end{aligned} \tag{3.10}$$

We can also write the equation in 3.10 as a linear combination of the columns of V_p. It is shown as:

$$m^+ = V_p S_p^{-1} U_p^T d = \sum_{i=1}^{p} \frac{U_{.i}^T d}{s_i} V_{.i} \tag{3.11}$$

The equations in 3.10 and 3.11 can be used to estimate the least square solutions of $d = Gm$ which satisfies

$$\tilde{m} = \underset{m}{argmin} \|d - Gm\|_2 \tag{3.12}$$

The vectors $U_{.,i}$ in Equation 3.11 form a basis for measurement space whereas the vectors $V_{.,i}$ form a basis for source space. In the presence of a noise in measurements, measurement d will have a nonzero projection onto each of the directions specified by the vectors $U_{.,i}$. In the presence of a very small s_i in the denominator of Equation 3.11, we will have a very large coefficient for the corresponding vector $V_{.,i}$ and the basis vectors $V_{.,i}$ with small singular values will dominate the solution. The singular values s_i decreases with increasing i. The number of zero-crossing of eigenvectors $U_{.,i}$ and $V_{.,i}$ is growing with decreasing eigenvalues si. In other words, the eigenvectors with smaller eigenvalues represent the higher spatial frequencies. Thus, the generalized inverse solution, or the least square solution becomes a noise amplifier in the presence of high frequency components in measurement noise. In this case, even a slightly perturbed data results in unstable solutions.

The instability of the solution can measured by a measure called condition number. This condition number is computed from the transfer matrix G and it reflects the how the equations formed in the problem. The higher condition numbers means more ill-conditioned problems and in this case we get more unstable solutions. The least square solution can be regularized by decreasing the amplifying effect of smaller singular values. This achieved by regularization method such as TSVD and Tikhonov solution. In the next section we will represent regularization methods that are studied in this thesis.

3.2 Regularization Methods for Solving Inverse ECG Problem

As mentioned in previous section, the least square solution is unstable and can oscillate wildly with small noise due to the ill-posed nature of the ECG inverse problem. The ill-posed nature

needs to be stabilized by using some regularization methods. In this part of thesis, some studied regularization methods will be discussed.

3.2.1 Tikhonov Regularization

Tikhonov regularization is a widely used method in stabilizing the ill-posed problems. In Tikhonov regularization, a regularization term is introduced into the formulation in 3.12 and the method solves the following minimization problem:

$$m_\lambda = \underset{arg\ m}{min} \left\{ \|d - Am\|_2^2 + \lambda \|Rm\|_2^2 \right\} \tag{3.13}$$

where $m_\lambda$is the estimated solution for a particular regularization parameter λ, A is the transfer function between the heart and the torso and $\|Rm\|_2^2$ term is the regularization constraint. The equation 3.13 has an analytical solution as follows:

$$m_\lambda = (A^T A + \lambda R^T R)^{-1} A^T d \tag{3.14}$$

Tikhonov or regularization matrix R is a regularization operator. It is usually chosen as the identity matrix $R = I$ and the equation in 3.13 is called zero order Tikhonov regularization in that case. In zero order Tikhonov regularization amplitudes of the norms of epicardial potentials are penalized. In the first-order and second-order Tikhonov regularization, the surface gradient and the surface Laplacian of the epicardial potential values are penalized, respectively.

In this thesis, zero-order Tikhonov regularization is studied. This technique attempts to minimize both the energy of the desired solution and the residual errors of fitness to ECG data. The first term in Equation 3.13 represents the residual errors of fitness to ECG data and second term represents the energy of the solution.The zero-order Tikhonov regularization solution Gm = d, has the following unique solution in terms of singular values:

$$m_\lambda = \sum_{i=1}^{k} \frac{s_i^2}{s_i^2 + \lambda^2} \frac{U_{.,i}^T d}{s_i} V_{.,i} \tag{3.15}$$

where $k = min(M, N)$.

The quantities $f_i = \frac{s_i^2}{s_i^2+\lambda^2}$ in equation 3.15 is called the filter factors. This term avoids the amplification in the small values of singular values.

The regularization parameter λ plays an important role in Equation 3.13. As $\lambda \rightarrow 0$ the estimate approaches the least-squares solution and as $\lambda \rightarrow \infty$ the estimate tends to zero. Thus, Tikhonov regularization method needs decision optimal regularization parameter before implementation. There are some methods to find the optimal regularization parameter such as L-curve, GCV (Generalized Cross Validation), QUASI (Quasi Optimality Criterion).In this thesis, the optimal regularization parameter (λ_{opt}) is estimated by using L-curve method. In L-curve method, L-shaped curve is obtained by plotting the norms $\|d - Gm\|_2$ and $\|m\|_2$ on log-log scale.

The main advantage of Tikhonov regularization is that it does not need prior information in order to solve the inverse problem. It also creates a robust and reasonable solution to a certain degree. However, due to L_2-norm (energy) minimization, edges in the estimated solutions are smoothed and solutions may contain limited information and some misinformation about the real data.

3.2.2 Conic Quadratic Programming

Conic Quadratic Problem is an optimization problem with linear objective and finitely many ice-cream (or second-orderLorentz) cone constraints. It is a type of convex nonlinear optimization problems and its computational complexity lies between linear programming (LP) problems and general convex nonlinear problems. It has the following form[70]:

$$\begin{aligned} &\min_{arg\ x} && c^T x \\ &\text{subject to} && \|D_i x - d_i\|_2 \leq c_i^T x - q_i \text{ (for } i = 1, 2, ...k \text{)} \end{aligned} \tag{3.16}$$

where c, D_i, d_i, c_i and q_i are vectors.

Most convex quadratic programming and quadratically constrained programming problems can be formulated as conic optimization problems. Conic Quadratic Programming can be used as an alternative optimization technique to Tikhonov Regularization for regularizing and solving the inverse problems. Tikhonov Regularization formulation given equation 3.13 can be reformulated as the following optimization problem [70]:

$$\begin{aligned} \min_{arg\ m} \quad & \|Gm - d\|_2^2 \\ \text{subject to} \quad & \|Rm\|_2^2 \leq M \end{aligned} \tag{3.17}$$

The objective function in optimization problem 3.17 is not linear, it has a quadratic form. In order to obtain a linear objective function, the quadratic objective function in 3.17 can be moved to the list of constraints and we write the following equivalent equation:

$$\begin{aligned} \min_{arg\ m,t} \quad & t \\ \text{subject to} \quad & \|Gm - d\|_2^2 \leq t^2 \\ & \|Rm\|_2^2 \leq M \end{aligned} \tag{3.18}$$

The formulation in 3.17 is also equivalent to the following conic quadratic formulation:

$$\begin{aligned} \min_{arg\ m,t} \quad & t \\ \text{subject to} \quad & \|Gm - d\|_2 \leq t \\ & \|Rm\|_2 \leq \sqrt{M} \end{aligned} \tag{3.19}$$

For each value of the penalty parameter λ in Equation 3.13, there exists a corresponding bound parameter, M, in equation 3.19 that gives the same solution. The bound parameter , M, limits the total energy of the solution, this kind of formulation is useful when we have a prior knowledge about the total energy of the solution. However, the equation 3.19 does not have an analytical solution while the problem 3.13 can be solved directly using the equation 3.14.

3.2.3 Two Step Tikhonov Regularization - Linearly Constrained Optimization

As mentioned in section 3.2.1, Tikhonov regularization provides a stabilized solution to the ill-posed inverse problems. However, the accuracy of the estimated solutions using this method strongly depends on the choice of regularization parameter. Optimal choice of the regularization parameter results in more accurate solutions. There some methods those enable to choose regularization parameter without any prior information about the solution. If we have any a priori knowledge about the data or geometry errors, this prior information can be used

to obtain an optimal value of the regularization parameter. In addition, imposing constraints depending on the prior information about the solution can improve the obtained solution.

However, having proper prior information is difficult. Iakovidis[15] proposed a method deriving constraints in the form of linear bounds on the values of the solution without any a priori knowledge of either the data or geometry errors or of any particular characteristics of the epicardial potentials. The method is based on the assumptions that the over regularized ($\lambda_{over} << \lambda opt$) zero-order Tikhonov regularization generates smoother solutions tend to recover more accurately the distribution of the positive and negative values of epicardial potentials or, equivalently, to recover more accurately the zero line of epicardial potentials whereas under-regularized solution corresponding to under-regularized ($\lambda_{opt} << \lambda_{under}$) zero-order Tikhonov inverse solution, recovers more accurately the magnitudes and location of the extrema. Therefore, Iakovidis[15] examined a two-step Tikhonov regularization to obtain more accurate solutions than the unconstrained Tikhonov method can provide. In the first step, Tikhonov regularization applied to the problem in order to obtain a accurate around the zero line. Then, we derive a solution set shown in equation 3.20 in the form of linear bounds the using the obtained over-regularized solution. At the second step, the problem is solved with an under-regularization parameter by imposing this solution set as constraint. In other words, we try to construct an under-regularized solution that satisfies the solution set M.

$$M = \left\{ m \in R^n | a_i \leq m^i \leq b_i, i = 1, 2, \ldots, n \right\} \tag{3.20}$$

where,

$$\begin{aligned}
&a_i = \epsilon, \quad && b_i = K \quad && \text{when} \quad m^i_{t_0} > \epsilon > 0, \\
&a_i = -K, \quad && b_i = -\epsilon \quad && \text{when} \quad m^i_{t_0} < -\epsilon < 0, \\
&a_i = m^i_{t_0}, \quad && b_i = m^i_{t_0} \quad && \text{when} \quad \left| m^i_{t_0} \right| < \epsilon
\end{aligned}$$

Here, ϵ is small positive number that defines the value around zero while K is large number defines the upper bound on the magnitudes of the epicardial potentials.In this thesis, both zero-order Tikhonov Regularization and a two step zero-order Tikhonov Regularization are used to obtain the desired solution of inverse ECG problem. In the thesis, K is taken as infinity. Method is tested with various over-regularization and under -regularization parameters and ϵ values.

3.2.4 Twomey Regularization

Twomey regularization is a modified form of Tikhonov regularization. This technique attempts to simultaneously minimize the distance between the desired solution and the prediction about solution and the residual errors of fitness to ECG data. This minimization is represented as:

$$m_{k+1} = \underset{argm_{k+1}}{min} \left\{ \|d_{k+1} - Gm_{k+1}\|_2^2 + \lambda_{opt} \|m_{k+1} - Fm_k\|_2^2 \right\} \tag{3.21}$$

The prediction or initial estimate of solution can be obtained by multiplication of STM and previous time instant solution as in Equation 3.21.

3.2.5 Admissible Solution Approach

In literature, there are methods which consist of two or more steps to find a solution that satisfies certain constraints. It is aimed to satisfy only a single constraint in each step. In obtaining a solution in multiple-steps, it is easy to get a solution in each step. However, decision on the strategy to combine these solutions and obtaining a good posterior solution is a problem.

Instead of finding a solution in multiple-steps, Ahmad et. Al. [17] reported an admissible solution approach to inverse electrocardiography that allows easier integration of multiple constraints simultaneously. The problem is now treated as finding one solution in the set of solutions that satisfy all these constraints. Any solution that simultaneously satisfies all the constraints is said to be admissible.

In admissible solution approach, it is concentrated on incorporating multiple constraints into the inverse problem formulation. Inverse problem reformulated as a convex optimization problem and problem is solved by using convex optimization methods. The motivation for imposing multiple constraints in inverse electrocardiography is described by Srinidhi [18] as

1) No single priori constraint is clearly superior from a physical point of view, but many have some validity.

2) Some constraints, needed to stabilize the solution, may introduce bias. By using more than

one constraint one can hope to reduce the severity of each constraint.

Most of the approaches in inverse electrocardiography regularization are L_2-norm based constraints as in Tikhonov regularization. However, these kinds of constraints generally are smoothing constraints. The drawback is that regions of large potential gradients are smoothed out as an effect of these kinds of constraints. In this thesis, admissible approach is one of the studied methods. In this method, I have formulated both L_2 and L_1 (TV) norm constraints in the same problem. L_2 norm constraint bounds the total energy of solution. The effect of L_2 norm constraint is same as the Tikhonov regularization. L_1 norms include potential gradients depending on topology and position of nodes. Similar to L_2 norm constraint, the L_1 (TV) norm constraints make solution spatially regularized. However, L_1 norm constraint based regularization methods do not penalize edges (discontinuous transitions) in the model whereas L_2 norm based constraint regularization methods such as Tikhonov regularization tend to broaden peaks in the solution. In order to recover edges more accurately, both L_2 and L_1 norm constraints are imposed into the formulation of inverse problem as in 3.22.

Activation wavefronts are characterized by a large spatial gradient separating the depolarized and the repolarized tissue on the epicardium. An activation wavefront is formally similar to an edge on an image. The TV norm is essentially an L1 norm of the gradient of the image and has the property that it suppresses small oscillations and spikes but allows or even encourages edges. Unlike the L_2 norm based methods, TV norm based methods are non-linear and therefore are computationally complex.

In the admissible solution approach that is studied in this thesis, both L_2 and L_1 norm based constraints are simultaneously used to regularize the solution. Formulation of this method is as follows:

$$m_k = \underset{argm_k}{min} \left\{ \|d_k - Gm_k\|_2^2 + \lambda_1 \|m_k\|_2^2 + \lambda_1 \|m_k\|_2^2 + \lambda_2 \|G_\theta m_k\|_1^2 + \lambda_3 \left\|G_\phi m_k\right\|_1^2 \right\} \tag{3.22}$$

The first two terms in Equation 3.22 contain $L2$ norm and other two contain $L1$ norm. $L2$ norms are similar to the norms in the Tikhonov regularization method. However,$L1$ norms include potential gradients depending on topology and position of nodes.

3.2.5.1 Spatial Gradient Estimation

Due to non-uniform spatial sampling and the highly irregular geometry of the heart, gradient estimation on its surface is non-trivial.

The method for gradient estimation is based on a triangulated geometric representation of the epicardial surface. Consider a node on the heart surface, p_0, and let f(x, y) denote the value of the potentials at p_0 where (x, y) denotes the position of p_0 on the surface in some local coordinate system. The Taylor series expansion yields:

$$f(x+h,y) = f(x,y) + h\frac{\partial f}{\partial x}|_{p_0} + \frac{1}{2}h^2\frac{\partial^2 f}{\partial x^2}|_{p_0} + \dots \tag{3.23}$$

Similarly,

$$f(x,y+h) = f(x,y) + h\frac{\partial f}{\partial x}|_{p_0} + \frac{1}{2}h^2\frac{\partial^2 f}{\partial x^2}|_{p_0} + \dots \tag{3.24}$$

Therefore, the gradient at p_0 along the x coordinate may be approximated as

$$\frac{\partial f}{\partial x} = \frac{f(x+h,y) - f(x-h,y)}{2h} \tag{3.25}$$

Similarly, the gradient at p_0 along the y coordinate may be approximated as

$$\frac{\partial f}{\partial x} = \frac{f(x,y+h) - f(x,y-h)}{2h} \tag{3.26}$$

Equations 3.25 and 3.26 are known as central difference equations. On a regular geometry gradient matrices can be estimated easily using these central difference equations. However, heart has an irregular geometry and nodes are non-uniformly distributed over the surface of heart. Therefore following procedure followed in order to estimate gradient matrices:

1) Select a central node

2) Find the first order neighbors of central node p_o.

3) Determine surface that passes through central node po and best fits to its first order neighbors

4) Project the coordinates of the first order neighbors onto the best fit surface

5) Change the coordinate system so that all the points on the plane are now represented with two dimensions instead of three and projection of central node is at the origin.

6) Get distance of projections of neighboring nodes from origin and calculate average distance from origin.

7) Linearly interpolate/extrapolate all potentials to average distance (onto a circle)

8) Determine the two closest points to x+ axis from both sides of x+ axis; similarly determine the two closest points to x- axis, y+ axis and y- axis.

9) Find the potential on x+ axis by averaging the potential of closest points to x+ axis. Then find the potential on to x- axis, y+ axis and y- axis using similar method.

10) Find the gradients using Equation 3.25 and Equation 3.26.

Repeat the same procedure 1-10 for each node by changing central node.

Gradient matrices $G_\theta$and G_ϕ are obtained by using the procedure above.

3.2.5.2 Implementation of Admissible Solution Method

In order to solve the minimization problem in 3.22 is reformulated as convex optimization problem:

$$\begin{aligned} \min_{argm_k} \quad & \|d_k - Gm_k\|_2^2 \\ \text{subject to} \quad & \|m_k\|_2^2 \leq \epsilon_1 \\ & \|G_\theta m_k\|_1^2 \leq \epsilon_2 \\ & \left\|G_\phi m_k\right\|_1^2 \leq \epsilon_3 \end{aligned} \tag{3.27}$$

Actually, equation 3.22 is a Lagrange dual problem of the convex optimization problem in 3.27. In other words, equation 3.22 is a weighted sum of the objective and constraint functions

in 3.27. For each weighting factors λ_i in 3.22, there is a corresponding constant value of bound parameter ϵ_i that makes the problems 3.22 and 3.27 equivalent.

The problem in 3.27 is solved by using the CVX toolbox. CVX is a Matlab-based modeling system for disciplined convex optimization. In order to solve the problem in 3.27 constraint parameter values ϵ_1, ϵ_2 and ϵ_3 are need to determine. The problem is solved using different constraint parameters that are obtained from Tikhonov solution and real epicardial potential distributions. The details about the reconstructed solutions by different constraint parameters are represented in section 4.4.

3.3 Minimum Relative Entropy Method in the Solution of Inverse ECG Problem

The minimum entropy method is a useful method in solution of the problem of linear inverse problems [67]. These Inverse problems have a form $\mathbf{d} = \mathbf{Gm}$ where $\mathbf{m}$ is a vector of unknown model parameters, $\mathbf{d}$ is a vector of measurements and $\mathbf{G}$ is the forward transfer matrix. MRE method is a method of statistical inference that treats the elements of m as random variables and obtains the solution as mean value of posterior distribution using the prior information and measurements. The prior information, which is used in this thesis, contains the lower and upper limits of $\mathbf{m}$ and a prior expected value of $\mathbf{m}$.

3.3.1 Motivation

In literature, there are some statistical methods -such as Bayesian MAP Estimation [20] that use prior information in order to solve inverse ECG problem. The truth of the posterior distribution, obtained through this method, is highly dependent on the prior distribution. If the prior distribution is close to the actual data then the results are good. Otherwise, the posterior distribution may be irrelevant to the actual model parameters. In addition, detailed prior information is necessary in order to get a good result. The regularization methods such as truncated singular value decomposition and Tikhonov regularization are also used in solution of inverse ECG problem. Prior information about the model parameters is not necessary for these methods. However, the results of these methods may have limited relevance to the real model parameters.

The minimum relative entropy method is a useful tool to find a posterior distribution when there is a prior distribution and constraints on the random variable obtained from the measurements. It gives the optimal solution to the information available. Therefore, it can be used to obtain good results with robust prior information of model parameters. In this thesis, MRE method is studied in order to get better results with limited prior information.

3.3.2 Overview of MRE Method

In this method, linear inverse ECG problem is formulated in the the form $\mathbf{d} = \mathbf{Gm}$, where $\mathbf{m}$ is a vector of unknown model parameters (epicardial potentials), $\mathbf{d}$ is a vector of measurements (torso potentials) and $\mathbf{G}$ is the forward transfer matrix. The model parameters (epicardial potentials) $\mathbf{m}$ are handled as random variable and the solution is obtained as mean value of distribution using the prior information about epicardial potentials. The prior information used in this thesis involves the upper and lower limits of $\mathbf{m}$ and the average value of $\mathbf{m}$. A posterior distribution (solution) for $\mathbf{m}$ is obtained by using this prior information and measurements of torso potentials $\mathbf{d}$.

Method consists of two steps. In the first step, a prior distribution is generated by maximization of entropy subject to prior information i.e. the lower and upper bounds of $\mathbf{m}$ and expected value of $\mathbf{m}$. In the second step, a posterior distribution (solution) for m is obtained by minimizing entropy relative to prior distribution and subject to imposed constraints by measurements. The details of these stages are represented in the latter parts of this chapter.

3.3.3 Generating Prior Distribution - Maximum Entropy Method

In the first step of this method, a prior distribution is produced whose entropy is maximized subject to the forced constraints. These constraints are the lower and upper bounds of model parameters m and expected value of $\mathbf{m}$.

In inverse ECG problem, model parameters are assumed to have independent elements. Therefore, $p(\mathbf{m}) = \prod_{i=1}^{M} p(m_i)$ where M is the number of model parameters. We have also assumed that lower bound for each element is zero. For non-zero lower bounds, this is done by a change of random variable. Then the formulation of maximization of entropy step is as given:

$$
\begin{aligned}
\text{maximize} \quad & H(p) = \int p(\mathbf{m}) ln\left[1/p(\mathbf{m})\right] d\mathbf{m} \\
\text{subject to} \quad & \int p(\mathbf{m}) d\mathbf{m} = 1 \\
& \int p(\mathbf{m}) m_i d\mathbf{m} = s_i \\
& 0 \leq m_i \leq U_i
\end{aligned}
\tag{3.28}
$$

where s_i is the mean of parameter i and U_i is the upper bound of parameter i.

It is shown by Woodbury [59] that the maximum entropy distribution is a multivariable truncated exponential distribution for independent continuous random variables with a zero lower bounds, upper bounds U_i and means s_i. This prior distribution is

$$
\begin{aligned}
p(m_i) &= \frac{\beta_i exp(-\beta_i m_i)}{1 - exp(-\beta_i U_i)}, \text{ for } \beta_i \neq 0 \\
p(m_i) &= \frac{1}{U_i}, \text{ for } \beta_i = 0 \\
p(\mathbf{m}) &= \prod_{i=1}^{M} p(m_i)
\end{aligned}
\tag{3.29}
$$

where β_i is a Lagrange multiplier whose value is determined by

$$
\frac{-(\beta_i U_i + 1) exp(-\beta_i U_i) + 1}{\beta_i \left[1 - exp(-\beta_i U_i)\right]} = s_i \tag{3.30}
$$

3.3.4 Estimation of the Posterior Distribution - MRE Method

In the second step of this method, aim is to obtain a posterior distribution that is an estimate of the true distribution. This is achieved by minimizing the entropy of the posterior distribution, $q(\mathbf{m})$, relative to the prior distribution, $p(\mathbf{m})$, subject to the measurements. In the minimization of entropy of the posterior distribution, $q(\mathbf{m})$, we have two constraints: the normalization constraint $\int q(\mathbf{m}) d\mathbf{m} = 1$, and the requirement of the mean of the posterior distribution fit the measured data $\overline{\mathbf{d}} = \mathbf{G}\hat{\mathbf{m}}$ where $\overline{\mathbf{d}}$ is the measured data and $\hat{\mathbf{m}}$ is the mean of the posterior distribution. Formulation of this minimization as follows:

$$\begin{aligned} \text{minimize} \quad & H(q,p) = \int q(\mathbf{m}) ln\left[q(\mathbf{m})/p(\mathbf{m})\right] d\mathbf{m} \\ \text{subject to} \quad & \int q(\mathbf{m}) d\mathbf{m} = 1 \\ & \overline{d}_j = \int_{\mathbf{m}} q(\mathbf{m}) \sum_{i=1}^{M} g_{ji} m_i d\mathbf{m} \end{aligned} \tag{3.31}$$

where $\overline{d}_j$ is the j^{th} measured data point, g_{ji} is the j, i^{th} element of the G matrix and m_i is the i^{th} model parameter for $j = 1, 2, 3, \ldots, N$ and $i = 1, 2, 3, \ldots, M$.

The first constraint in minimization is a normalization factor while the second one is the measured data. Measured data constraint enables model to agree with the measurement. This optimization problem can be rewritten by the method of Lagrange multiplier by minimizing:

$$\phi = H(q,p) + \mu\left[\int q(\mathbf{m}) d\mathbf{m} - 1\right] + \sum_{j=1}^{N} \lambda_j \left[\int_m q(\mathbf{m}) \sum_{i=1}^{M} g_{ji} m_i d\mathbf{m} - \overline{d}_j\right] \tag{3.32}$$

where μ and λ are Lagrange Multipliers.

Minimizing variation in ϕ with respect to $q(m)$ yields [59, 71]:

$$0 = ln\left[q(\mathbf{m})/p(\mathbf{m})\right] + 1 + \mu + \sum_{j=1}^{N} \lambda_j \left[\sum_{i=1}^{M} g_{ji} m_i\right] \tag{3.33}$$

This equation results in following expression:

$$q(\mathbf{m}) = cp(\mathbf{m}) exp\left(-\sum_{j=1}^{N}\left[\lambda_j \sum_{i=1}^{M} g_{ji} m_i\right]\right) \tag{3.34}$$

where $c = exp(-1-\mu)$. Then, the resulting posterior distribution takes the form

$$\begin{aligned} q(m_i) &= \frac{\alpha_i exp(-\alpha_i m_i)}{1 - exp(-\alpha_i U_i)}, \text{ for } \alpha_i \neq 0 \\ q(m_i) &= \frac{1}{U_i}, \text{ for } \alpha_i = 0 \\ q(\mathbf{m}) &= \prod_{i=1}^{M} q(m_i) \end{aligned} \tag{3.35}$$

where $\alpha_i = \beta_i + \sum_{i=1}^{N} \lambda_j g_{ji}$.

Finally, solution of problem is obtained by calculating the mean of posterior distribution and it is:

$$\begin{aligned} \hat{m}_i &= \frac{1-(\alpha_i U_i+1)exp(-\alpha_i U_i)}{\alpha_i\left[1-exp(-\alpha_i U_i)\right]} \text{ for } \alpha_i \neq 0 \\ \hat{m}_i &= \frac{U_i}{2} \text{ for } \alpha_i = 0 \end{aligned} \tag{3.36}$$

The Lagrange multipliers μ and λ_j's are calculated using the the two constraints: normalization and measurements. λ_j's are estimated from the following equation satisfying the measurement constraint:

$$\overline{d}_j = \sum_{i=1}^{M} g_{ji}\hat{m}_i(\lambda) \tag{3.37}$$

where $\hat{m}_i$ is the expected value of the reconstructed model parameter m_i and it is a is function the Lagrange multipliers $\lambda = [\lambda_1, \lambda_2, ...\lambda_j]^T$.

However, 3.37 may cause a over-fitting in model parameters or it may be non-existing due to the invisible set in problem formulation. In order to avoid the over-fitting and to account for measurement and model errors, the measurement contraint in 3.31 is replaced the the following constraint:

$$\left\|\overline{\mathbf{d}} - \mathbf{G}\hat{\mathbf{m}}\right\|_2^2 \leq \epsilon^2 \tag{3.38}$$

The inequality in 3.38 yields the reconstructed solution to fit the measurement data within a specified tolerance. The inequality in 3.38 can be rewritten in the following form:

$$\sum_{j=1}^{N}\left[\overline{d}_j - \sum_{i=1}^{M} g_{ji}\hat{m}_i(\lambda)\right]^2 \leq \epsilon^2 \tag{3.39}$$

The data constraint in 3.39 when λ statisfies the following nonlinear equation:

$$d_j - \sum_{i=1}^{M} g_{ji}\hat{m}_i(\lambda) + \epsilon\frac{\lambda_j}{||\lambda||} = 0 \tag{3.40}$$

The details for estimation of the Lagrange multipliers are shown in the following section.

3.3.5 Implementation of MRE Method

The MRE method that is represented above is implemented in MATLAB. In this section, several numerical issues in implementation and the details of the estimation of Lagrange multipliers in equation 3.40 will be represented in this section.

3.3.5.1 Estimation of Prior Distribution

The equations given in section 3.3.3 for the estimation of the prior distribution using maximum entropy method assume the lower bound of the model parameter as zero. For non-zero lower bounds, the problem is reformulated by change of variable. For this purpose, $m = m_L + l$ where m is the true solution, m_L is the corresponding model solution for a zero lower bound and l is the vector of the lower bound of the true solution. Similiarly, measurement data d is modified as $d_L = d - Gl$ for using in problem. The upper bounds and the expected values are also replaced by $U_i - l_i$ and $s_i - l_i$ respectively.

The equations for the estimation of the prior distribution are given in 3.29 in terms of the Lagrange multipliers, β_i. In order to find a prior distribution, first we need to determine the values of the Lagrange multipliers, β_i individually using the equation 3.30. The Lagrange multipliers are estimated from the equation 3.30 using the bisection method which is a robust method in finding the root of an equation. The method repeatedly bisects an interval then selects a subinterval in which a root must lie for further processing.

3.3.5.2 Estimation of Posterior Distribution

The posterior distribution can be estimated using the equations in 3.35. However, we need to determine the values of the Lagrange multipliers, λ_j's, which are used in calculation of the values $\alpha_i = \beta_i + \sum_{i=1}^{N} \lambda_j g_{ji}$. The values of the Lagrange multipliers, λ_j, are calculated using the Newton-Raphson method to solve the equation 3.40. We define :

$$F(\lambda)_j = d_j - \sum_{i=1}^{M} g_{ji}\hat{m}_i(\lambda) + \epsilon\frac{\lambda_j}{||\lambda||} \tag{3.41}$$

Then, we use Newton-Raphson method to solve for the zeroes of $F(\lambda)_j$ iteratively using

$$\lambda^k = \lambda^{k-1} - \left(\frac{\partial F}{\partial \lambda}|_{\lambda^{k-1}}\right)^{-1} F^{k-1} \tag{3.42}$$

where the superscripts k denote the iteration number. The terms of the Jacobian matrix, $\partial F/\partial\lambda$, are

$$\frac{\partial F_j}{\partial \lambda_l} = -\sum_{i=1}^{M} g_{ji}\left[\frac{\partial \hat{m}_i}{\partial \alpha_i} g_{li}\right] + \frac{\epsilon}{||\lambda||}\left[\delta_{jl} - \frac{\lambda_j\lambda_l}{||\lambda||^2}\right] \tag{3.43}$$

where l=1,2....N δ_{jl} is the Kronecker delta and

$$\frac{\hat{m}_i}{\partial \alpha_i} = \frac{\alpha_i^2 U_i^2 exp(-\alpha_i U_i) - \left[1 - exp(-\alpha_i U_i)\right]^2}{\alpha_i^2 \left[1 - exp(-\alpha_i U_i)\right]^2} \tag{3.44}$$

The iterations are carried out until $||F|| / (1 + ||d||)$ is less than a reasonable tolerance or iteration number reaches to user-defined the maximum iteration number. we need to make several asymptotic approximations to solve these equations numerically.

CHAPTER 4

RESULTS AND DISCUSSION

In this chapter, first we explain the simulation data that is used for solving inverse problem. In the later subsections, the reconstruction results of inverse problem of electrocardiography for different methods are given.

4.1 Experimental Data and Validation Of Methods

As mentioned in previous sections, inverse ECG problem is the estimation of cardiac sources using the body surface measurements and the volume conductor model. In this thesis, epicardial potentials are used the equivalent cardiac source. Therefore, our aim in this study is estimating the epicardial potentials using body surface potentials and forward transfer matrix. Therefore, in order to solve the inverse problem, we need the body surface potentials and the forward transfer matrix.

The forward transfer matrix describing the relation between the epicardial potentials and the body surface potentials is estimated by boundary element method [13, 45] using conductivity values in the torso model. The torso model contains thorax volume and the lungs i.e. thorax volume and the lungs have different conductivities.

The body surface potentials used in reconstruction of the epicardial potentials are simulated using the true epicardial potentials instead of taking the measurements from a body surface. In other words, the body surface measurements are estimated from the true epicardial potentials by solving forward electrocardiography problem. First, the epicardial potential measurements are multiplied by the forward transfer matrix estimated using torso geometry and a torso noise is added to the product. The obtained results from this process are used as body surface

measurements. Finally, the simulated body surface potentials are used in inverse problem in order to reconstruct the epicardial potentials.

The true epicardial potentials used in simulation of the body surface potentials and in validation of reconstructed solution of the inverse problem were measured from an isolated dog heart. The measurements were taken by a team at University of Utah Nora Eccles Harrison Cardiovascular Research and Training Institute (CVRTI) [72, 73]. The isolated dog heart was perfused by from a second dog's circulatory system and suspended in an electrolytic tank that had an adolescence thorax shape. The epicardial potentials were recorded from 490 points with 1 kHz sample rate using a nylon sock electrode with silver wires slipped over the ventricles. The forward transfer matrix relates these 490 points with 771 points on body surface.

In order to compare the reconstructed solutions from the inverse problem using different methods and the true epicardial potentials recorded from a dog heart, we have used correlation coefficient (CC) and relative difference measurement star (RDMS) values. The higher CC and the lower RDMS values are correspond to more accurate solutions. In addition to these quantitative values, we have also compared the reconstructed epicardial potentials with the true ones by plotting 3D potential maps. For this purpose, map3d software [74] prepared in CVRTI was used.

4.2 Reconstruction of Solution By Conic Quadratic Programming

As mentioned in the methods section, Conic Quadratic Programming is an alternative technique for regularizing and solving the inverse problem instead of using Tikhonov Regularization. The formulation of Tikhonov Regularization that is represented in equation 4.1 and the formulation in equation 4.2 are equivalent. For each value of the penalty parameter δ in Equation 4.1, there exists a corresponding bound parameter in equation 4.2 that gives the same solution. The value of the parameter δ can be chosen by several methods such as "composite residual and smoothing operator" (CRESO) and L-curve method [2]. In this thesis L-curve method is used to find the optimum penalty parameter. L-curve is a log scale plot that is obtained by putting each of the two norms in equation 4.1 onto one axis and plotting them in log scale. In this method, the corner of the L shaped curve enables both of these norms to attain low values simultaneously. Therefore, the value of the penalty parameter is selected at the

corner of L-curve. By this way, L-curve method enables to select a penalty parameter without any prior information. However, if we have prior information about the bound parameter such as the knowledge of the bound for the total energy of the solution, it may be useful to formulate the regularization problem as in equation 4.2. The equation 4.1 can be solved using Conic Quadratic Programming technique.

$$\min_{m} ||Gm - d||_2^2 + \delta^2 ||Rm||_2^2 \tag{4.1}$$

$$\begin{aligned} \underset{arg\ m}{\text{minimize}} \quad & ||Gm - d||_2^2 \\ \text{subject to} \quad & ||Rm||_2^2 \leq M \end{aligned} \tag{4.2}$$

In the following subsections, Conic Quadratic Programming will be tested for solving 4 different cases of the inverse ECG problem and performance of method will be compared with Tikhonov Regularization. In two cases, only Gaussian white noise is added to measurements at two different levels (30 dB and 10 dB). In other two cases, the effects of geometric errors due to the shift in heart location and error in cardiac size will be investigated.

4.2.1 Conic Quadratic Programming Results of 30 dB Gaussian White Noise Added Measurements

In the first scenario of the test of Conic Quadratic Programming method, Gaussian white noise with 30 dB SNR is added to the body surface measurements that are simulated from the real epicardial potentials. Then, the noisy data is used for the solution of inverse problem. In Conic Quadratic Programming method, we need a priori information about the Euclidean (L_2) norm of the solution (epicardial potentials). This prior is included in equation 4.2 as a constraint that bounds the total energy of the solution. Thus, we need to obtain the total energy of the solution. For this purpose, we have used the optimal Tikhonov solution since the inverse problem can be solved without any prior by Tikhonov Regularization. In other words, the prior about the total energy of the solution can be obtained by means of Tikhonov results.

For that purpose, we have compared the Euclidean norm of the real epicardial potentials with the Euclidean norm of the optimal Tikhonov solutions at the first stage. It is observed that the

total energy of the optimal Tikhonov solution is always less than the total energy of the real epicardial potentials at the each time instant of the QRS interval for 30 dB noisy data as shown in Figure 4.1.According to this plot, it is possible to obtain the norms that are much closer to the norm of real epicardial potentials than the case in the Tikhonov solution by multiplying the norm of Tikhonov solution by a scaling factor. Therefore, the norms of optimal Tikhonov solution is multiplied by a scaling factor and the resultant norms can be used as prior for Conic Quadratic Programming. If we use the norm of the Tikhonov Solution without multiplying by a scaling factor as prior, we will obtain the same solution with Tikhonov Solution since Tikhonov Regularization and Conic Quadratic Programming are identically formulated. The average CC and RDMS values in a QRS interval for different norms that are obtained by multiplying the norm of Tikhonov solution are given in 4.1.

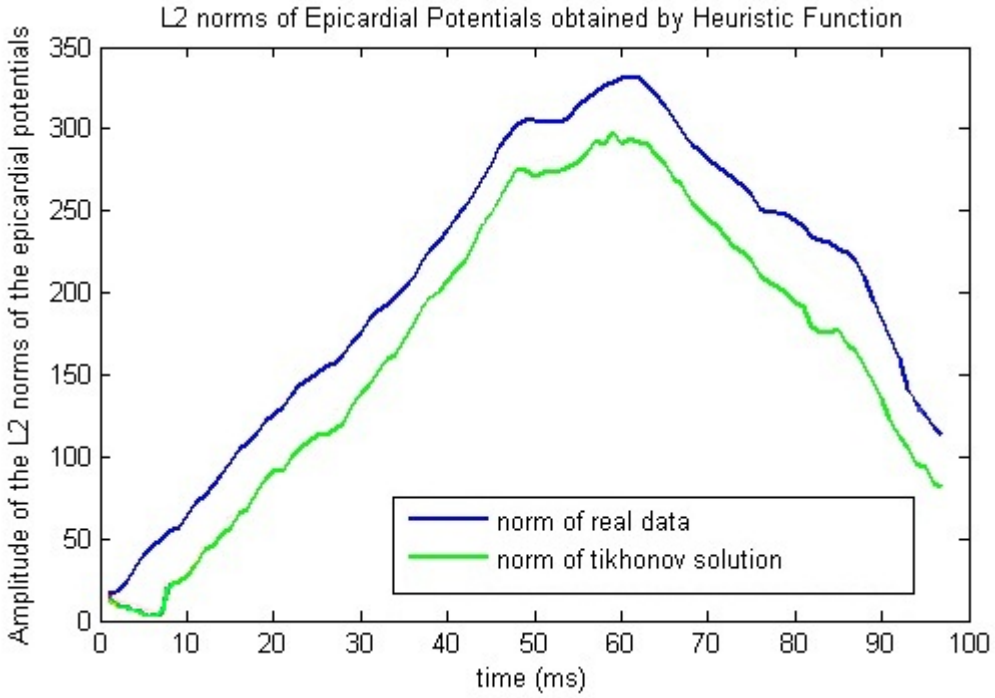

Figure 4.1: L_2 Norms of Epicardial Potential For Real Data and Tikhonov Solution

As given in Table 4.1, the best solution is obtained when scaling factor is equal to 1.0. This is the case where the Conic Quadratic programming yields a solution identical to optimal Tikhonov solution. When scaling factor is less than 1, the epicardial potential solutions have worse CC and RDMS values than the values in the optimal Tikhonov solution case. These results are expected by looking into the norms that are shown in Figure 4.1. By Figure 4.1, it is also expected that better solutions can be obtained when scaling factor is 1.1 and 1.2 since

Table 4.1: Averages and standard deviations of CC and RDMS values for different norms that are obtained by multiplying the norm of Tikhonov solution with different scaling factors

Scaling Factor	Average CC ± std	Average RDMS ± std
0.8	0.6952±0.1999	0.7101±0.1734
0.9	0.7288±0.1979	0.6635±0.1873
1.0	0.7698±0.1958	0.6039±0.2060
1.1	0.7621±0.1730	0.6269±0.1777
1.2	0.7241±0.1544	0.6889±0.1482
1.3	0.6824±0.1403	0.7984±0.1271
1.4	0.6426±0.1288	0.8018±0.1109

the norms at these scales are much more similar to the norm of real epicardial potentials. However, the results are different from the expected ones as shown in Table 4.1.

Figure 4.2 shows the CC and RDMS plots of these results for different time instants in the QRS interval. These plots show that scaling the norm of optimal Tikhonov solution with a scalar greater than 1 leads to better the solution at $[0-25]$ ms interval and $[75-97]$ ms interval. One common property of these intervals is that the norm of epicardial potentials in these intervals is lower than the half of the maximum norm in the whole QRS interval. Thus, this result leads us to the idea of scaling the lower norms by greater scales and higher norms by lower scales. In order to do this, we have established a heuristic function that depends on the norm of the optimal Tikhonov solution at that time instant and the maximum norm of real epicardial potential over the whole QRS interval. This heuristic function is used to determine the bound for the L_2- norm (Euclidian norm) of solution. This heuristic function is:

$$f_h(\left\|m_{opt}\right\|) = \begin{cases} \frac{6maxnorm-\left\|m_{opt}\right\|_2}{5maxnorm}\left\|m_{opt}\right\|_2 & \text{if} \quad \left\|m_{opt}\right\|_2 < 3maxnorm \\ \frac{9maxnorm}{5} & otherwise \end{cases} \tag{4.3}$$

where maxnorm is the maximum value of the L_2- norm of real epicardial potentials $\left\|m_{opt}\right\|_2$ is the L_2-norm of optimal Tikhonov solution.

The maximum value of the L_2-norm of real epicardial potentials in a QRS interval is 331 for the data used in this study. Therefore, this value is taken as 350 for the estimation of the heuristic function in Equation 4.3. The characteristic of this heuristic function with respect to

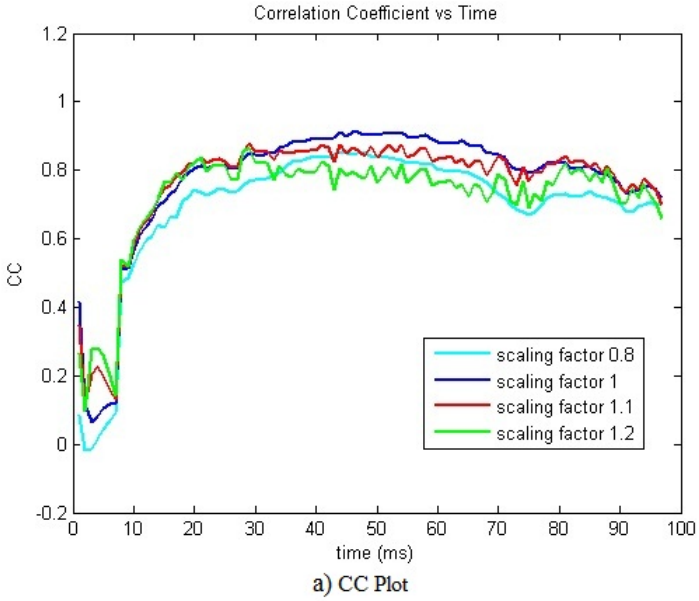

a) CC Plot

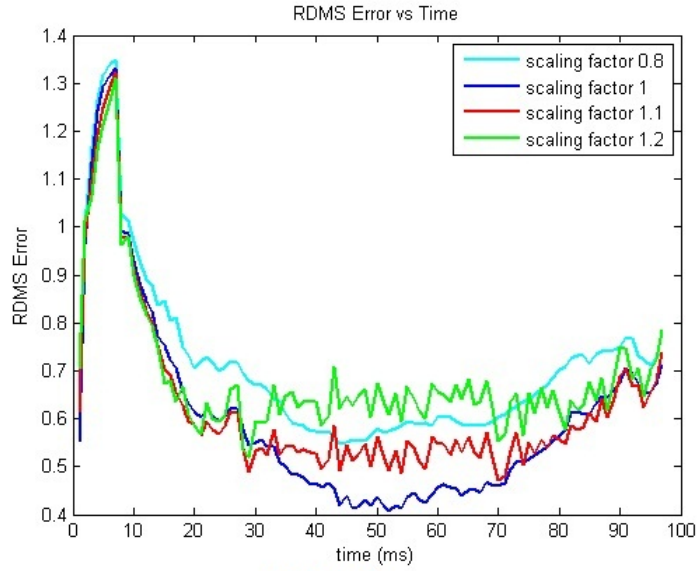

b) RDMS Plot

Figure 4.2: The CC and RDMS values of different norm bounds

the norm of optimal Tikhonov solution is shown in 4.3 for the maximum norm real epicardial norm taken as 350.

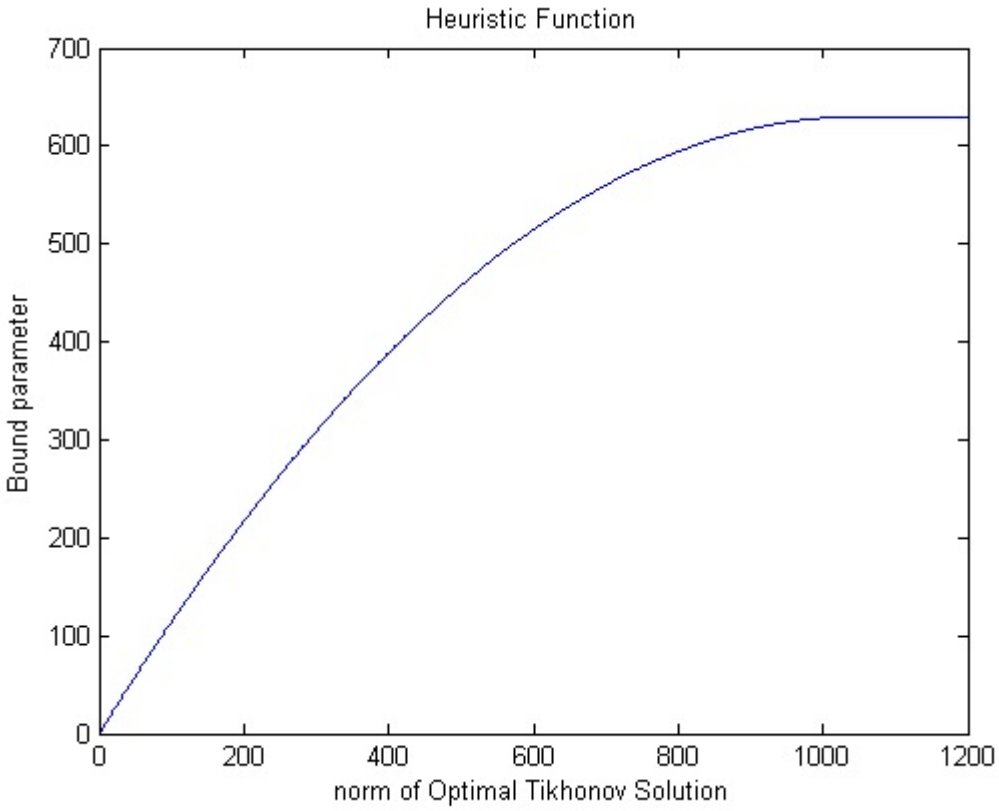

Figure 4.3: The characteristic of the heuristic function that is used for determining the upper bound of L2-norm of solution

This heuristic function enables to generate the prior information that will be used as the total energy of the solution in Conic Quadratic Programming method. The new L2-norm bound obtained by this function, the L2-norms of the real epicardial potentials and optimal Tikhonov solution epicardial potentials are shown in Figure 4.4. As seen in this figure, the new norms built by heuristic function are much more similar to the norm of real epicardial potentials. The average CC and RDMS values of the results that are reconstructed by putting these norm values into Conic Quadratic Programming method as constrain is given in Table 4.2. The CC plot of these results in a QRS interval is also shown in 4.5. As seen in Figure 4.5, the heuristic function leads to a small improvement at the beginning of the stimulus in a QRS interval.

Epicardial maps estimated from these methods and real epicardial map are shown in Figure

Table 4.2: Averages and standard deviations of CC and RDMS values for optimal Tikhonov solution and solution using heuristic function

Method	Average CC ± std	Average RDMS ± std
Tikhonov	0.7698±0.1958	0.6039±0.2060
Heuristic	0.7753±0.1742	0.6054±0.1881

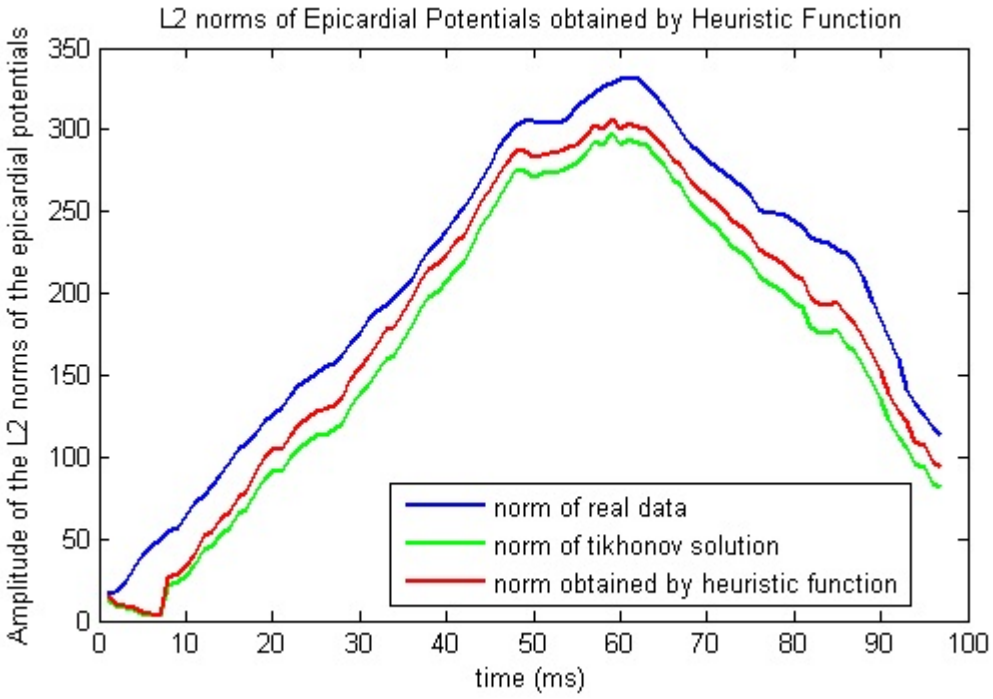

Figure 4.4: The L2- Norms for 30 dB noisy data

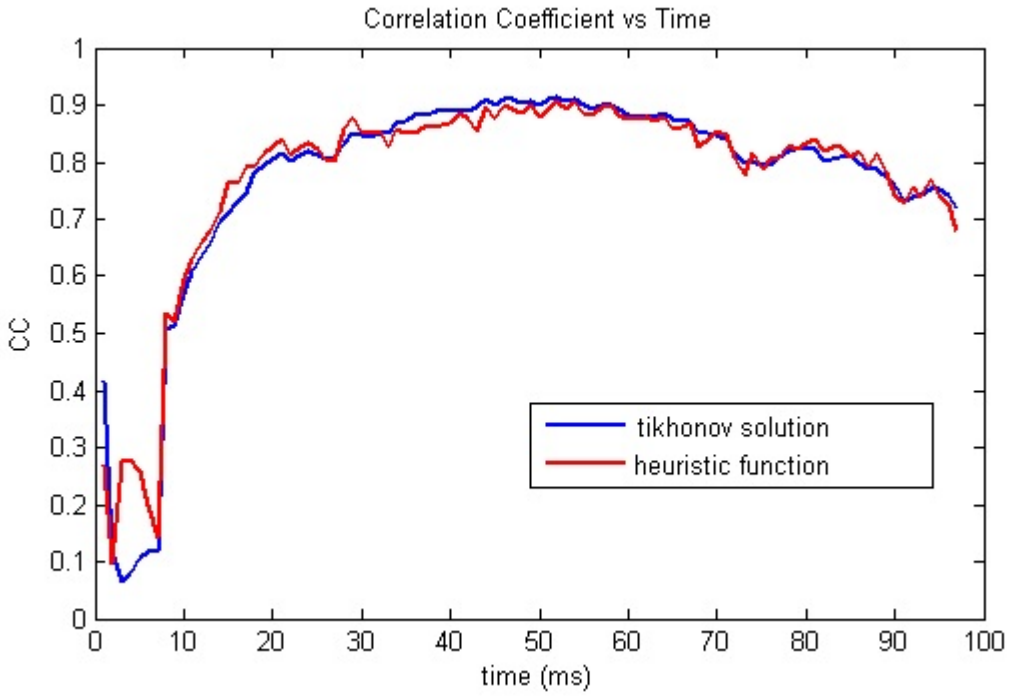

Figure 4.5: The CCvalue for optimal Tikhonov solution and solution using heuristic function

4.6. As seen from this figure and Figure 4.5, heuristic function provides a solution very similar to optimal Tikhonov solution, but it slightly improves the reconstructed solution at some time instants in QRS interval.

4.2.2 Conic Quadratic Programming Results of 10 dB Gaussian White Noise Added Measurements

In this section, we have tested the Conic Quadratic Programming method with 10 dB noisy measurement data. Similar to the previous section, Euclidean norms of the real epicardial potentials and optimal Tikhonov solutions and the bound values that are obtained using heuristic function is plotted in Figure 4.7 for comparison. It is observed that the total energy of the optimal Tikhonov solution is always less than the total energy of the real epicardial potentials. It is also clear that the heuristic function generates the norms which are much similar to the norms of the real epicardial potentials at the each time instant of the QRS interval.

The average CC and RDMS values of the results that are reconstructed by using different bound constraints are given in Table 4.3. The CC plot of these results in a QRS interval is

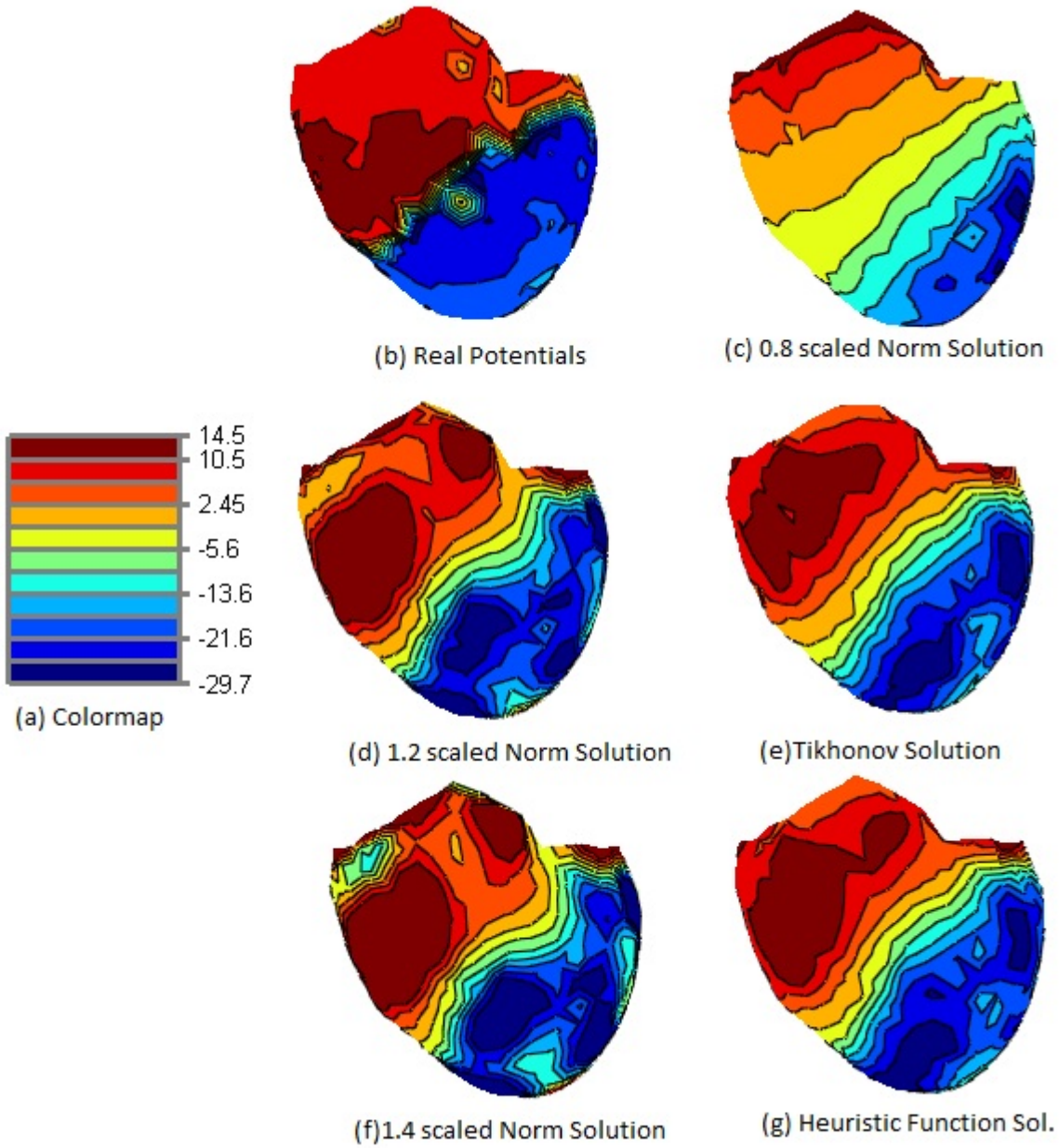

Figure 4.6: Epicardial Maps of Solution at 61 ms after stimulus for 30dB Noisy Data

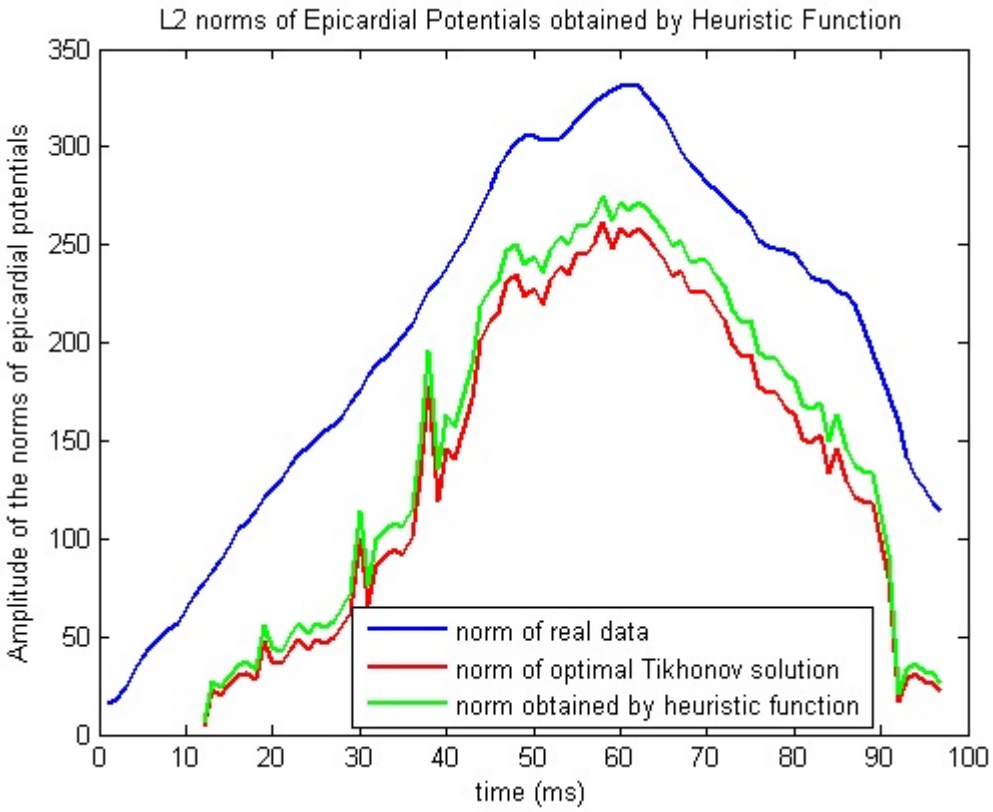

Figure 4.7: The Euclidean Norms for 10 dB noisy data

also shown in Figure 4.8. As seen in this figure, heuristic function enables us to generate better solutions interms of the CC measure almost during the whole QRS interval. It is also observed that the heuristic function leads to better improvement compared to the Tikhonov solution in 10 dB noisy case than in the 30 dB case.

Table 4.3: Averages and standard deviations of CC and RDMS values of different test methods for 10 dB Noisy Data

Method	Average CC ± std	Average RDMS ± std
0.8 scale	0.5349 ± 0.2978	0.8719 ± 0.2475
0.9 scale	0.5563 ± 0.2968	0.8457 ± 0.2552
1 scale (Tikhonov)	0.5796 ± 0.2899	0.8196 ± 0.2621
1.1 scale	0.5958 ± 0.2721	0.8039 ± 0.2601
1.2 scale	0.5995 ± 0.2505	0.8123 ± 0.2403
1.3 scale	0.5885 ± 0.235	0.8323 ± 0.2193
1.4 scale	0.574 ± 0.2214	0.8545 ± 0.2002
Heuristic	0.6123 ± 0.2599	0.7946 ± 0.2553

In Figure 4.9, the epicardial maps that are estimated for the 44 milliseconds after the stimulus is shown. In 10 dB noisy case, the heuristic function yields a more significant improvement on Tikhonov solution than in the 30 dB noisy case. It can be also observed that smaller norms lead to smoother solutions whereas higher norms lead to oscillating results.

4.2.3 Conic Quadratic Programming Results of 30 dB Gaussian White Noise Added Measurements with 0.6 Scale Geometric Error

In this subsection, the inverse problem having 30 dB Gaussian white noise added measurements has been solved using the transfer matrix calculated by wrong estimation of heart's size. This geometric error has been created by adjusting the heart's size with a scalar of 0.6. We have generated and solved this problem in order to investigate the performance of Conic Quadratic Programming in geometric error.

We have first generated the measurement data (torso potentials) using real epicardial potentials and true transfer matrix. Then we have added a 30 dB Gaussian noise to these results. Finally, this inverse problem was solved by Conic Quadratic Programming method using the transfer matrix calculated by wrong estimation of heart's size. Similar to the previous subsections, different bound values were used as the norm constraint in Equation 4.2 .

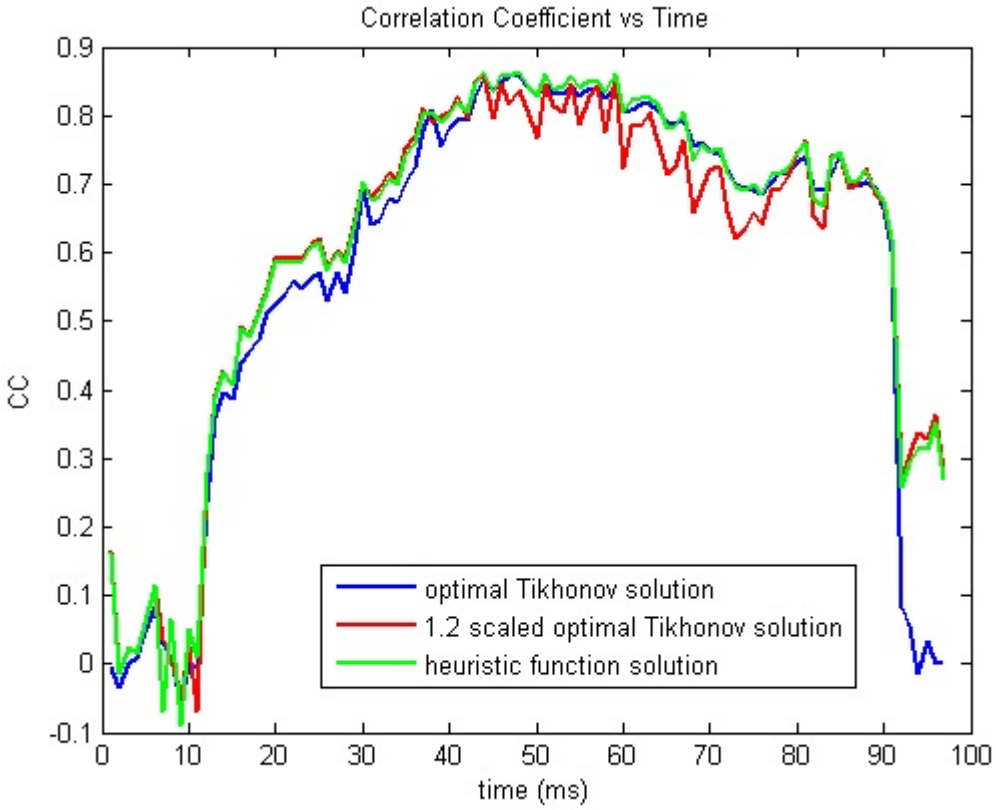

Figure 4.8: The CC values of different methods in a QRS interval

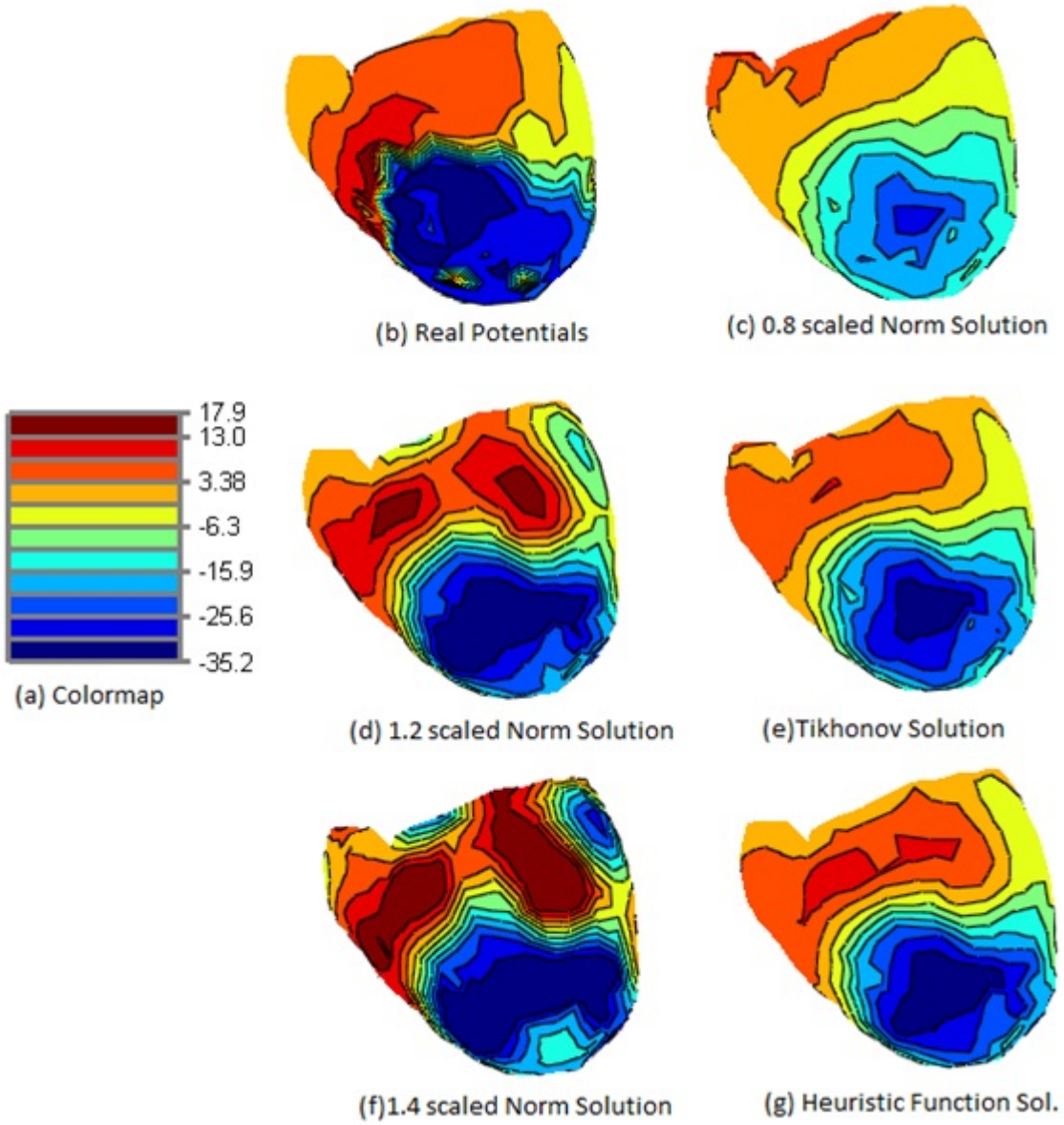

Figure 4.9: Epicardial Maps of solutions at 44 ms after stimulus for 10 dB Noisy Data

In Figure 4.10, the norms of the real epicardial potentials and optimal Tikhonov solutions and the bound values that are obtained using heuristic function are shown. Here, the norm of optimal Tikhonov solution is much greater than the the real epicardial potential norms which differs from the previous cases where the problem do not have the geometric errors. The norm values that are generated by heuristic function are also much similar to the norms real epicardial potentials for this inverse problem. However, the norm generated by heuristic function has the shape of the norm of optimal Tikhonov solution.

We have solved this inverse problem having 30 dB measurement error and geometric error originated from the wrong estimation of cardiac size using different bounds for L_2-norms. The results of Conic Quadratic Programming using different bounds of the norm are shown in Table 4.4. Average CC and RDMS values in this table indicate that the best result is estimated by the bound values generated by heuristic function. The heuristic function provides significant improvements in CC and RDMS values. The CC values over a QRS interval are also shown in Figure 4.11. As seen from this figure, the conic quadratic programming that has constraint bounds from heuristic function yields the best CC values nearly whole interval.

Table 4.4: Averages and standard deviations of CC and RDMS values of different test methods for 30 dB Noisy Data with 0.6 Scale Geometric Error

Method	Average CC ± std	Average RDMS ± std
0.8 scale	0.5741 ± 0.2628	0.822 ± 0.2475
0.9 scale	0.5751 ± 0.3218	0.8305 ± 0.2516
1 scale (Tikhonov)	0.5895 ± 0.2915	0.8316 ± 0.2421
1.1 scale	0.609 ± 0.2495	0.8327 ± 0.2276
1.2 scale	0.6126 ± 0.2247	0.8413 ± 0.2112
1.3 scale	0.6072 ± 0.2075	0.8547 ± 0.1952
1.4 scale	0.5968 ± 0.1941	0.8711 ± 0.1802
Heuristic	0.6307 ± 0.2356	0.801 ± 0.2329

The epicardial potential maps are shown in Figure 4.12 in order to analyze the reconstructed solution in a three dimensional view. The improvement in reconstructed epicardial potential using the heuristic function is also apparent in this figure. This solution is smoother than the other reconstructed solution, but it is closer to the real epicardial potential distribution.

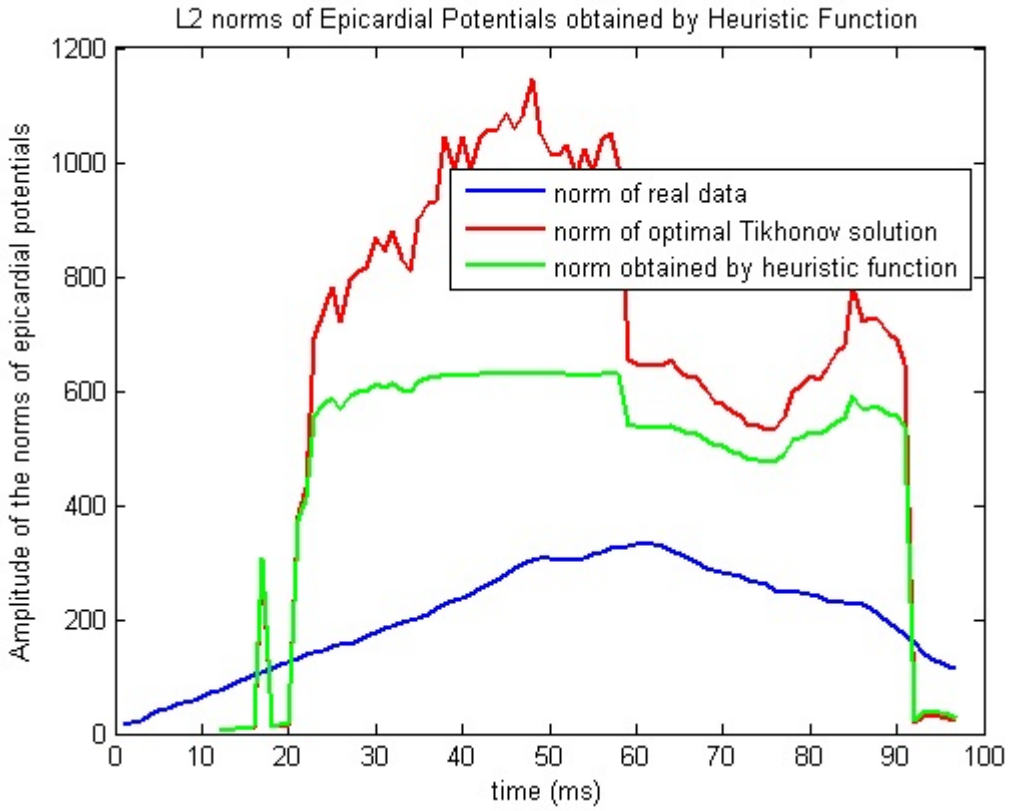

Figure 4.10: The Euclidean Norms for 30 dB Noisy Data with 0.6 Scale Geometric Error

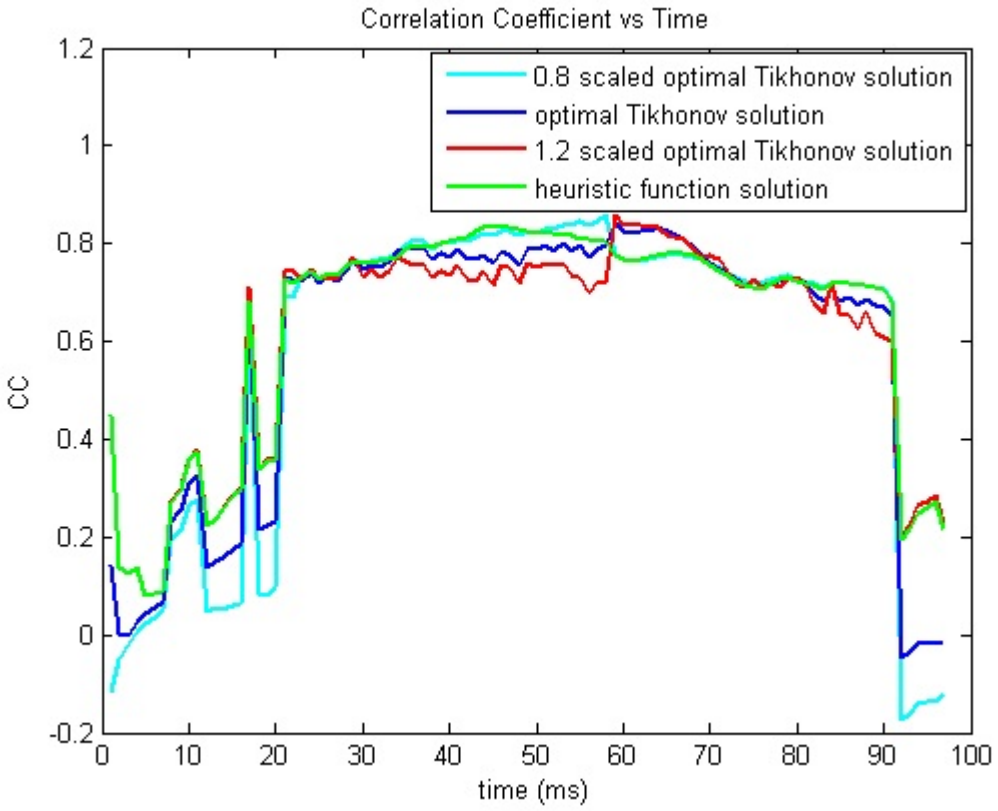

Figure 4.11: The CC values of different methods in a QRS interval for 30 dB Noisy Data with 0.6 Scale Geometric Error

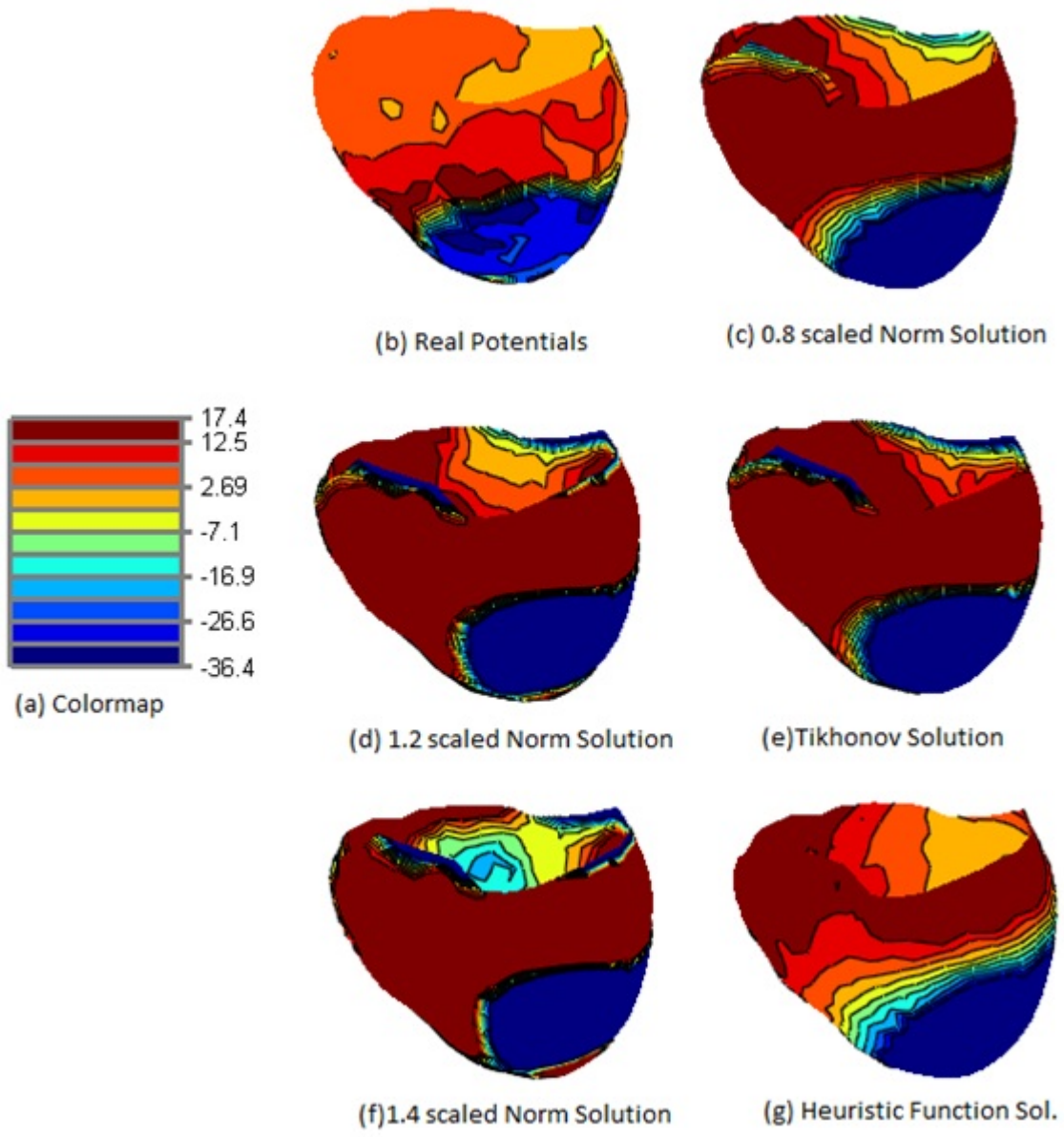

Figure 4.12: Epicardial Maps of solutions at 51 ms after stimulus for 30 dB Noisy Data with 0.6 Scale Geometric Error

4.2.4 Conic Quadratic Programming Results of 30 dB Gaussian White Noise Added Measurements with 15mm Shifted Geometric Error

The inverse problem studied in this subsection involves the errors due to the noise in measurements and shift in the location of heart. Errors in measurements are similar to the previous sections, a 30 dB noise added to the simulated torso potentials. However, geometric error is originated from wrong location of heart at mediastinum. Here, we have reconstructed the epicardial potential from noisy torso potential using the transfer matrix estimated from the wrong location of heart, instead of true transfer matrix.

This problem was also solved using different bound constraints. These bound values were obtained by scaling the norm of optimal Tikhonov solution or using the norm of optimal solution and heuristic function. In Figure 4.13, the norms of the real epicardial potentials and optimal Tikhonov solutions and the bound values obtained from heuristic function are plotted. The norm values that are generated by heuristic function have the shape of the norm of optimal Tikhonov solution, however, they are closer to the real norms.

In Table 4.5, the average CC and RDMS values of reconstructed solutions using different bound constraints in Conic Quadratic Programming are given. The results in this case are quite different from three cases represented in the previous cases. The highest CC values were obtained by using the bounds generated by scaling norm optimal Tikhonov solution with 0.8. Figure 4.14 also supports this result. 0.8 scaled norms lead to the highest CC values nearly over whole QRS interval. In addition, heuristic generates worse CC and RDMS values than the optimal Tikhonov solution.

Table 4.5: Averages and standard deviations of CC and RDMS values of different test methods for 30 dB Noisy Data with 15mm Shifted Geometric Error

Method	Average CC ± std	Average RDMS ± std
0.8 scale	0.5815 ± 0.1802	0.8474 ± 0.1452
0.9 scale	0.5578 ± 0.162	0.8795 ± 0.1398
1 scale (Tikhonov)	0.5328 ± 0.1422	0.9133 ± 0.1310
1.1 scale	0.5013 ± 0.1179	0.9519 ± 0.1107
1.2 scale	0.4696 ± 0.1078	0.9872 ± 0.0970
1.3 scale	0.4408 ± 0.103	1.0179 ± 0.0897
1.4 scale	0.4151 ± 0.1008	1.0444 ± 0.0861
Heuristic	0.5282 ± 0.1249	0.9239 ± 0.1160

Epicardial potential maps drawn in Figure 4.15 illustrate the reconstructed potential distri-

butions 43 ms after the stimulus. This figure also shows that the closest result to the real epicardial potentials is obtained by narrowing the norm bound with 0.8 scaling factor. Moreover, results of optimal Tikhonov solution and heuristic function are very similar. This is an expected result since constraints of both methods are very similar. Having better result by narrowing bound constraint is also meaningful since optimal Tikhonov solution has greater norm than the real epicardial potential norm as shown in Figure 4.13.

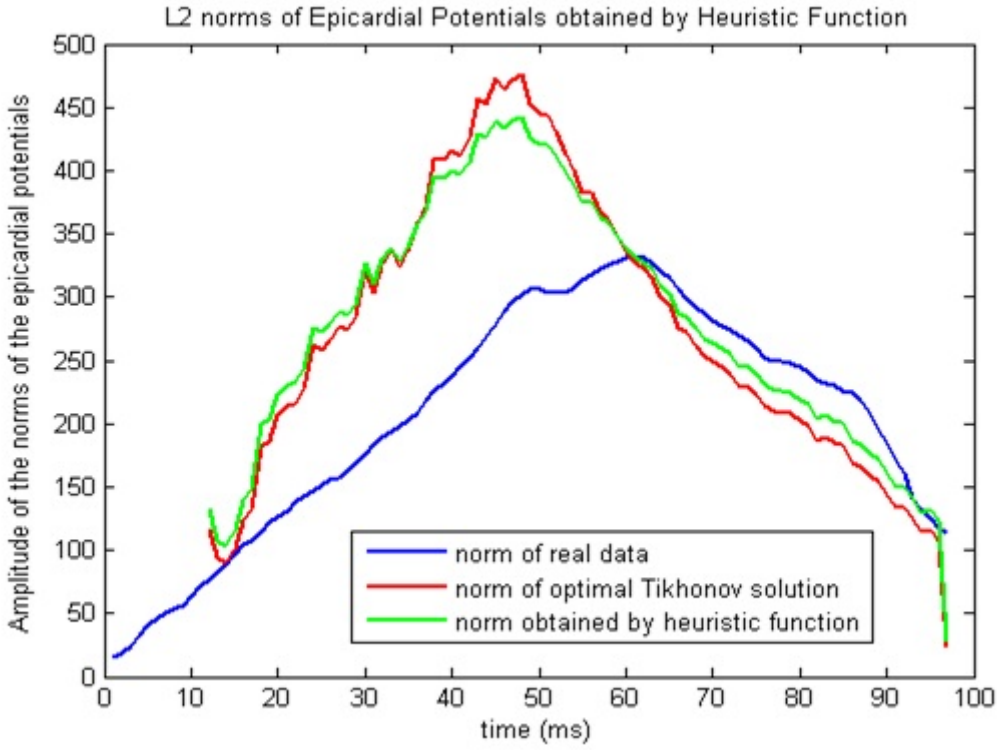

Figure 4.13: The Euclidean Norms for 30 dB Noisy Data with 15mm Shifted Geometric Error

The results in all cases show that Conic Quadratic Programming method provides an improvement in reconstructed solution, if we have a prior knowledge about the norm of solution. This consequence is valid for the inverse problem having both measurement error and/or geometric error. This is more obvious when geometric error is present since the norm of optimal Tikhonov solution is quite different from the norm of real epicardial potentials.

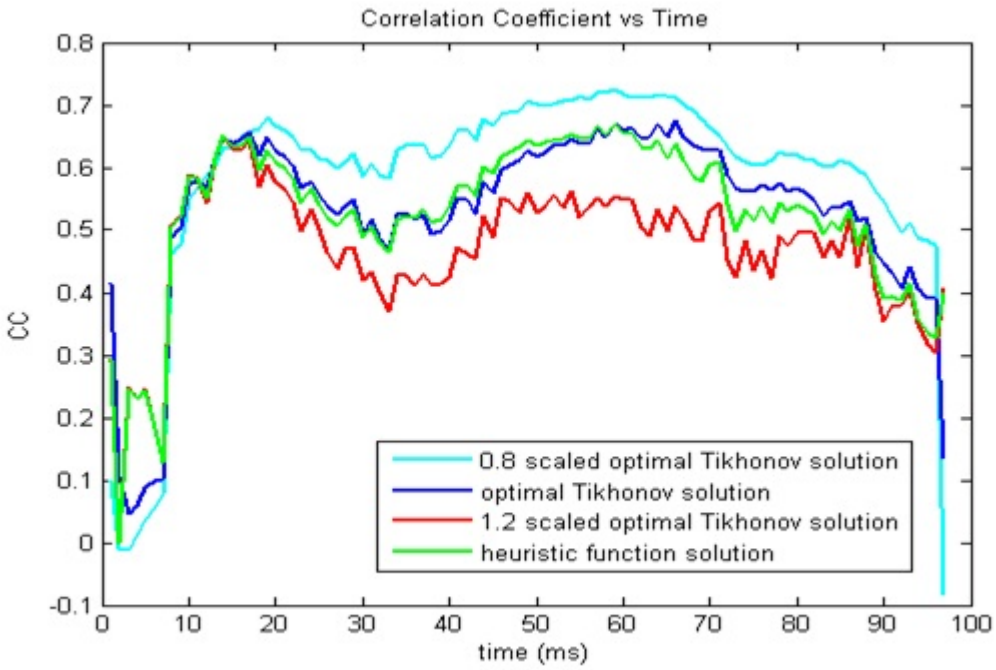

Figure 4.14: The CC values of different methods in a QRS interval for 30 dB Noisy Data with 15mm Shifted Geometric Error

4.3 Linearly Constrained Tikhonov Solutions

In this section, results of a two step Tikhonov regularization method consisting of over-regularized and under-regularized solutions are represented. As mentioned in previous sections, Tikhonov regularization technique does not need a priori knowledge of the properties of the solution or the error to solve inverse problem. The over-regularized solutions in Tikhonov regularization provide smoother solutions tend to recover more accurately the distribution of the positive and negative values of epicardial potentials or, equivalently, to recover more accurately the zero line of epicardial potentials. On the other hand, under-regularized solutions recover more accurately the magnitudes and location of the extrema in epicardial distributions [15]. The method that is applied in this section is based on these principles and it solves the problem in two steps without any prior information. At the first step, problem is solved with a regularization parameter that is bigger than the optimal value of the regularization parameter. This provides a smoother solution that recovers more accurately the zero line of epicardial potentials. This solution is then used to derive constraints in the form of linear bounds on the values of the solution. At the second step, problem is solved with an under-regularizing parameter by imposing these linear bound constraints. The details of the method are represented

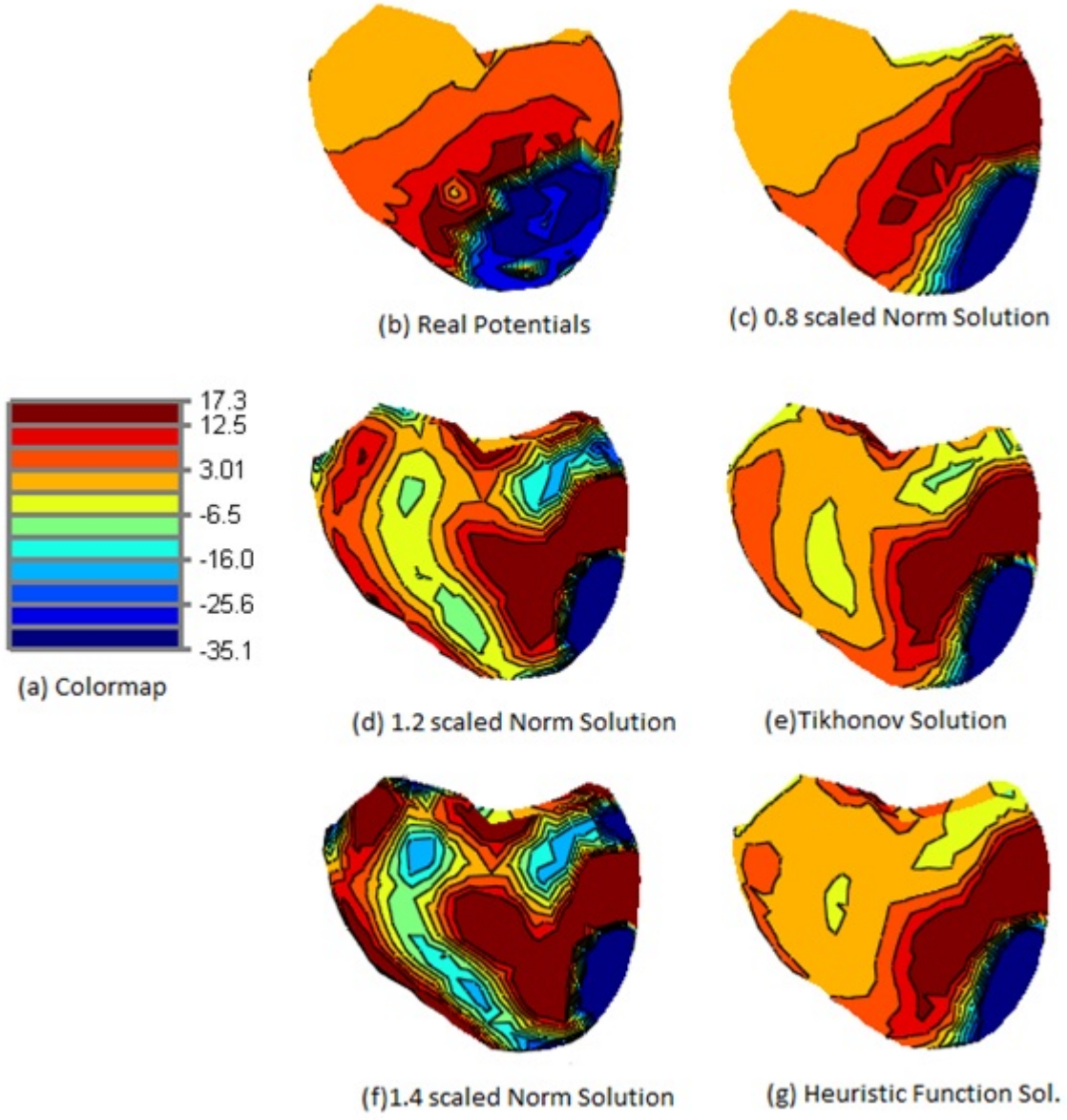

Figure 4.15: Epicardial Maps of solutions at 43 ms after stimulus for 30 dB Noisy Data with 15mm Shifted Geometric Error

in section 3.2.3.

In the following subsections, the linearly constrained Tikhonov regularization method will be tested for solving 4 different cases of the inverse ECG problem and performance of method will be compared with Tikhonov Regularization. In two cases, only Gaussian white noise is added to measurements at two different levels (30 dB and 10 dB). In other two cases, geometric errors due to the shift in heart location and error in cardiac size is present in addition to measurement errors.

4.3.1 Linearly Constrained Tikhonov Results of 30 dB Gaussian White Noise Added Measurements

In the first step of the test of method, Gaussian white noise with 30 dB SNR is added to the body surface measurements that are simulated from the real epicardial potentials and this noisy data is used for the solution of inverse problem. The construction of the solution set in linearly constrained Tikhonov Regularization method depends on the choice of the three parameter values. These parameters are over-regularization parameter λ_o, under-regularization parameter λ_u and the band parameter ϵ that describes the width of the bound around the baseline. Different values for these parameters result in different reconstructed results. During the tests, this method is studied with different values of these parameters.

As mention before, the over-regularization parameter, λ_o, is higher than optimal regularization parameter λ_{opt}. Thus, we have used different values of the over-regularization parameter obtained by multiplying optimal regularization parameter with a scaling factor between 1 and 2. Similarly, we have obtained values of the under-regularization parameter, λ_u, which is smaller than the value of optimal regularization parameter, by multiplying optimal regularization parameter with a scaling factor between 0.4 and 0.8. We have taken the value of band parameter ϵ in 3.20 as a small positive number that corresponds to a value 1% of the norm of optimal Tikhonov solution. Instead of using zero as baseline, we have selected the mean of optimal Tikhonov solution as baseline. During the test of method, we have observed that this choice gives better results than the choice of zero as baseline.

The average CC and RDMS values of the results that are reconstructed by using different over-regularization and under-regularization parameters are given in Table 4.6 and Table 4.7. The

CC and RDMS values in these tables show the slight improvement in reconstructed solutions. The best results for linearly constrained Tikhonov Regularization are obtained when the value of λ_o is around the 1.2 times the value of λ_{opt} and the value of λ_u is around 0.5 times the value of λ_{opt}. The CC plot of the case where the value of λ_o is scaled value of λ_{opt} with 1.2 and the value of λ_u is is scaled value of λ_{opt} with 0.5 and optimal Tikhonov solution in a QRS interval is also shown in Figure 4.16. Figure 4.17 shows the epicardial maps of the same results.

Table 4.6: Averages of CC values of the reconstructed solution using different regularization parameters for 30 dB Noisy Data (optimal Tikhonov solution has 0.7698 CC value)

λ_o \ λ_u	0.4	0.5	0.6	0.7	0.8
1	0 .778	**0 .7804**	0 .7799	0 .778	0.7755
1 .2	0 .7768	**0 .7793**	0 .7788	0 .777	0.7746
1 .4	0 .7677	0 .7776	0 .7774	0 .7757	0.7734
1 .6	0 .7503	0 .7684	0 .7757	0 .7742	0.772
1 .8	0 .7306	0 .76	0 .7705	0 .7727	0.7705

Table 4.7: Averages of RDMS values of the reconstructed solution using different regularization parameters for 30 dB Noisy Data (optimal Tikhonov solution has 0.6039 RDMS value)

λ_o \ λ_u	0.4	0.5	0.6	0.7	0.8
1	0 .5993	0 .5932	0 .5924	0 .594	0.5968
1 .2	0 .6008	**0 .5944**	0 .5934	0 .5949	0.5977
1 .4	0 .6118	0 .5966	0 .5953	0 .5965	0.5991
1 .6	0 .6341	0 .6077	0 .5977	0 .5987	0.601
1 .8	0 .6577	0 .6181	0 .6037	0 .6007	0.6029

4.3.2 Linearly Constrained Tikhonov Regularization Results of 10 dB Gaussian White Noise Added Measurements

In this section, the results of linearly constrained Tikhonov Regularization method for 10 dB noise measurement added data will be represented. Similar to previous section, we have tested this method with different values of over-regularization parameter λ_o, under-regularization parameter λ_u and the band parameter ϵ.

The average CC and RDMS values of the reconstructed solutions by using different over-regularization and under-regularization parameters are given in Table 4.8 and 4.9. In these results, the band parameter ϵ is taken as 1% of the norm of optimal Tikhonov solution. Similar

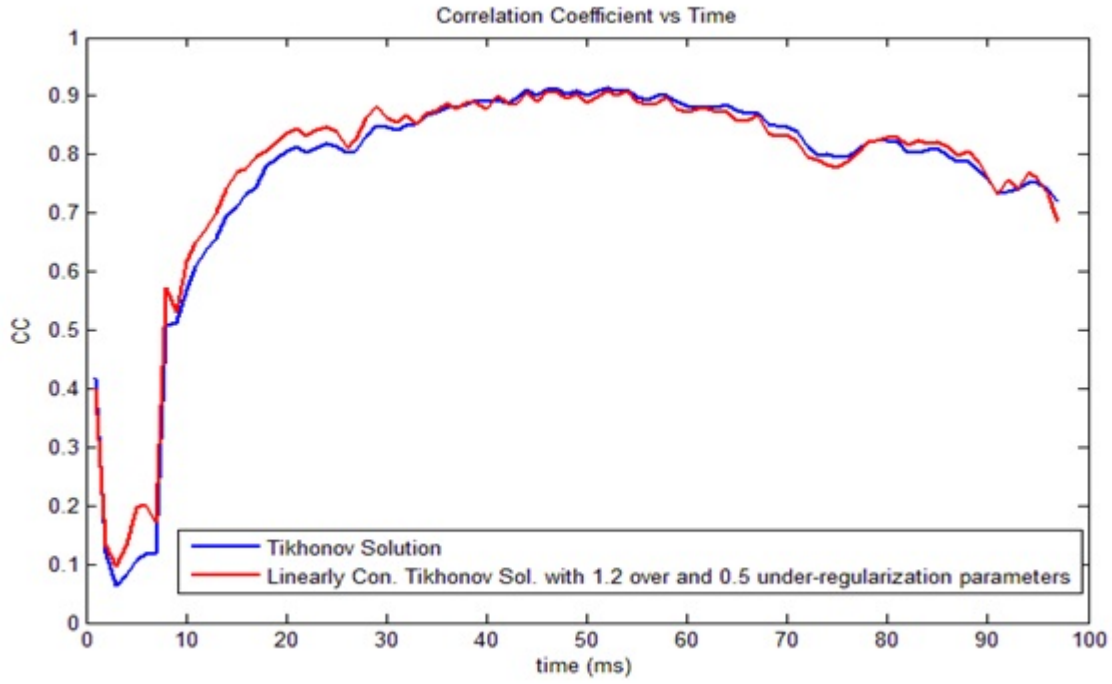

Figure 4.16: The CC values of Tikhonov Solution and Linearly Constrained Tikhonov Solution in a QRS interval for 30 dB Noisy Data

to previous section, the CC plot of the solutions where the value of λ_o is 1.2 times the value of λ_{opt} and the value of λ_u is 0.5 times the value of λ_{opt} and the CC plot of optimal Tikhonov solutions in a QRS interval are also shown in Figure 4.18. In Figure 4.19, the epicardial maps of the these results are shown.

Table 4.8: Averages of CC values of the reconstructed solution using different regularization parameters for 10 dB Noisy Data (optimal Tikhonov solution has 0.5796 CC value)

λ_o \ λ_u	0.4	0.5	0.6	0.7	0.8
1	0 .6033	**0 .6048**	0 .6022	0 .5974	0.5916
1 .2	0 .5957	**0 .5978**	0 .5961	0 .5919	0.5866
1 .4	0 .5873	0 .5904	0 .5894	0 .5858	0.5811
1 .6	0 .5797	0 .5837	0 .5831	0 .5799	0.5757
1 .8	0 .5739	0 .5784	0 .5779	0 .5751	0.5713

Similar to 30 dB noisy measurements, linearly constrained Tikhonov Regularization provides a slight improvement in reconstruction of epicardial potential distribution when compared with Tikhonov solution.

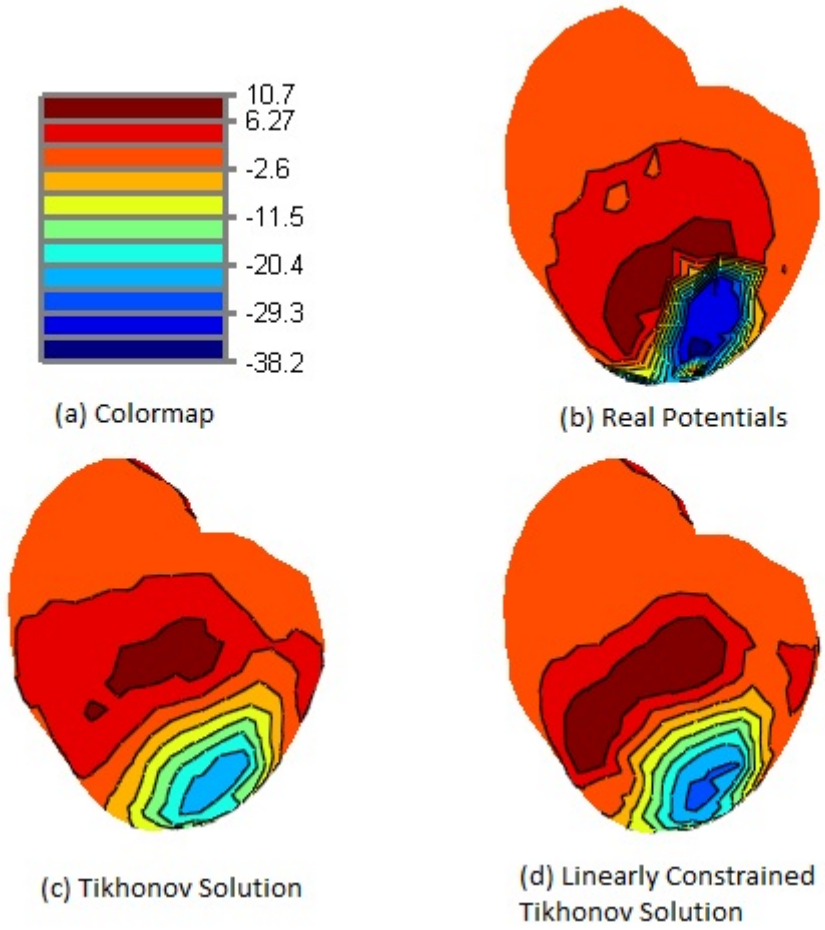

Figure 4.17: Epicardial Maps of Solution at 25th ms

Table 4.9: Averages of RDMS values of the reconstructed solution using different regularization parameters for 10 dB Noisy Data (optimal Tikhonov solution has 0.8196 RDMS value)

λ_o \ λ_u	0.4	0.5	0.6	0.7	0.8
1	0 .802	**0 .7971**	0 .7982	0 .8022	0.8076
1 .2	0 .81	**0 .8047**	0 .8046	0 .8079	0.8126
1 .4	0 .8191	0 .8126	0 .8118	0 .8143	0.8184
1 .6	0 .8275	0 .8203	0 .819	0 .821	0.8245
1 .8	0 .8347	0 .8272	0 .8256	0 .8272	0.8303

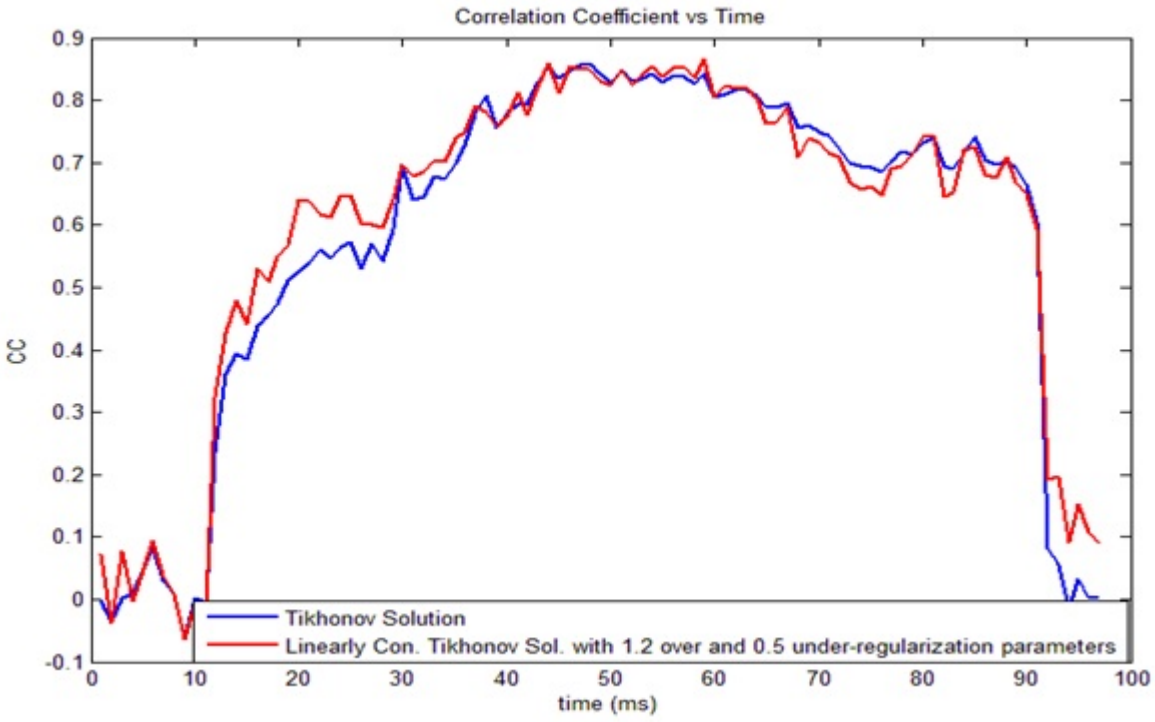

Figure 4.18: The CC values of Tikhonov Solution and Linearly Constrained Tikhonov Solution in a QRS interval for 10 dB Noisy Data

4.3.3 Linearly Constrained Tikhonov Regularization Results of 30 dB Gaussian White Noise Added Measurements with 0.6 Scale Geometric Error

We have also tested the linearly constrained Tikhonov Regularization method for the inverse problem having an error in heart's size in addition to 30 dB measurement noise. We have followed the same way in two previous cases. The inverse problem has been solved with different values of over-regularization parameter λ_o, under-regularization parameter λ_u and the band parameter ϵ.

We have used the average CC and RDMS values of the reconstructed solutions in validation of method. These average CC and RDMS values for different over-regularization and under-regularization parameters are given in Table 4.10and Table 4.11. The average CC and RDMS results in these tables show that it is possible to obtain a slight improvement in reconstructed solution by two step Tikhonov regularization. However, this improvement is limited. In Figure 4.20, the CC plots of optimal Tikhonov solutions and the reconstructed solutions where the value of λ_o is 1.2 times the value of λ_{opt} and the value of λ_u is 0.5 times the value of λ_{opt} are shown in a QRS interval. The epicardial maps of these results 65 ms after the stimulus are

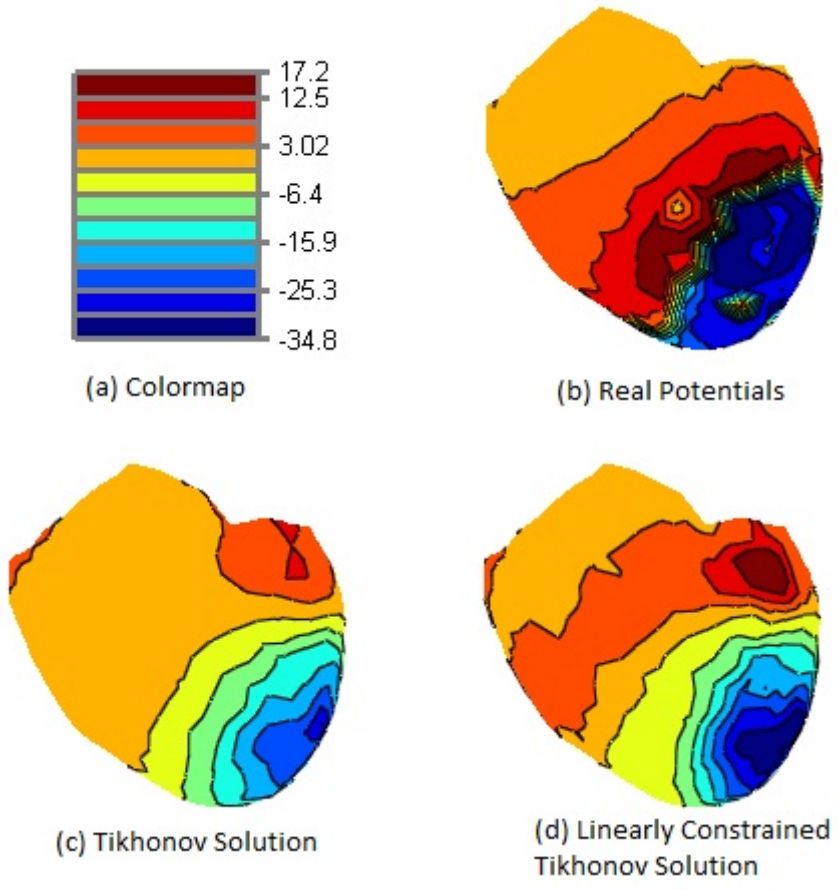

Figure 4.19: Epicardial Maps of Solution at 42 ms for 10dB Noisy Data

also shown in Figure 4.21. These epicardial maps show that two step Tikhonov regularization and zero order Tikhonov regularization produces very similar results and the improvement in estimated solution from linearly constrained Tikhonov solution is very limited when it is compared with zero order Tikhonov solution.

Table 4.10: Averages of CC values of the reconstructed solution using different regularization parameters for 30 dB Noisy Data with 0.6 Scale Geometric Error (optimal Tikhonov solution has 0.5895 CC value)

λ_o \ λ_u	0.4	0.5	0.6	0.7	0.8
1	0.6076	**0.609**	0.6071	0.6033	0.5986
1.2	0.5858	**0.5953**	0.5947	0.5924	0.5896
1.4	0.57	0.5838	0.5841	0.5826	0.5808
1.6	0.5611	0.5724	0.5763	0.5755	0.5743
1.8	0.556	0.5644	0.5718	0.5715	0.5707

Table 4.11: Averages of RDMS values of the reconstructed solution using different regularization parameters for 30 dB Noisy Data with 0.6 Scale Geometric Error (optimal Tikhonov solution has 0.8316 RDMS value)

λ_o \ λ_u	0.4	0.5	0.6	0.7	0.8
1	0.8372	**0.8312**	0.8294	0.8295	0.8302
1.2	0.8558	0.838	**0.8345**	0.8332	0.8328
1.4	0.8691	0.845	0.8399	0.8375	0.8363
1.6	0.8765	0.8557	0.8452	0.8418	0.8399
1.8	0.8817	0.8649	0.8492	0.8452	0.8427

4.3.4 Linearly Constrained Tikhonov Regularization Results of 30 dB Gaussian White Noise Added Measurements with 15mm Shift Geometric Error

In this part, results of linearly constrained Tikhonov regularization method for the inverse problem having a geometric error due to the wrong location of heart and a measurement error will be represented. During the tests of method, we have repeated the procedure similar to the previous cases i.e. different over-regularization and under-regularization parameters have been used for the estimation of solution. The average CC and RDMS values of the reconstructed solutions are given in Table 4.12 and Table 4.13. The results for the geometric error due to the shift in location of heart differ from the results of previous cases since the method cannot provide an improvement when we compare with Tikhonov solution. This

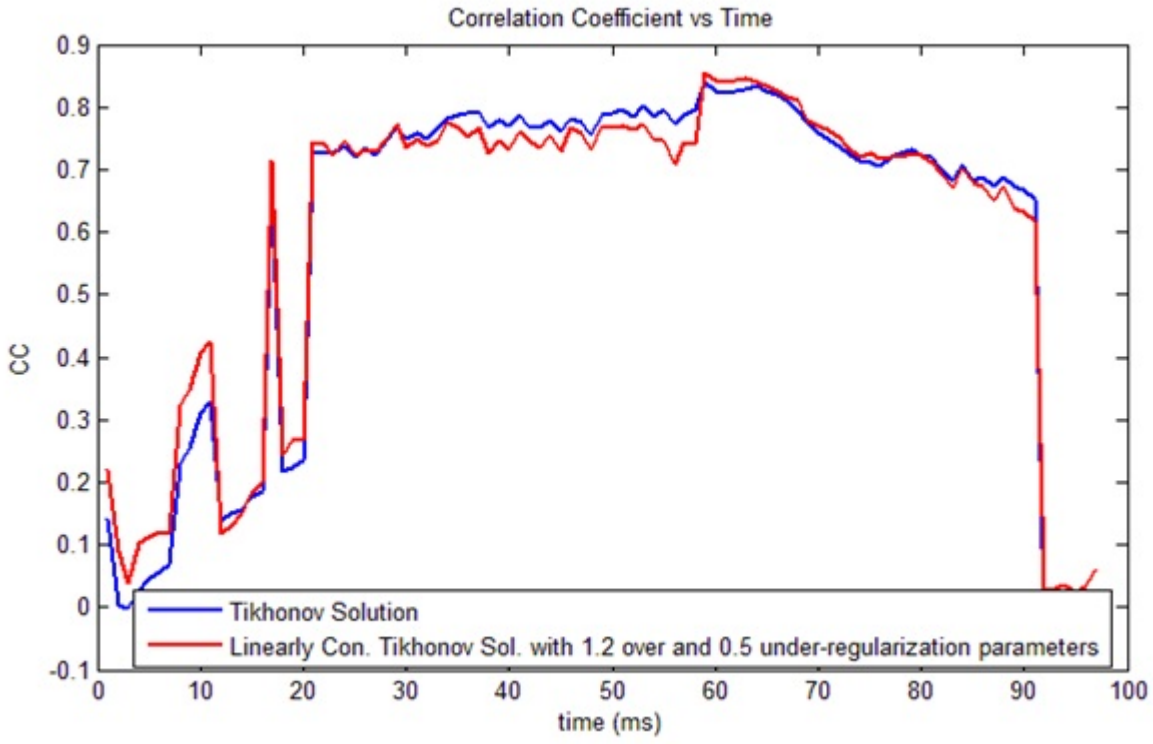

Figure 4.20: The CC values of Tikhonov Solution and Linearly Constrained Tikhonov Solution in a QRS interval for 0.6 Scale Geometric Error

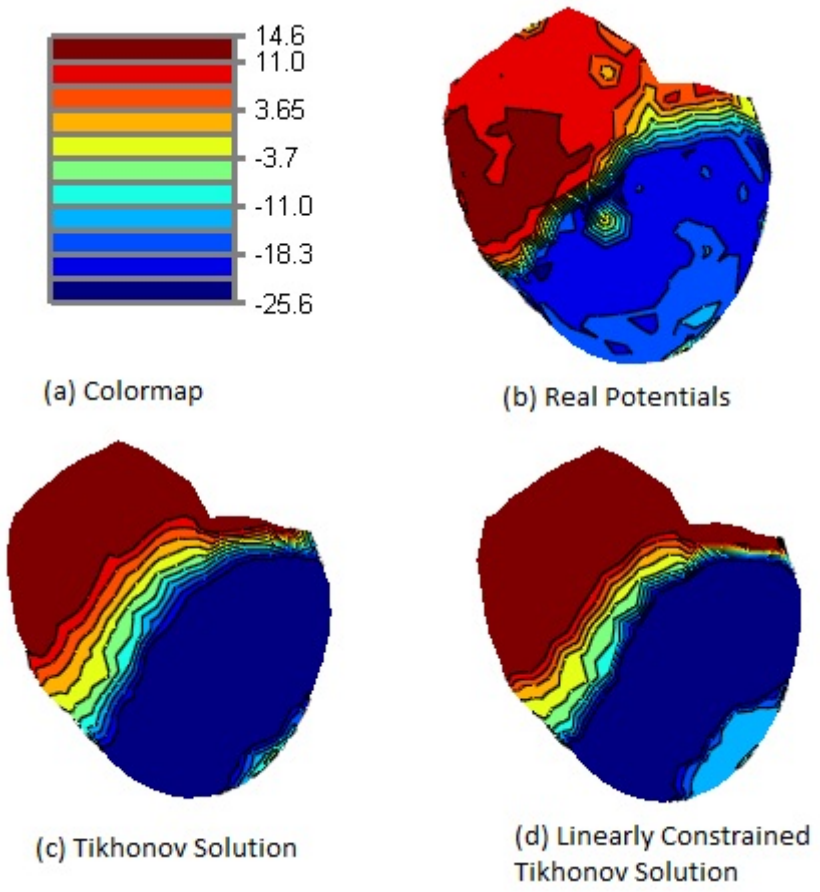

Figure 4.21: Epicardial Maps of Solution at 65 ms for 0.6 Scale Geometric Error

consequence is also obvious in the Figure 4.22 and Figure 4.23 showing the CC plot of reconstructed solutions in a QRS interval and epicardial maps, respectively.

Table 4.12: Averages of CC values of the reconstructed solution using different regularization parameters for 30 dB Noisy Data with 15mm Shifted Geometric Error (optimal Tikhonov solution has 0.5328 CC value)

λ_o \ λ_u	0.4	0.5	0.6	0.7	0.8
1	0.4866	0.4999	0.5095	0.517	0.5231
1.2	0.4833	0.4975	0.5079	0.516	0.5226
1.4	0.4749	0.4954	0.5064	0.5149	0.5218
1.6	0.4713	0.4926	0.5041	0.5131	0.5204
1.8	0.4663	0.4824	0.5017	0.5111	0.5187

Table 4.13: Averages of RDMS values of the reconstructed solution using different regularization parameters for 30 dB Noisy Data with 15mm Shifted Geometric Error (optimal Tikhonov solution has 0.9133 RDMS value)

λ_o \ λ_u	0.4	0.5	0.6	0.7	0.8
1	0.9665	0.9518	0.9408	0.9321	0.9248
1.2	0.9692	0.9536	0.9419	0.9327	0.925
1.4	0.9781	0.9554	0.9432	0.9335	0.9256
1.6	0.9813	0.9581	0.9454	0.9352	0.9269
1.8	0.9864	0.9688	0.9478	0.9372	0.9286

4.4 Regularization of Inverse ECG Problem with Multiple Constraints

Instead of using single constraint, which usually leads to biased solutions, it is aimed to obtain qualified solution by regularizing the problem with multiple spatial constraints. For this purpose, we studied the convex optimization problem described in equation 3.22 in section sec:AdmSol. We have formulated the problem into the equivalent form shown in Equation 4.4 in order to solve problem by the CVX toolbox.

$$\begin{aligned} \min_{arg\ m_k} \quad & \|d_k - Gm_k\|_2^2 \\ \text{subject to} \quad & \|m_k\|_2^2 \leq \epsilon_1 \\ & \|G_\theta m_k\|_1^2 \leq \epsilon_2 \\ & \left\|G_\phi m_k\right\|_1^2 \leq \epsilon_3 \end{aligned} \tag{4.4}$$

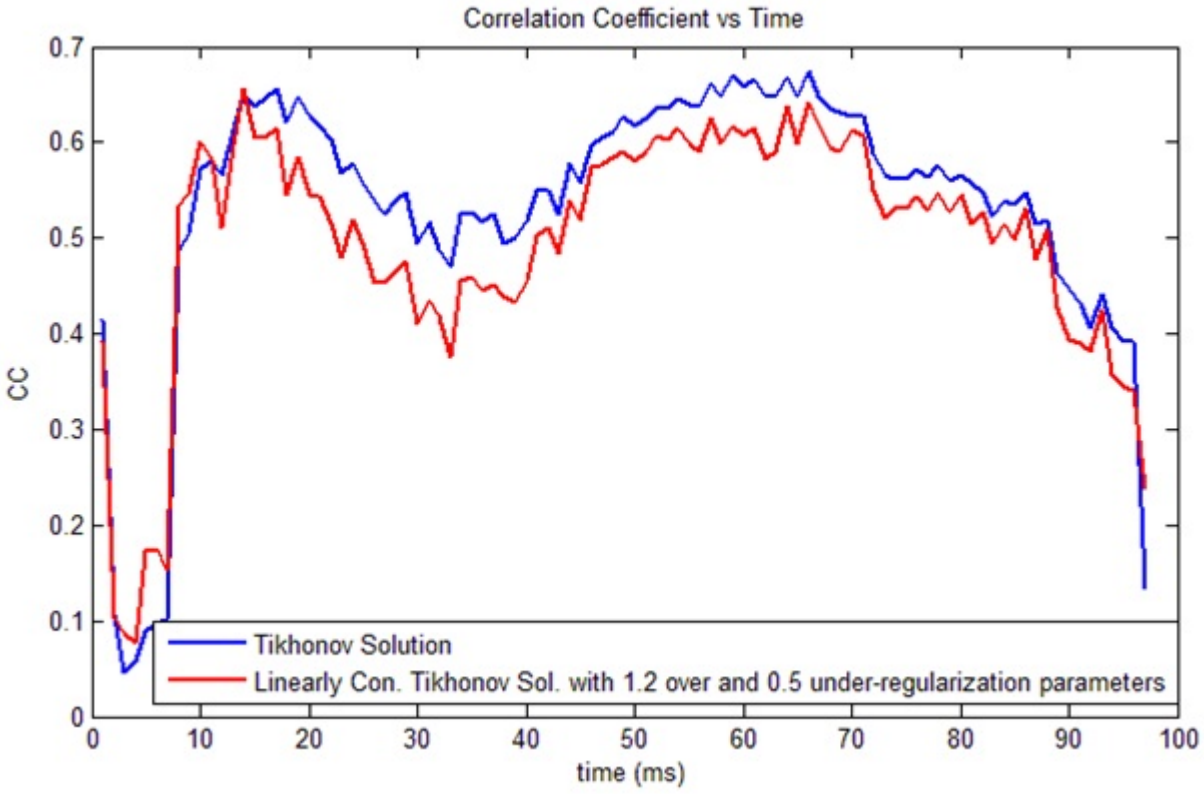

Figure 4.22: The CC values of Tikhonov Solution and Linearly Constrained Tikhonov Solution in a QRS interval for 15mm Shifted Geometric Error

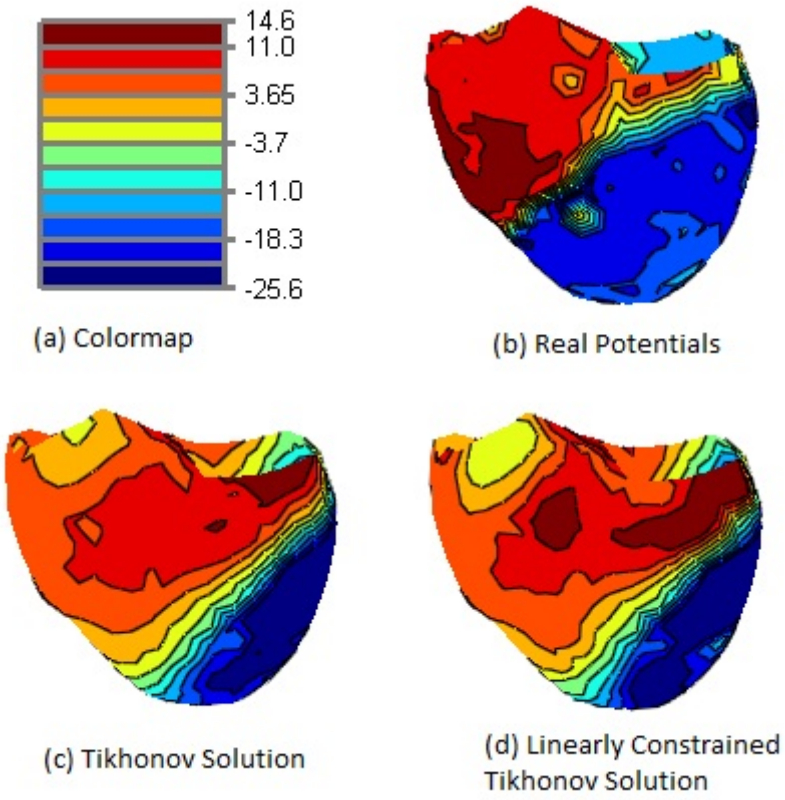

Figure 4.23: Epicardial Maps of Solutions at 65 ms for 15 mm Shifted Geometric Errors

In order to estimate a solution by this method, we need to develop the constraint values ϵ_1, ϵ_2 and ϵ_3 . We developed different constraint values based on the optimal Tikhonov solution and exact epicardial potentials. We have investigated the performance of method for different cases including different measurement error in data and geometric error in model as in previous methods.

In the following subsections, method is studied with different data having different level of noise and different geometric errors in model. For each case, we used different constraints values that were developed from the optimal Tikhonov solution and exact solution. We will investigate the validation of solution by means of CC and RDMS values and epicardial maps as in previous methods.

4.4.1 Results of 30 dB Gaussian White Noise Added Measurements by Imposing Multiple Constraints

Here we will discuss the simulation results of the inverse ECG problem having 30 dB noise in measurements and true geometry model. The transfer matrix G that is used for reconstruction of solution is the same as the one used for forward simulation of problem. However, measurements have 30 dB Gaussian noise. This problem is solved using the formulation in equation 4.4. We have used different constraint values ϵ_1, ϵ_2 and ϵ_3 in equation 4.4 during the test of method.

These constraints values, ϵ_1, ϵ_2 and ϵ_3, were generated by different methods. First, we have used real epicardial potentials in order to obtain these values. The value of ϵ_1 was directly computed by taking the L- norm of epicardial potentials. Similarly, values of , ϵ_2 and ϵ_3 were calculated by taking the L1-norm of the result of the gradient matrices times the real potential values. This is an unrealistic case since we use the real potential that we try to estimate. As a second method, we have optimal Tikhonov solution in order to develop constraint values. Here we have computed the L2-norm of the Tikhonov solution and L1-norms of gradient matrices times Tikhonov solution and we have obtained the values $\epsilon_{1,tik}$, $\epsilon_{2,tik}$ and $\epsilon_{3,tik}$, respectively. Then, we have generated different ϵ_1, ϵ_2 and ϵ_3 values by multiplying the values of $\epsilon_{1,tik}$, $\epsilon_{2,tik}$ and $\epsilon_{3,tik}$ with different scaling factors. In other words, we calculated the constraint values in the following way:

$$\epsilon_1 = \alpha_1 \epsilon_{1,tik}$$
$$\epsilon_2 = \alpha_2 \epsilon_{2,tik}$$
$$\epsilon_3 = \alpha_2 \epsilon_{3,tik} \tag{4.5}$$

Finally, we have used the heuristic function described in Equation 4.3 in order to establish the value of ϵ_1. This function had been used in Conic Quadratic Programming as a heuristic method. Similarly, we have used this function in multiple constraint regularization as a heuristic method. In the heuristic method, the constraint values, ϵ_2 and ϵ_3 were computed from optimal Tikhonov solution as shown in Equation 4.5. The average CC value of the reconstructed result using the norm values of the real epicardial potentials is 0.73 and the average RDMS this result is 0.67 whereas these values are 0.77 and 0.60 for optimal Tikhonov solution, respectively. The average CC and RDMS values of reconstructed solution using the true epicardial potentials are worse than the values of optimal Tikhonov solution. This is a surprising result that we get worse result even when we have used the real potentials determination of the constraint values. When we examined the results more closely, we found out that the norm values of real epicardial potentials are higher than the optimal Tikhonov solution. These higher norm values lead to a over-fitting in solution of inverse problem and due to this over-fitting we get more unstable and inaccurate solutions. The epicardial maps of reconstructed solution are shown in Figure 4.25.

As a second approach, we have used the optimal Tikhonov solution in building the constraint values. We have estimated the epicardial potentials using different constraint values generated by multiplying the norm values of the optimal Tikhonov solution with different scaling factors as shown in equation 4.5. Table 4.14 shows the average CC values of the reconstructed solution by different scaling factors α_1 and α_2. The same results are also illustrated in Figure 4.24. The average RDMS values of the estimated solutions are also given in Table 4.15. As seen in these tables, we have the most accurate results when the scaling factors α_1 is around 1.05 and α_2 is around 0.8. This is an expected result, since our aim in imposing multiple constraints is obtaining more accurate results by enlarging the energy constraint used in Tikhonov regularization. The expansion in energy norm provides a decrease in smoothing effect of Tikhonov solution, however, it causes an over-fitting and instability in reconstructed

solution. This instability is handled by imposing narrower L_1-norms. As seen in average CC and RDMS tables, change in α_2 affects the results less than the change in the value of α_1.

Table 4.14: Averages of CC values of the reconstructed solution using different scaling factors for 30 dB Noisy Data (optimal Tikhonov solution has 0. 77 CC value)

α_1 \ α_2	0.70	0.75	0.80	0.85	0.90	0.95	1.00	1.05	1.10	1.15
0.70	0.665	0.666	0.666	0.666	0.666	0.666	0.666	0.666	0.666	0.666
0.75	0.68	0.68	0.68	0.68	0.68	0.68	0.68	0.68	0.68	0.68
0.80	0.696	0.695	0.695	0.695	0.695	0.695	0.695	0.695	0.695	0.695
0.85	0.714	0.712	0.711	0.711	0.711	0.711	0.711	0.711	0.711	0.711
0.90	0.734	0.732	0.73	0.729	0.729	0.729	0.729	0.729	0.729	0.729
0.95	0.756	0.756	0.754	0.751	0.75	0.749	0.749	0.749	0.749	0.749
1.00	0.776	0.78	0.78	0.778	0.775	0.772	0.77	0.77	0.77	0.77
1.05	0.784	0.79	0.793	0.792	0.789	0.786	0.783	0.78	0.777	0.775
1.10	0.775	0.784	0.788	0.789	**0.788**	0.785	0.782	0.779	0.776	0.773
1.15	0.755	0.766	0.772	0.774	0.774	0.773	0.772	0.769	0.767	0.764
heuristic	0.779	0.789	**0.795**	0.797	-	-	-	-	-	-

Table 4.15: Averages of RDMS values of the reconstructed solution using different scaling factors for 30 dB Noisy Data (optimal Tikhonov solution has 0. 604 RDMS value)

α_1 \ α_2	0.70	0.75	0.80	0.85	0.90	0.95	1.00	1.05	1.10	1.15
0.70	0.751	0.751	0.751	0.751	0.751	0.751	0.751	0.751	0.751	0.751
0.75	0.73	0.73	0.73	0.73	0.73	0.73	0.73	0.73	0.73	0.73
0.80	0.708	0.71	0.71	0.71	0.71	0.71	0.71	0.71	0.71	0.71
0.85	0.683	0.686	0.688	0.688	0.688	0.688	0.688	0.688	0.688	0.688
0.90	0.654	0.658	0.661	0.663	0.663	0.663	0.663	0.663	0.663	0.663
0.95	0.62	0.622	0.625	0.63	0.633	0.634	0.634	0.634	0.634	0.634
1.00	0.589	0.584	0.585	0.589	0.595	0.599	0.604	0.604	0.604	0.604
1.05	0.581	0.57	0.568	**0.57**	0.575	0.58	0.587	0.592	0.597	0.601
1.10	0.601	0.587	0.581	0.58	0.582	0.587	0.592	0.598	0.603	0.609
1.15	0.635	0.619	0.611	0.607	0.607	0.609	0.612	0.617	0.621	0.626
heuristic	0.59	0.574	**0.566**	0.564	-	-	-	-	-	-

As mentioned before, we have also used the heuristic function in Equation 4.3 as a heuristic approach in order to construct the value of ϵ_1. In the heuristic approach, the constraint values, ϵ_2 and ϵ_3 were determined from optimal Tikhonov solution using Equation 4.5. In the last rows of Table 4.14 and Table 4.15, the average CC and RDMS values of the reconstructed solution by the heuristic approach are given. As shown in these tables the average CC and RDMS values are better than the values of the results reconstructed using the exact epicardial potentials and optimal Tikhonov solution.

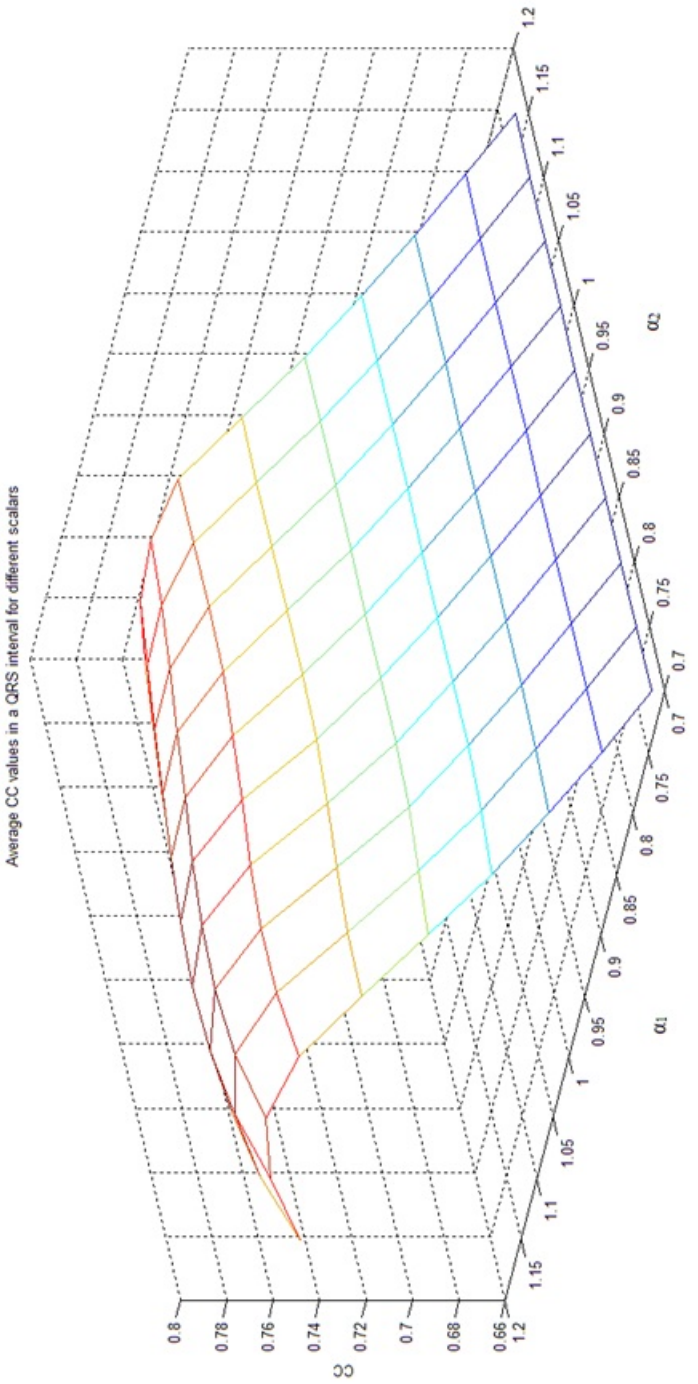

Figure 4.24: The Average CC values of solutions using different scaling factors in construction constraint values

In Figure 4.25, the epicardial maps of reconstructed solutions by imposing different constraint values into the problem Equation 4.4 are shown. These maps show that the solutions by this method have sharper edges than the optimal Tikhonov solution. However, the estimated solution in Figure 4.25-d using the norms of exact epicardial potentials has mislocalized extremas. This originates from the fact that the norms of the real potentials are much higher than the optimal Tikhonov solution and this causes under-regularized solutions. As in this figure, we get more accurate results using the heuristic function.

4.4.2 Results of 10 dB Gaussian White Noise Added Measurements by Imposing Multiple Constraints

In this section, we represent the obtained results of 10 dB noisy data by imposing the multiple constraints into formulation shown in Equation 4.4. We have repeated the same procedure mentioned in section 4.4.1 to compare the reconstructed solution of different constraints. We have used the true epicardial potential norms, optimal Tikhonov norms and heuristic function outputs in construction of constraint values as in previous section.

The average CC and RDMS values of obtained solution using the exact potential norms are 0.58 and 0.851, respectively. The obtained average CC and RDMS values over a QRS interval by using the optimal Tikhonov solution and the heuristic function are also given in Table 4.16 and Table 4.17. As in section previous section, we have the best CC and RDMS values by heuristic approach.

Epicardial maps of reconstructed solution and the true epicardial potentials 45 ms after the stimulus is illustrated in Figure 4.26. This figure also supports the results shown in the average CC and average RDMS value tables. Similar to the 30 dB noisy case, we get the most accurate results by using the heuristic function. The edges of estimated solution using this method are sharper than the edges in optimal Tikhonov solution. The reconstructed solution using the norm of exact epicardial potential contains wrong extrema in the potential map.

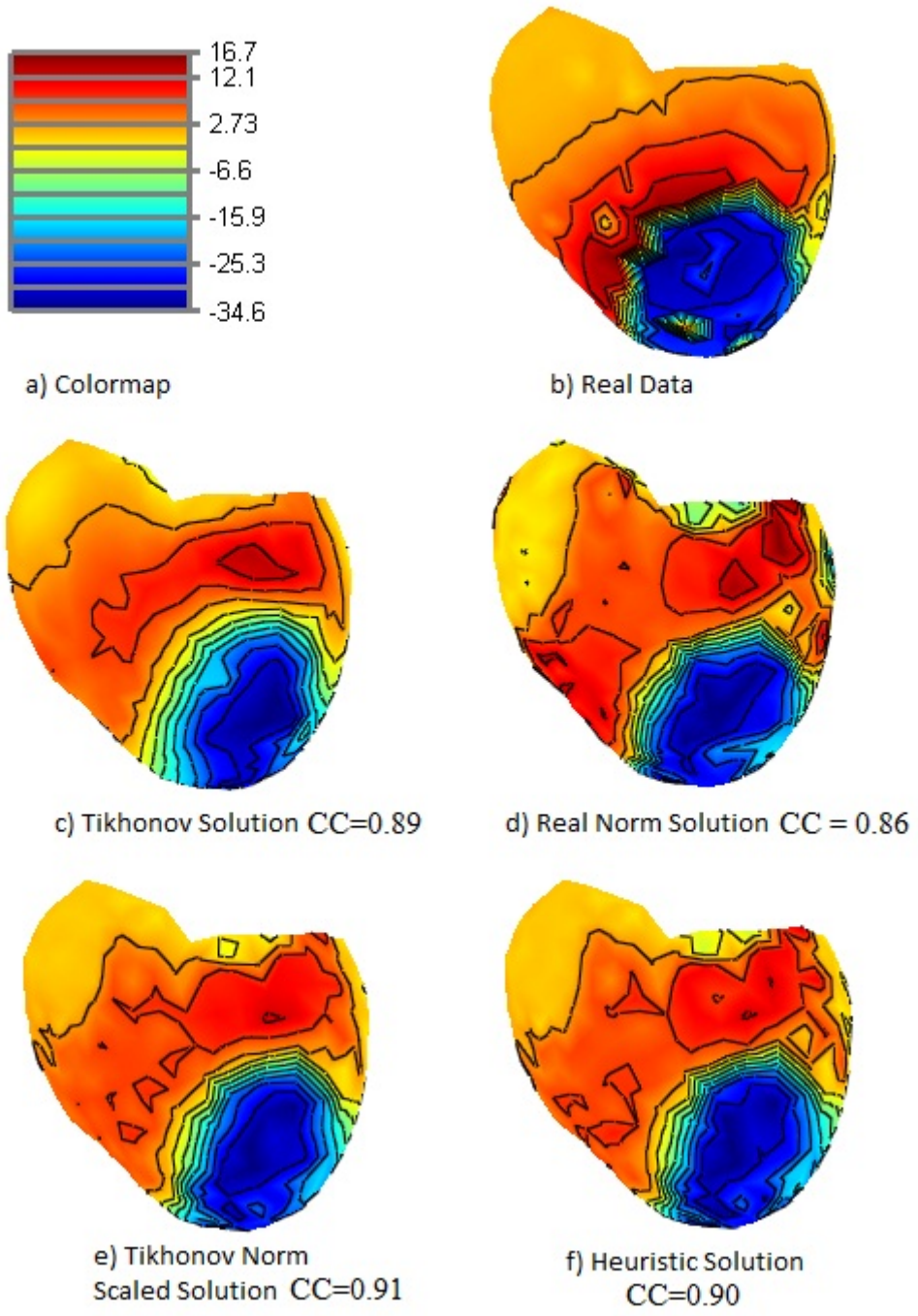

Figure 4.25: Epicardial Potential Maps for 30 dB noisy data : a) Colormap b) Real Potential Distribution at the 40ms c) Optimal Tikhonov Solution d) Reconstructed solution using real norms in multiple constraints imposed method e) Reconstructed solution by imposing the constraint values as $\epsilon_1 = 1.05\epsilon_{1,tik}$, $\epsilon_2 = 0.8\epsilon_{2,tik}$ and $\epsilon_3 = 0.8\epsilon_{3,tik}$ f)Reconstructed solution from heuristic method

Table 4.16: Averages of CC values of the reconstructed solution using different scaling factors for 10 dB Noisy Data (optimal Tikhonov solution has 0. 58 CC value)

α_1 \ α_2	0.70	0.75	0.80	0.85	0.90	0.95	1.00	1.05	1.10	1.15
0.70	0.519	0.517	0.517	0.516	0.517	0.516	0.516	0.516	0.516	0.516
0.75	0.53	0.528	0.528	0.526	0.527	0.527	0.527	0.527	0.527	0.527
0.80	0.542	0.54	0.538	0.537	0.537	0.537	0.537	0.537	0.537	0.537
0.85	0.554	0.552	0.549	0.548	0.547	0.547	0.547	0.547	0.547	0.547
0.90	0.566	0.564	0.562	0.56	0.558	0.557	0.558	0.558	0.558	0.558
0.95	0.578	0.577	0.576	0.573	0.571	0.569	0.568	0.57	0.569	0.569
1.00	0.59	0.59	0.589	0.587	0.585	0.583	0.581	0.581	0.58	0.581
1.05	0.601	0.604	**0.604**	0.602	0.6	0.598	0.597	0.594	0.593	0.593
1.10	0.609	0.614	0.616	0.614	0.613	0.611	0.608	0.606	0.604	0.603
1.15	0.611	0.618	0.622	0.623	0.621	0.619	0.617	0.614	0.612	0.609
heuristic	0.618	0.623	**0.626**	0.626	-	-	-	-	-	-

Table 4.17: Averages of RDMS values of the reconstructed solution using different scaling factors for 10 dB Noisy Data (optimal Tikhonov solution has 0.819 RDMS value)

α_1 \ α_2	0.70	0.75	0.80	0.85	0.90	0.95	1.00	1.05	1.10	1.15
0.70	0.894	0.896	0.896	0.897	0.896	0.897	0.897	0.897	0.897	0.897
0.75	0.879	0.882	0.883	0.884	0.884	0.884	0.884	0.884	0.884	0.883
0.80	0.864	0.867	0.869	0.87	0.871	0.871	0.871	0.871	0.871	0.871
0.85	0.849	0.852	0.855	0.856	0.858	0.858	0.858	0.858	0.858	0.858
0.90	0.834	0.837	0.84	0.842	0.844	0.845	0.845	0.845	0.845	0.845
0.95	0.82	0.822	0.823	0.826	0.829	0.831	0.832	0.831	0.832	0.832
1.00	0.807	0.807	0.808	0.811	0.813	0.816	0.819	0.819	0.819	0.819
1.05	0.797	0.793	**0.793**	0.795	0.798	0.8	0.803	0.806	0.808	0.807
1.10	0.791	0.784	0.782	0.784	0.786	0.789	0.792	0.795	0.798	0.8
1.15	0.794	0.784	0.779	0.778	0.78	0.783	0.786	0.789	0.793	0.796
heuristic	0.786	0.78	**0.777**	0.777	-	-	-	-	-	-

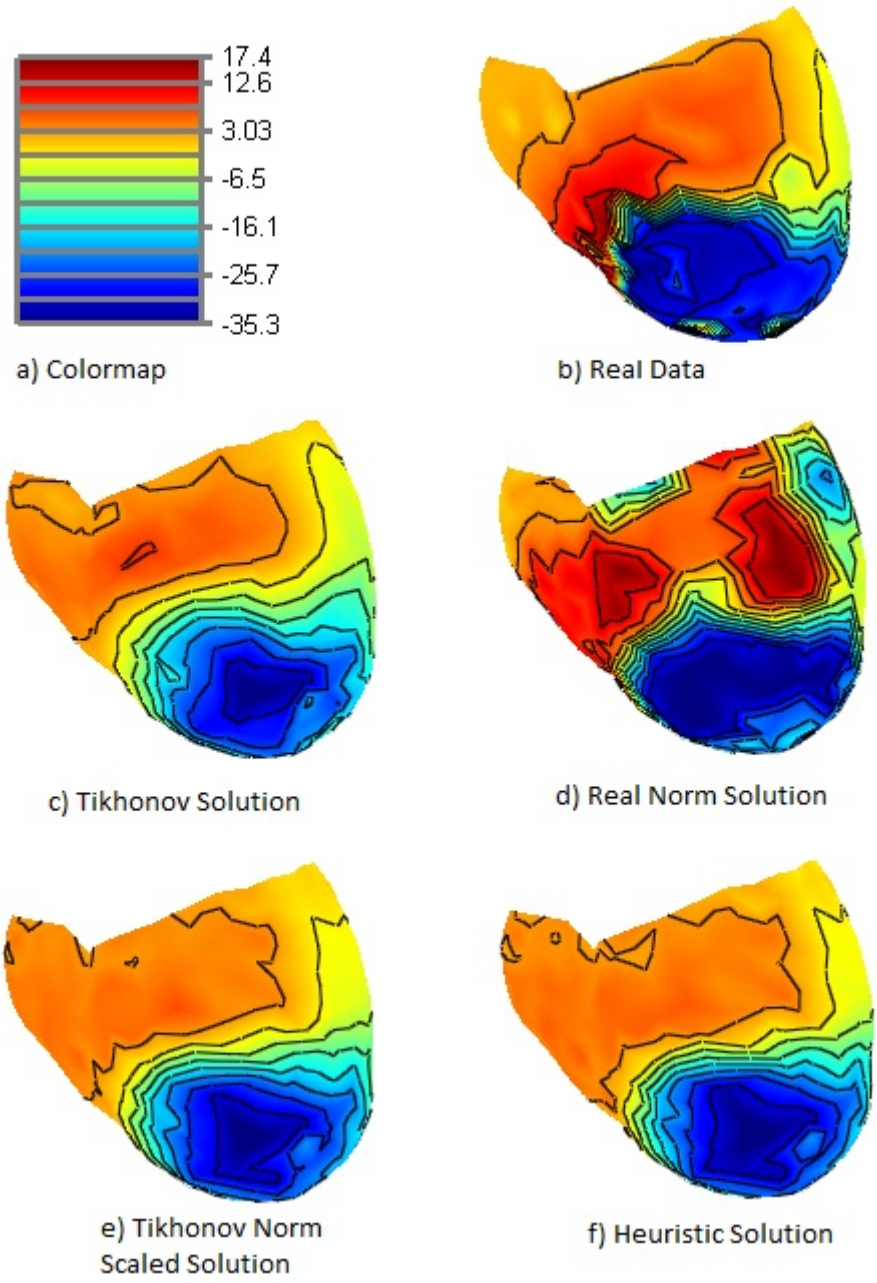

Figure 4.26: Epicardial Potential Maps for 10 dB noisy data : a) Colormap b) Real Potential Distribution at the 45ms c) Optimal Tikhonov Solution d) Reconstructed solution using real norms in multiple constraints imposed method e) Reconstructed solution by imposing the constraint values as $\epsilon_1 = 1.05\epsilon_{1,tik}$, $\epsilon_2 = 0.8\epsilon_{2,tik}$ and $\epsilon_3 = 0.8\epsilon_{3,tik}$ f)Reconstructed solution from heuristic method

4.4.3 Results of 30 dB Noisy Measurement Containing 0.6 Scale Geometric Error by Imposing Multiple Constraints

In this subsection, we have used the 30 dB noisy data as body surface potentials and we have solved this problem using the wrong estimated transfer matrix due to 0.6 scaled cardiac size. Similar to the two previous cases, we have imposed different constraints into problem formulation.

During the validation of the method, we have first imposed the norms estimated from the real epicardial potentials. The average CC and RDMS values are 0.642 and 0.822, respectively. This result is better than the optimal Tikhonov solution. We have also solved the problem using the norms obtained from optimal Tikhonov solution and heuristic function. The average CC and RDMS values of the attained solutions are shown in Figures 4.22 and 4.23. Similar to the previous cases, the best average CC and RDMS values over a QRS interval were achieved by means of the heuristic function.

The epicardial potential maps of the reconstructed solutions using the different norm constraints are shown in Figure 4.27. As seen in this figure, we have the most accurate solution in the heuristic function results. It enables the more accurate magnitudes and the correct position of extrema whereas the optimal Tikhonov solution has incorrect magnitudes and wrong positioned extrema. In case, the real epicardial norms provide smoother solutions since this norms are narrower than the norms of the optimal Tikhonov solution. This result differs from the two previous cases where inverse problem does not contain any geometric error. In the previous two cases, real potentials norms are higher than the norms of optimal Tikhonov solution.

4.4.4 Results of the Inverse Problem Containing 30 dB Noisy Measurements and 15 Shift Geometric Error by Imposing Multiple Constraints

In this subsection, we have reconstructed the solution of a inverse problem having 30 dB measurement noise and geometric error due to the wrong placed heart at the mediastinum by imposing multiple norm constraints. The geometric error is added to the problem by shifting the heart 15mm and by obtaining a new transfer matrix for the new position of the heart. This problem is also solved using different constraints obtained from real epicardial potentials and

Table 4.18: Averages of CC values of the reconstructed solution of the problem containing the 30 dB Noise Data and 0.6 Scale Geometric Error using different scaling factors (optimal Tikhonov solution has 0.589 CC value)

α_1 \ α_2	0.70	0.75	0.80	0.85	0.90	0.95	1.00	1.05	1.10	1.15
0.70	0.571	0.57	0.57	0.57	0.57	0.57	0.57	0.57	0.57	0.57
0.75	0.575	0.574	0.573	0.573	0.573	0.573	0.573	0.573	0.573	0.573
0.80	0.578	0.576	0.575	0.574	0.574	0.574	0.574	0.574	0.574	0.574
0.85	0.582	0.579	0.577	0.575	0.575	0.575	0.575	0.575	0.575	0.575
0.90	0.585	0.582	0.58	0.577	0.576	0.575	0.575	0.575	0.575	0.575
0.95	0.589	0.588	0.586	0.583	0.581	0.579	0.579	0.579	0.579	0.579
1.00	0.596	0.598	0.598	0.597	0.595	0.592	0.589	0.589	0.589	0.589
1.05	0.602	0.608	0.611	**0.611**	0.61	0.608	0.605	0.603	0.602	0.602
1.10	0.601	0.61	0.616	0.619	0.619	0.618	0.616	0.613	0.611	0.61
1.15	0.594	0.605	0.614	0.619	0.622	0.622	0.621	0.62	0.618	0.616
heuristic	0.639	0.637	**0.636**	0.634	-	-	-	-	-	-

Table 4.19: Averages of RDMS values of the reconstructed solution of the problem containing the 30 dB Noise Data and 0.6 Scale Geometric Error using different scaling factors (optimal Tikhonov solution has 0.832 RDMS value)

α_1 \ α_2	0.70	0.75	0.80	0.85	0.90	0.95	1.00	1.05	1.10	1.15
0.70	0.819	0.82	0.82	0.82	0.82	0.82	0.82	0.82	0.82	0.82
0.75	0.818	0.819	0.82	0.82	0.82	0.82	0.82	0.82	0.82	0.82
0.80	0.817	0.82	0.821	0.822	0.822	0.822	0.822	0.822	0.822	0.822
0.85	0.817	0.821	0.824	0.825	0.826	0.826	0.826	0.826	0.826	0.826
0.90	0.819	0.822	0.825	0.829	0.83	0.831	0.831	0.831	0.831	0.831
0.95	0.822	0.822	0.825	0.828	0.831	0.833	0.833	0.833	0.833	0.833
1.00	0.826	0.822	0.821	0.823	0.825	0.829	0.832	0.832	0.832	0.832
1.05	0.834	0.825	**0.82**	0.819	0.821	0.823	0.827	0.829	0.831	0.831
1.10	0.847	0.834	0.826	0.822	0.821	0.822	0.824	0.827	0.829	0.832
1.15	0.862	0.848	0.837	0.829	0.825	0.824	0.824	0.826	0.829	0.831
heuristic	0.796	0.797	**0.798**	0.799	-	-	-	-	-	-

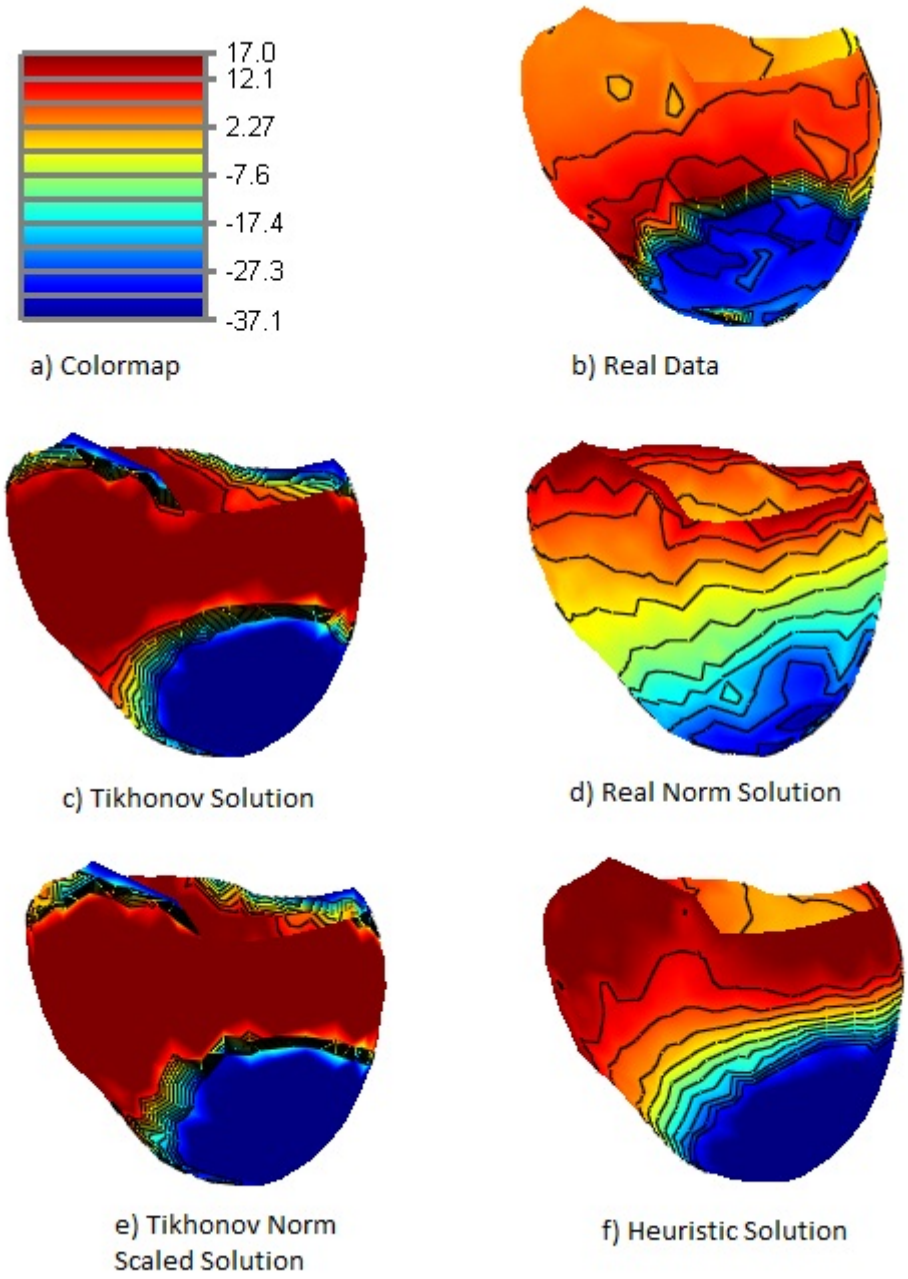

Figure 4.27: Epicardial Potential Maps for 30 dB noisy data with 0.6 Scale Geometric Error: a) Colormap b) Real Potential Distribution at the 49 ms c) Optimal Tikhonov Solution d) Reconstructed solution using real norms in multiple constraints imposed method e) Reconstructed solution by imposing the constraint values as $\epsilon_1 = 1.05\epsilon_{1,tik}$, $\epsilon_2 = 0.8\epsilon_{2,tik}$ and $\epsilon_3 = 0.8\epsilon_{3,tik}$ f)Reconstructed solution from heuristic method

optimal Tikhonov solution.

We have obtained 0.579 and 0.865 as average CC and RDMS values, respectively, over a QRS interval using the true norms estimated from exact epicardial potentials. This result implies an improvement when we compare the optimal Tikhonov solution results where the average CC value is 0.533 and average RDMS value is 0.913. This inverse problem was also solved with the constraint values estimated by multiplication of optimal Tikhonov norms with different scaling factor as in previous inverse problems. The results differ from the previous cases when we compare the average CC and RDMS values of estimated solutions. In the previous cases, we have achieved the improvement in Tikhonov solution by enlarging the L_2-norm constraint and narrowing the L_1-norm constraints. However, in this case, we have attained improvement in average CC and RDMS values by narrowing both L_2-norm and the L_1-norm constraints. Actually, this shows that the optimal Tikhonov solution using the optimum regularization parameter obtained from L-curve method is not the true optimal one. In other words, we can achieve a similar improvement in Tikhonov solution for this problem by only over-regularizing the Tikhonov solution instead of narrowing the all of the constraints.

The constraints obtained from heuristic function did not yield an improvement in solutions for this problem. The epicardial potential maps of reconstructed. solution are illustrated in Figure 4.28. As seen in this figure most accurate results are achieved by imposing the constraint values obtained from the exact epicardial potentials.

When we investigate all these results for different cases involving different level of noise in measurements and different errors in geometry, we are generally able to achieve improvement in reconstructed solution by imposing multiple constraints. We can derive that imposing multiple constraints into problem formulation yields an improvement in reconstructed solutions. We get the recovered solutions more accurately in the magnitudes and location of the extrema. The edges of the recovered solutions also become sharper by imposing multiple norm constraints.

4.5 Reconstruction of Solution by the MRE Method

As mentioned in section 3.3, MRE method is an optimization technique that can be used in reconstruction of solution of linear inverse problems. In order to estimate a solution using the

Table 4.20: Averages of CC values of the reconstructed solutions using different scaling factors for 30 dB Noisy Data with 15mm Shifted Geometric Error (optimal Tikhonov solution has 0.533 CC value)

α_1 \ α_2	0.70	0.75	0.80	0.85	0.90	0.95	1.00	1.05	1.10	1.15
0.70	0.597	0.597	**0.598**	0.598	0.598	0.598	0.598	0.598	0.598	0.598
0.75	0.59	0.59	0.591	0.591	0.591	0.591	0.591	0.591	0.591	0.591
0.80	0.581	0.581	0.581	0.581	0.581	0.581	0.581	0.581	0.581	0.581
0.85	0.57	0.57	0.57	0.57	0.57	0.57	0.57	0.57	0.57	0.57
0.90	0.559	0.558	0.558	0.558	0.558	0.558	0.558	0.558	0.558	0.558
0.95	0.548	0.548	0.547	0.547	0.546	0.546	0.546	0.546	0.546	0.546
1.00	0.536	0.535	0.535	0.534	0.534	0.533	0.533	0.533	0.533	0.533
1.05	0.521	0.522	0.521	0.52	0.519	0.519	0.518	0.518	0.518	0.518
1.10	0.503	0.505	0.505	0.505	0.504	0.503	0.503	0.503	0.502	0.502
1.15	0.485	0.488	0.489	0.489	0.489	0.488	0.488	0.488	0.487	0.487
heuristic	0.523	0.531	**0.532**	0.531	-	-	-	-	-	-

Table 4.21: Averages of RDMS values of the reconstructed solutions using different scaling factors for 30 dB Noisy Data with 15mm Shifted Geometric Error (optimal Tikhonov solution has 0.913 RDMS value)

α_1 \ α_2	0.70	0.75	0.80	0.85	0.90	0.95	1.00	1.05	1.10	1.15
0.70	0.824	0.824	**0.824**	0.824	0.824	0.824	0.824	0.824	0.824	0.824
0.75	0.834	0.834	0.834	0.834	0.834	0.834	0.834	0.834	0.834	0.834
0.80	0.847	0.847	0.847	0.847	0.847	0.847	0.847	0.847	0.847	0.847
0.85	0.862	0.862	0.863	0.863	0.863	0.863	0.863	0.863	0.863	0.863
0.90	0.877	0.878	0.879	0.879	0.879	0.879	0.879	0.879	0.879	0.879
0.95	0.892	0.893	0.893	0.894	0.895	0.895	0.895	0.895	0.895	0.895
1.00	0.909	0.909	0.91	0.911	0.912	0.913	0.913	0.913	0.913	0.913
1.05	0.928	0.927	0.929	0.93	0.931	0.931	0.932	0.932	0.933	0.933
1.10	0.948	0.946	0.946	0.947	0.948	0.949	0.95	0.95	0.951	0.951
1.15	0.968	0.965	0.964	0.965	0.965	0.966	0.966	0.967	0.967	0.968
heuristic	0.92	0.919	**0.918**	0.919	-	-	-	-	-	-

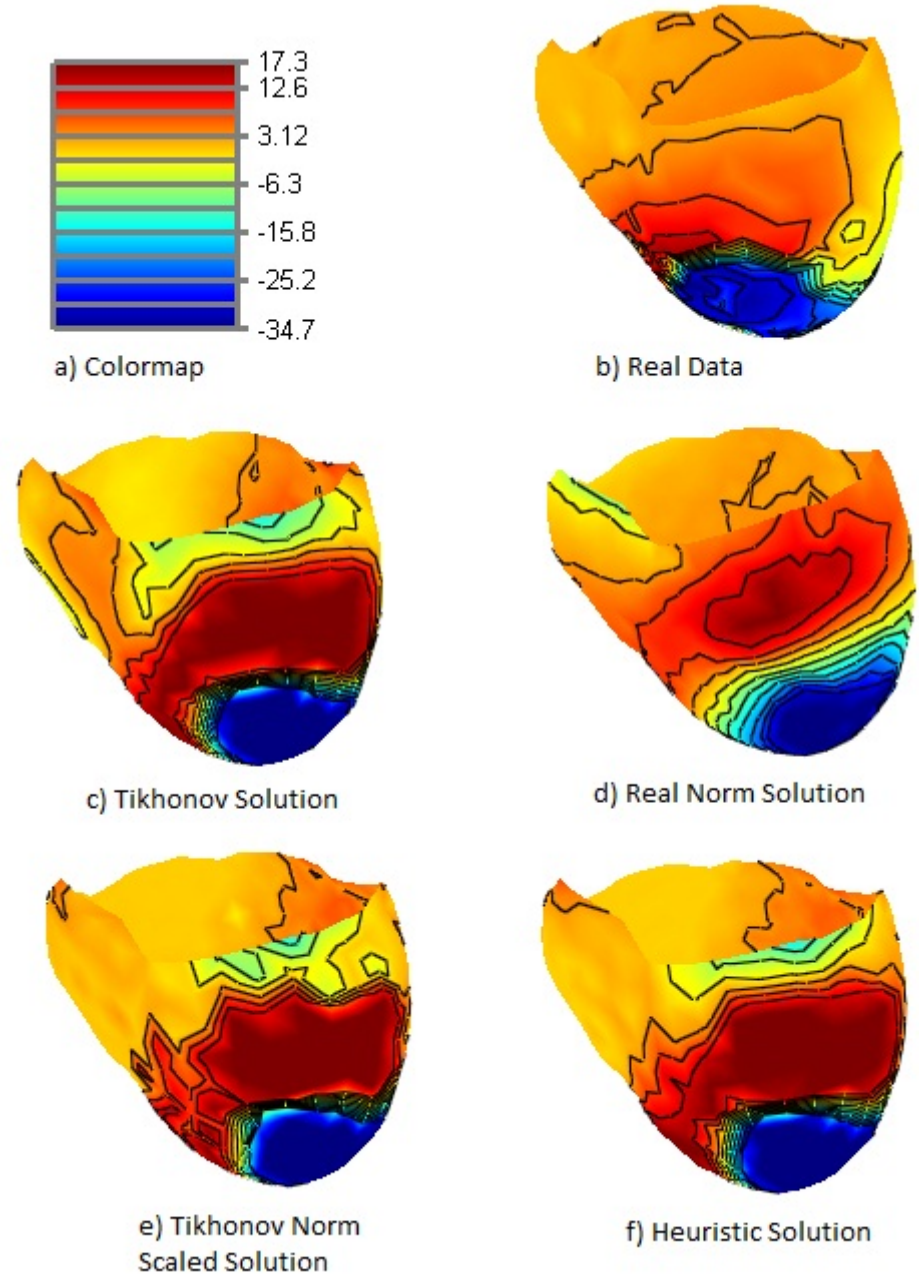

Figure 4.28: Epicardial Potential Maps for 30 dB noisy data with 15 mm Shift Geometric Error: a) Colormap b) Real Potential Distribution at the 39 ms c) Optimal Tikhonov Solution d) Reconstructed solution using real norms in multiple constraints imposed method e) Reconstructed solution by imposing the constraint values as $\epsilon_1 = 1.05\epsilon_{1,tik}$, $\epsilon_2 = 0.8\epsilon_{2,tik}$ and $\epsilon_3 = 0.8\epsilon_{3,tik}$ f)Reconstructed solution from heuristic method

MRE method, we need to impose the values of the upper, lower bounds of the model parameters and prior expected value of the model parameters into the formulation of optimization problem, respectively U_i, L_i, s_i. In addition, we need to determine the norm of the residual error $\epsilon = ||Gm - d||$ in order to estimate the posterior distribution. The norm of the residual error is important in how the posterior solution fits the measurement data. Very small values of the residual norm, ϵ, may lead to the over-fitting problem in the reconstructed solution or it may lead to an infeasible set that that result in no convergence of the method, while very big ϵ values cause the solutions that are irrelevant to the measurements.

The MRE method was tested with 4 different cases of the inverse ECG problem as in the previous methods presented in this Chapter. These cases are the inverse problems that contain different levels of Gaussian torso measurement noise and the geometric errors due to the shift in location of the heart and due to the wrong size of cardiac. The MRE method was tested with different prior expected value of the epicardial potentials while the upper and lower bounds of the epicardial potentials was taken as -45mV and +35 mV, respectively. In order to have an prior information about the solution, we have used different different training sets. For the training sets, the maximum and minimum values of potential value at any node over a QRS interval are 32 mV and -43 mV, respectively.

4.5.1 MRE Method Results of 30 dB Gaussian White Noise Added Measurements

In this section, MRE results of the reconstructed solutions of the inverse ECG problem having a 30 dB measurement data will be represented. As mentioned in section 3.3.3, we need upper, lower bounds of the epicardial potentials and the prior expected value of the epicardial potentials in order to estimate a prior distribution of the epicardial potentials using maximum entropy method. As mentioned above, during the test of MRE method, the upper values, U_i, and lower values, L_i, were taken as +35 mV and -45 mV, respectively. These values were same for all nodes and they were constant over the whole QRS interval. However, we have used different expected values of the epicardial potentials as prior knowledge. We have obtained the prior expected values using different techniques. These techniques are:

Fix Mean: The means of the epicardial potentials are taken as -5mV (midpoint of -45 and 35 mV) over the whole QRS interval and it is the same for all nodes.

Identity STM: The means of the epicardial potential, s, are estimated using the previous time instant solution of the MRE. For the first time instant they are taken as 0 for all nodes and for the remaining time instants they are estimated by multiplying 0.5 with the previous time solution i.e. $s_{i,t} = 0.5m_{i,t-1}$ for $t = 2, 3...$ where i is the i^{th} node, t is the time instant, $s_{i,t}$ is the mean at time t and $m_{i,t-1}$ is the MRE solution at $t - 1$.

Training Set STM: The means of the epicardial potentials, s, are estimated by multiplying the previous time instant solution of the MRE with the state transition matrix obtained from a training set i.e. $s_t = F_{train}m_{t-1}$ for $t = 2, 3...$ where s_t is the expected value vector of the epicardial potentials at time t, m_{t-1} is the MRE solution vector at $t-1$ and F_{train} is the training set STM. For the first time instant, the expected values of the epicardial potentials are taken as 0 for all nodes.

Real STM: The means of the epicardial potential, s, are estimated by multiplying the previous time instant solution of the MRE with the state transition matrix obtained from the true epicardial potentials i.e. $s_t = F_{real}m_{t-1}$ for $t = 2, 3...$ where s_t is the expected value vector of the epicardial potentials at time t, m_{t-1} is the MRE solution vector at $t - 1$ and F_{real} is the real STM. For the first time instant, the expected values of the epicardial potentials are taken as 0 for all nodes.

In table 4.22, average CC and RDMS values of the reconstructed solutions using different prior mean values are given. The CC plots of the obtained solutions over a QRS interval are also shown in Figure 4.29 . The results of the reconstructed solutions using constant value -5 mV and previous time instant solution times 0.5 as a prior expected value of the model parameters are very close to the optimal Tikhonov solution when we compare the CC values and RDMS values. However, the approaches that are using training set STM and the real STM in estimation of the prior expected value of the epicardial potentials yield a significant improvement in reconstructed solution.

Epicardial maps of the reconstructed solutions are also illustrated in Figure 4.30. These results show that we obtain solutions very similar to the optimal Tikhonov solution in fix value method where prior mean was taken as -5mV and in identity STM method where prior mean was estimated from previous time solution. However, the approaches in which prior mean values are estimated from training set STM and real STM, we have obtained a significant improvement in reconstructed solutions. The details and the edges in the epicardial potentials

Table 4.22: Averages values of CC and RDMS values of 30 dB noisy data reconstructed solutions using MRE Method

Method	Average CC	Average RDMS
Tikhonov	0.7698	0.6039
Fix Mean Sol.	0.7746	0.6082
Identity Stm Sol.	0.7825	0.5809
Training Stm Sol.	0.8358	0.4819
Real Stm Sol.	0.8852	0.3647

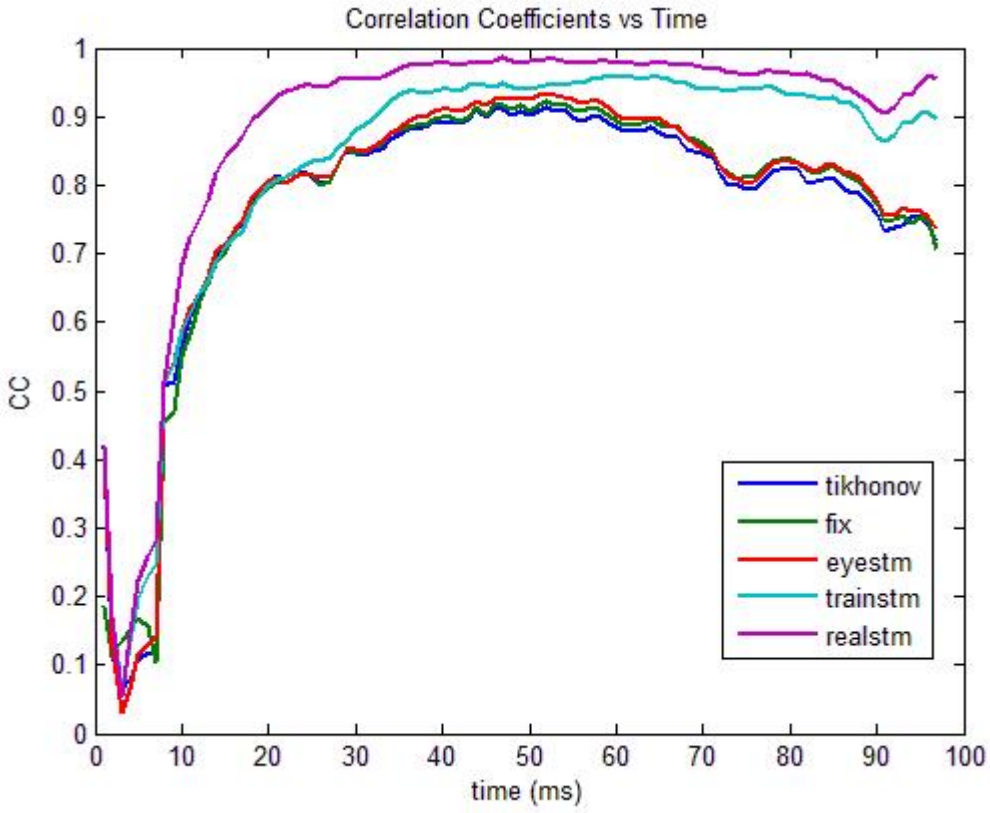

Figure 4.29: The CC values of different methods

maps for these approaches are much similar to the real epicardial map.

4.5.2 MRE Method Results of 10 dB Gaussian White Noise Added Measurements

Similar to the section 4.5.1, we have examined the results of the MRE method for 10 dB noisy measurements. The same procedure was followed during the tests. We have used the U_i and L_i bound values as 35 mV and -45 mV, respectively and we have the same approaches described in section 4.5.1 in calculation of a prior expected value of the epicardial potentials. Similar to the section 4.5.1, the residual norm, ϵ, was determined by solving the problem first using Tikhonov method and then estimating the norm value $\|d - Gm_{tik}\|_2$.

In table 4.23 , average CC and RDMS values of the reconstructed solutions by different approaches in calculation of prior mean values are given. The CC plots of the obtained solutions over a QRS interval are also shown in Figure 4.31. Similar to the results in section 4.5.1, the first two approaches, fix mean and identity STM generate similar results to the optimal Tikhonov solution. This is an expected result since the prior information that is used in estimating a prior distribution is very simple and it does not contain specific information about the real epicardial potentials. In addition, we use the same residual norm, ϵ, as the residual norm of the optimal Tikhonov solution. However, the other two approaches, training set STM and real STM improve the average CC and RDMS values.

Table 4.23: Averages values of CC and RDMS values of 10 dB noisy data reconstructed solutions using MRE Method

Method	Average CC	Average RDMS
Tikhonov	0.5796	0.8503
Fix Mean Sol.	0.5824	0.8401
Identity Stm Sol.	0.6068	0.7920
Training Stm Sol.	0.7672	0.5894
Real Stm Sol.	0.7678	0.5662

In Figure 4.32, epicardial maps of the reconstructed solutions by MRE method are also illustrated. These maps also support the results mentioned above. The first two approaches used in calculation of prior mean of the epicardial potentials yield the similar results to the optimal Tikhonov solution while the last two approaches improve the obtained solutions. Especially

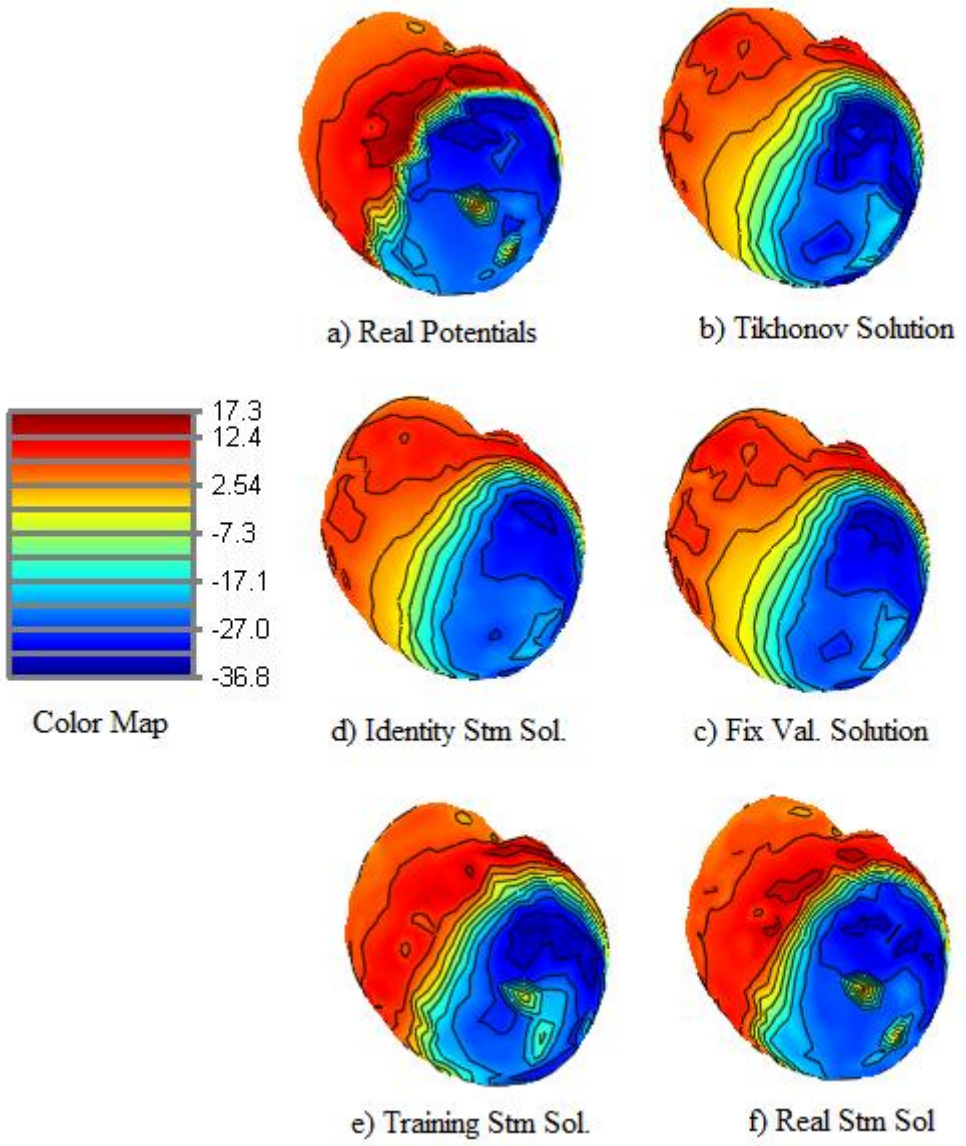

Figure 4.30: Epicardial Potential Maps of reconstructed solutions using MRE Method for 30 dB noisy data: a) Real Potential Distribution at the 50 ms b) Optimal Tikhonov Solution c) Reconstructed solution using -5 mV as mean value d) Reconstructed solution using the mean as identity matrix times previous time instant solution e) Reconstructed solution using the mean as training set stm matrix times previous time instant solution f) Reconstructed solution using the mean as real set stm matrix times previous time instant solution

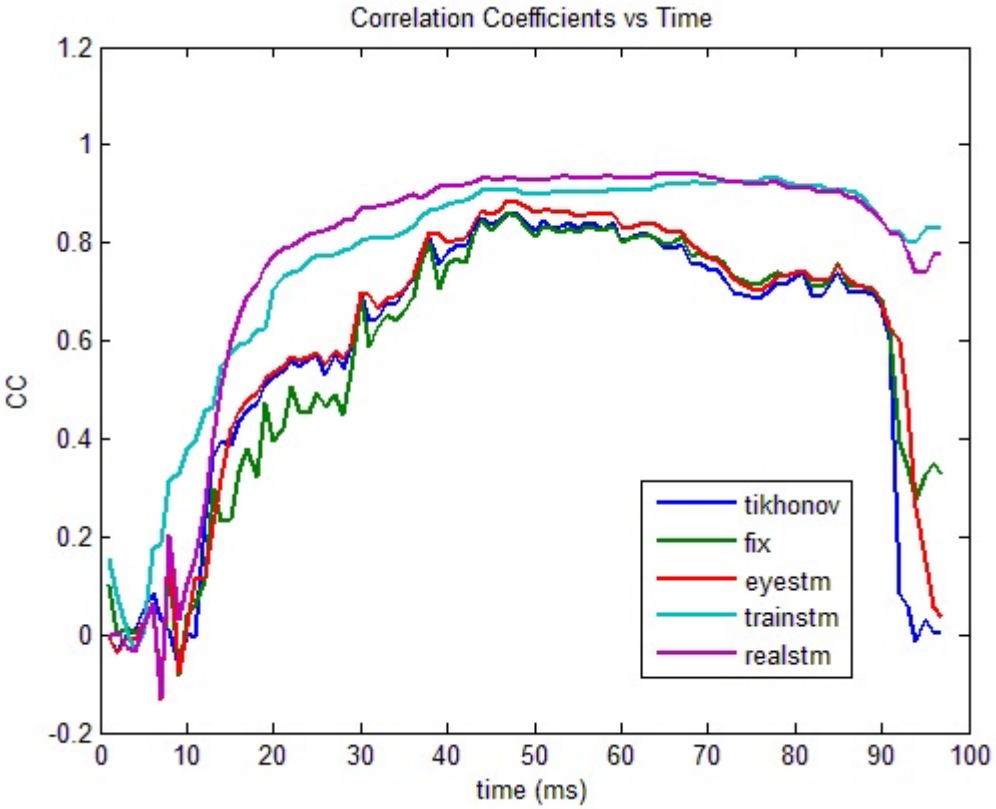

Figure 4.31: The CC values of different methods for 10 dB Noisy Measurements

in real STM case, the reconstructed solution can recover the details of the true epicardial potential map.

4.5.3 MRE Method Results of 30 dB Noisy Data with 0.6 Scaling Geometric Error

In this section, the results of the reconstructed solution of an inverse ECG problem containing a geometric error due to the wrong size of the heart will be represented. The MRE method was examined with the same U_i and L_i bound values in previous two cases. The expected values of the epicardial potentials were obtained using the same method in section 4.5.1. However, the residual norm used in this section was calculated using the true epicardial potentials i.e. $\epsilon = \|d - Gm_{real}\|_2$. During the tests, we have first the residual norms obtained from the optimal Tikhonov solution as previous two cases, inverse problems containing only noisy measurements. However, we have observed that the residual norms obtained from the optimal Tikhonov solution were small so that they caused the infeasible sets and the MRE method could not converge to a solution. Therefore, the residual norms estimated from the real epicardial potentials were used.

In table 4.24 , average CC and RDMS values of the reconstructed solutions by different approaches in calculation of prior mean values are given. The CC plots of the obtained solutions over a QRS interval are also shown in Figure 4.33 . Similar to previous sections, the significant improvement in average CC and RDMS values could be obtained by using the training set STM and real STM. The average CC values of the fix mean and identity STM solutions are close to the average CC value of the optimal Tikhonov solution. In Figure 4.33, we observe that the CC plots of the these two approaches have different shapes than the optimal Tikhonov solution CC plot. This differs from the inverse ECG problems containing only measurement noise. Actually, this result is expected since we have used the residual norms that were different from the residual norms of the optimal Tikhonov solution.

In 4.34, epicardial maps of the reconstructed solution for 50ms after the stimulus are shown. From this figure, we can see that the estimated solution using the training set STM and real STM are very similar to the true epicardial maps. In the fix mean and identity STM solutions, we have obtained smoother solutions than the optimal Tikhonov solution. However, the incorrect extreme points in optimal Tikhonov solution disappears in these solutions. Therefore, even if we could not obtain a significant improvement in CC values, these approaches provide

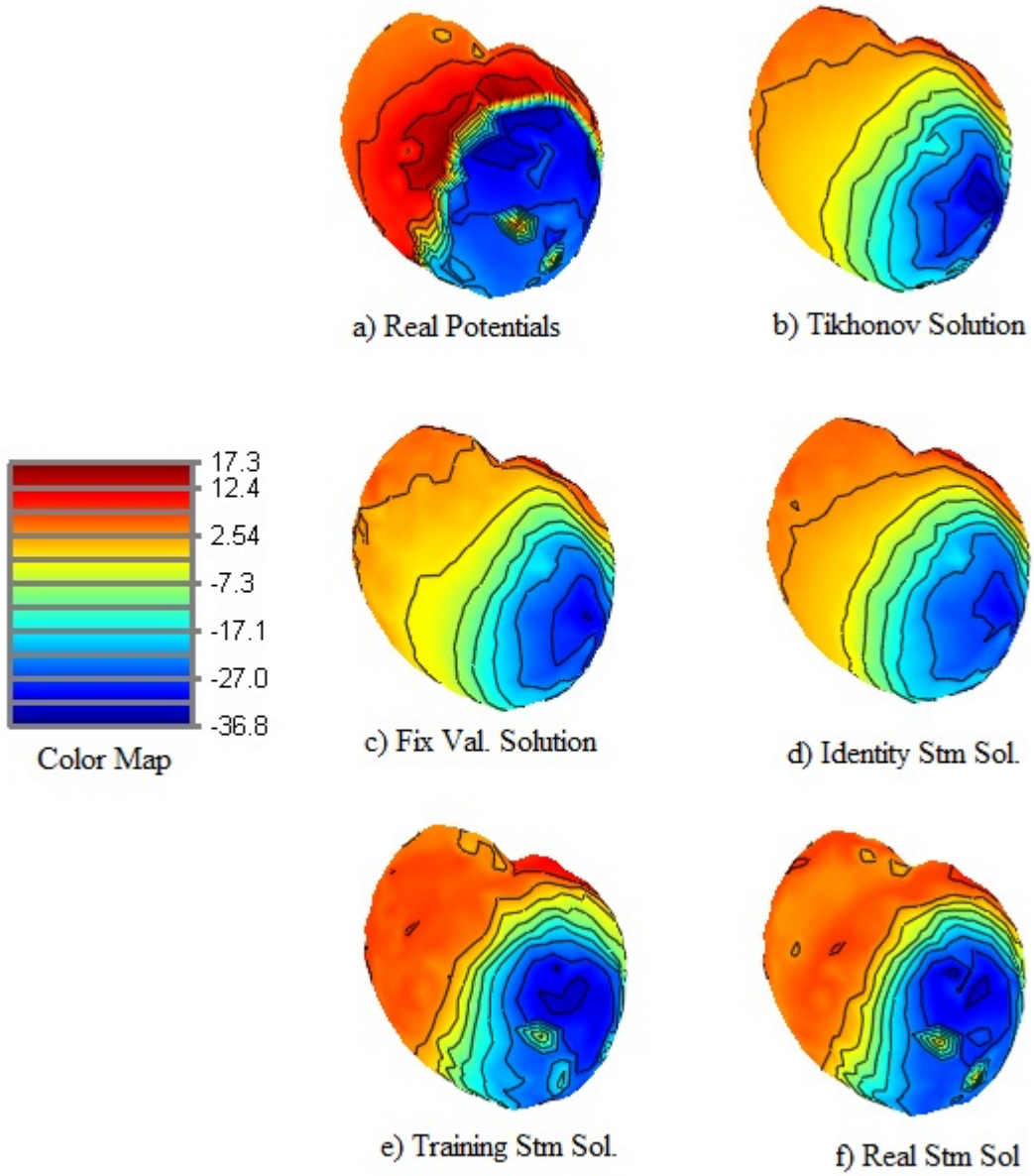

Figure 4.32: Epicardial Potential Maps of reconstructed solutions using MRE Method for 10 dB noisy data: a) Real Potential Distribution at the 50 ms b) Optimal Tikhonov Solution c) Reconstructed solution using -5 mV as mean value d) Reconstructed solution using the mean as identity matrix times previous time instant solution e) Reconstructed solution using the mean as training set stm matrix times previous time instant solution f) Reconstructed solution using the mean as real set stm matrix times previous time instant solution

Table 4.24: Averages values of CC and RDMS values of reconstructed solutions using MRE Method for 30 dB noisy data with 0.6 scaling geometric error

Method	Average CC	Average RDMS
Tikhonov	0.5895	0.8465
Fix Mean Sol.	0.6060	0.8401
Identity Stm Sol.	0.6087	0.8442
Training Stm Sol.	0.7167	0.7057
Real Stm Sol.	0.6910	0.7467

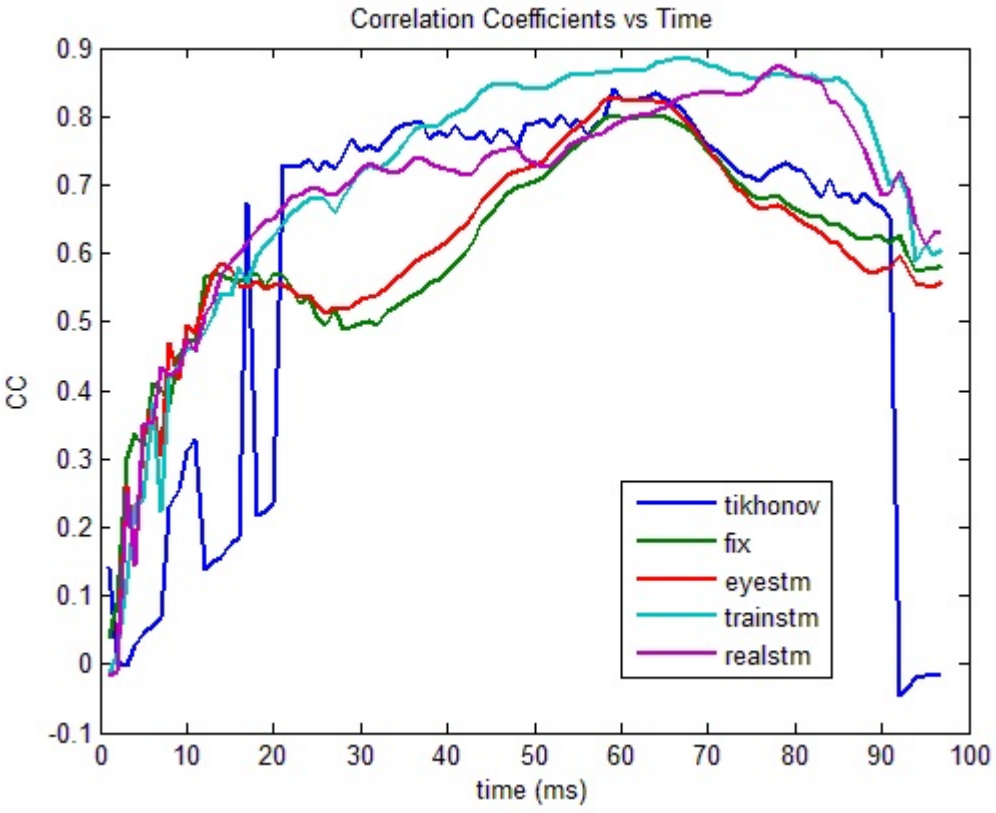

Figure 4.33: The CC plots of different methods for 30 dB noisy data with 0.6 scaling geometric error

solutions smoother but more accurate than the optimal Tikhonov solution.

4.5.4 MRE Method Results of 30 dB noisy data with 15mm shift geometric error

In this section, the results of the reconstructed solution of an inverse ECG problem containing a geometric error due to the wrong location of the heart will be represented. During the tests the same U_i and L_i bound values and the same method for obtaining expected values of the epicardial potentials in previous sections are used. The residual norm used in this section was calculated using the true epicardial potentials i.e. $\epsilon = \|d - Gm_{real}\|_2$ similar to the section 4.5.3.

In table 4.25 , average CC and RDMS values of the reconstructed solutions by different approaches in calculation of prior mean values are given. The MRE method provides improvement in the average CC and RDMS. Even in fix mean and identity STM solutions, we have obtained nearly %10 improvement in average CC and RDMS values. The CC plots of the obtained solutions over a QRS interval are also shown in Figure 4.35.

Table 4.25: Averages values of CC and RDMS values of reconstructed solutions using MRE Method for 30 dB noisy data with 15mm shift geometric error

Method	Average CC	Average RDMS
Tikhonov	0.5328	0.9133
Fix Mean Sol.	0.6143	0.8401
Identity Stm Sol.	0.6305	0.8009
Training Stm Sol.	0.7506	0.6434
Real Stm Sol.	0.7896	0.5902

In Figure 4.36, epicardial maps of the reconstructed solution for 50 ms after the stimulus are shown. From this figure, we can observe the improvements in the estimated solution using the training set STM and real STM. Similar to the section 4.5.3, the fix mean and identity STM approaches provide solutions that are smoother but more accurate than the optimal Tikhonov solution.

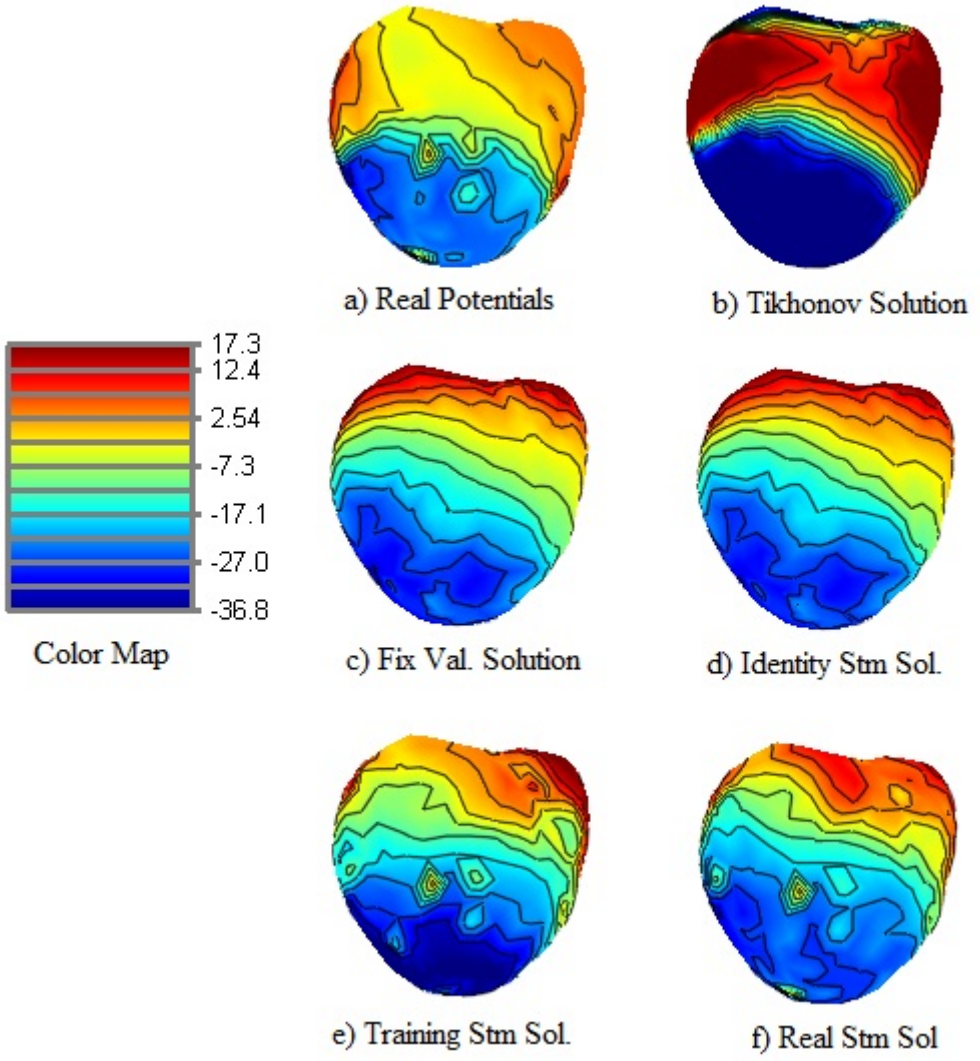

Figure 4.34: Epicardial Potential Maps of reconstructed solutions using MRE Method for 30 dB noisy data with 0.6 scaling geometric error: a) Real Potential Distribution at the 50 ms b) Optimal Tikhonov Solution c) Reconstructed solution using -5 mV as mean value d) Reconstructed solution using the mean as identity matrix times previous time instant solution e) Reconstructed solution using the mean as training set stm matrix times previous time instant solution f) Reconstructed solution using the mean as real set stm matrix times previous time instant solution

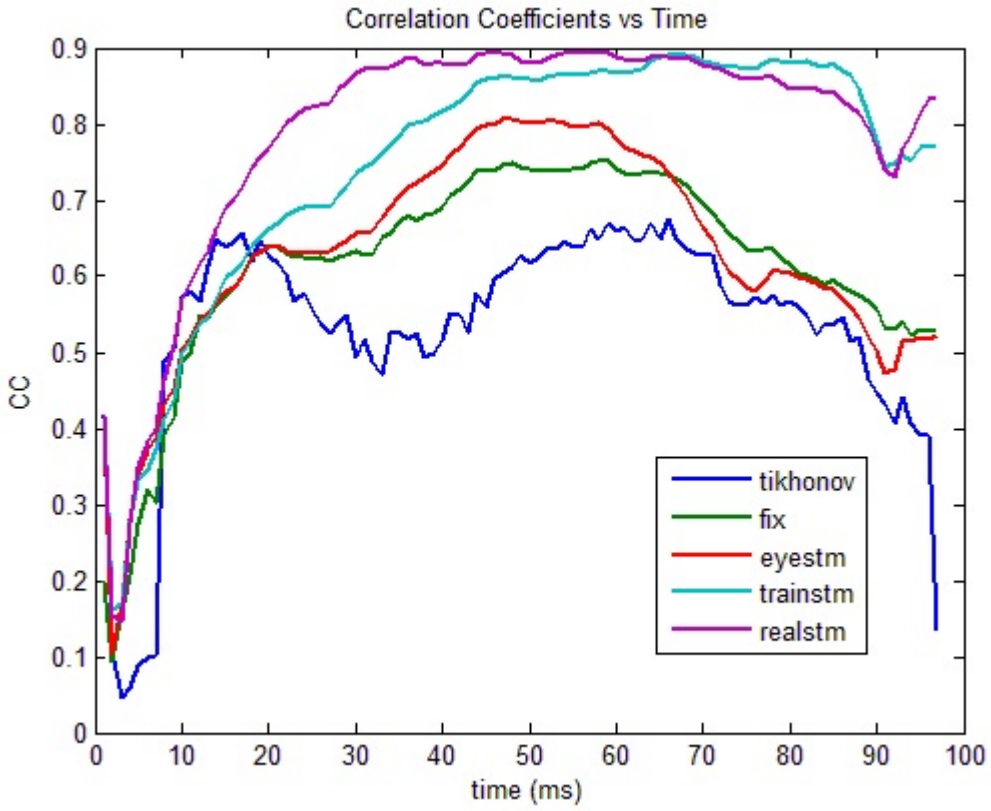

Figure 4.35: The CC plots of different methods for 30 dB Noisy Data with 15mm Shift Geometric Error

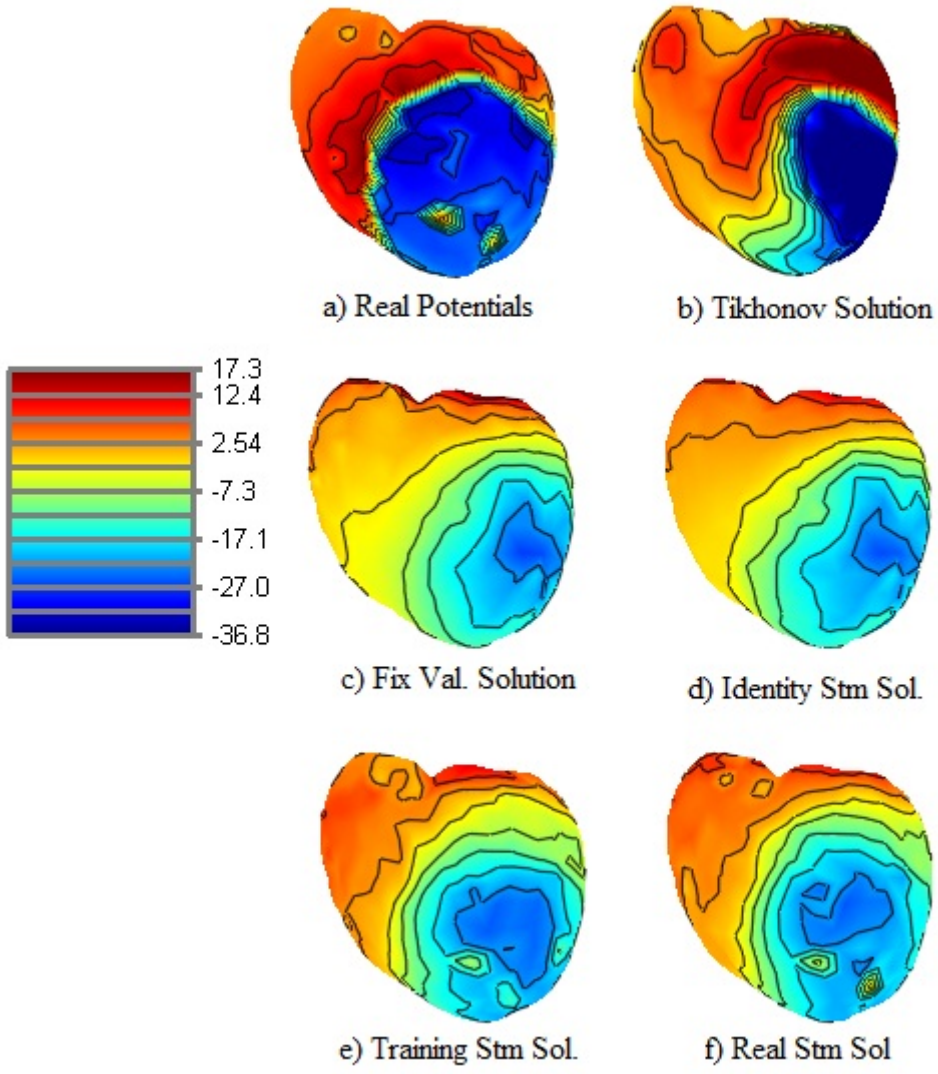

Figure 4.36: Epicardial Potential Maps of reconstructed solutions using MRE Method for 30 dB noisy data with 15mm shift geometric error: a) Real Potential Distribution at the 50 ms b) Optimal Tikhonov Solution c) Reconstructed solution using -5 mV as mean value d) Reconstructed solution using the mean as identity matrix times previous time instant solution e) Reconstructed solution using the mean as training set stm matrix times previous time instant solution f) Reconstructed solution using the mean as real set stm matrix times previous time instant solution

CHAPTER 5

CONCLUSIONS

5.1 Performance of Each Method

In this study, we have used 4 different solution methods for inverse problem of ECG. These methods are Conic Quadratic Programming, linearly constrained Tikhonov regularization, admissible solution approach (convex optimization with multiple constraints) and the MRE Method. The reconstructed results of these methods are compared with the optimal Tikhonov solution and the real epicardial potentials.The improvement in Conic Quadratic Programming, linearly constrained Tikhonov regularization and admissible solution is very limited. However, by using MRE method it is possible to obtain more accurate results compared to the Tikhonov solution.

As mentioned in the Theory Chapter, Conic Quadratic Programming has the equivalent formulation as the Tikhonov regularization. For each penalty parameter in Tikhonov regularization there is a corresponding bound value of the energy norm in Conic Quadratic Programming. The penalty parameter can be determined using a method such as the L-curve method. However, if we have prior information about the norm of the epicardial potentials it is more useful to use the norm values instead of using the penalty parameter. In results section it is shown that the L-curve method provides penalty parameters very close to the true optimal penalty parameters when the inverse problem contains only measurement noise and it does not take into account the geometric errors. However, in case of geometric errors, it provides penalty parameters that differ from the true optimal penalty parameter, especially when the geometric error is due to the shift in location of the heart. Therefore, determination of the optimal penalty parameter used in Tikhonov regularization is a problem. However, it may

be possible to obtain optimal bound parameter (norm of the epicardial potentials) used in Conic Quadratic Programming if we have prior information about the norm of the epicardial potentials. In section 4.2, we have developed a heuristic function that estimates the optimal norm value using the maximum norm in real epicardial potentials and the norm of the optimal Tikhonov solution. The heuristic approach yields the better solution than the optimal Tikhonov solution that is estimated using the L-curve, however, the improvements in reconstructed solutions are limited. We have also observed that it is not possible to obtain better results even when we have used the norm of the real epicardial in Conic Quadratic Programming as the bound value of norm of the potential. Due to the ill-posed nature of the problem, this interesting result is obtained. The norm of the real epicardial may lead to the under-regularized or over-regularized solutions depending on the noise level. However, the heuristic approach proposed in this thesis combines the optimal Tikhonov solution and the norm of the true potentials and it generates improvement in estimated solutions.

The second method studied in this thesis is the linearly constrained Tikhonov solution that composed of two step Tikhonov regularization. The method proposed by Iakovidis [15] generates a prior information by solving the problem using an over-regularization parameter and then it estimates the solution by solving the problem using an under-regularization parameter and the prior information at the first step. The results obtained in this thesis differs from the results in [15]. We could not obtain a significant improvement in reconstructed solutions. This is possibly due to the geometric model used in [15] differs from our geometric model. Iakovidis [15] have used a spherical geometry.

The admissible solution is another method studied in this thesis. In this method, we obtain a convex optimization problem by imposing multiple constraints that depend on the prior information about the real epicardial potentials. Then, we try to improve the solutions by imposing this multiple constraints into the formulation of the problem. We have examined this method using different prior information. The prior information was generated by adjusting the optimal Tikhonov solutions. Since we have used the optimal Tikhonov solutions in construction of the prior information, the improvements in reconstructed solution is limited and obtained solutions are similar to the optimal Tikhonov solution. However, we have obtained %1-2 improvement in CC values when we compare the results with the optimal Tikhonov solution. Instead of constructing the prior information from optimal Tikhonov solution, it may be useful different prior information in admissible solution. However, obtaining a good

prior is problem. In admissible solution, we have used the heuristic function developed for Conic Quadratic Programming in order to generate prior information about the norm of the solutions. The heuristic function yields an improvement here, too. The iterative calculation of the solution is the weakness of the method. It needs long time, 100 times more than Tikhonov method, to reconstruct a solution.

Finally, we have studied the Minimum relative entropy method in reconstruction the epicardial potentials. The method needs the prior information about the upper and lower bound of the epicardial potentials and the expected value of the epicardial potentials. It generates a posterior distribution using the prior distribution that is generated from the prior information. The method also needs the residual norm of the reconstructed solution as an input parameter in order to fit the posterior distribution to the measurements to some extent. In the presence of the only measurement noise in inverse problem, we have used the residual norm that was calculated from the optimal Tikhonov solution. In this case, we have obtained significant improvement if we have a good prior about the expected value of the epicardial potentials. The prior about the expected value of the potentials can be estimated using the training set STM and real STM. In other words, we have a good estimate of STM, we obtain a significant improvement in reconstructed solutions. In the presence of a geometric noise in inverse problem, the residual norm calculated by the optimal Tikhonov solution generates an infeasible set and the method cannot converge to a solution. Therefore, we have used the residual norms calculated from the real potentials in the presence of geometric noise. When we used the real potentials to calculate the residual norms, we have obtained improvements about %10 in CC value of reconstructed solution.

5.2 Future Work

- The constraint parameter used as upper limit for total energy of the solution in Conic Quadratic Programming was estimated from the real potentials and optimal Tikhonov solution in this study. Estimation of this constraint parameter directly from torso potentials could be studied.
- The MRE method was tested with different prior information about the lower, upper and and mean values of epicardial potentials. Generation of proper prior lower, upper and and mean values of epicardial potentials in MRE method could be studied as a

future work.

- The residual norm value used in MRE method determines the fitting level of reconstructed solution with body surface measurements. Therefore, it is very important in reconstruction of solution. During this study, it is observed that determination of an appropriate value of residual norm is a problem in the presence of geometric noise in inverse problem. Determination of residual norm value that leads to proper fitting of model parameters to the measurements could be studied.

REFERENCES

[1] P. M. Okin, R. B. Devereux, E. T. Lee, J. M. Galloway, and B. V. Howard. Electrocardiographic repolarization complexity and abnormality predict all-cause and cardiovascular mortality in diabetes. *Diabetes*, 53:434–440, 2004.

[2] Y. Jiang. Solving the inverse problem of electrocardiography in a realistic environment, 2010. Karisruhe Transactions on Biomedical Engineering.

[3] C. Ramanathan, R. N. Ghanem, P. Jia, K. Ryu, and Y. Rudy. Noninvasive electrocardiographic imaging for cardiac electrophysiology and arrhythmia. *Nature Medicine*, 10 (4):422–428, 2004.

[4] R. Mohindra, J.L. Sapp, J.C. Clements, and B.M. Horacek. Use of body-surface potential mapping and computer model simulations for optimal programming of cardiac resynchronization therapy devices. *Computers in Cardiology*, 34:69–72, 2007.

[5] R. R. Bond, D. D. Finlay, C. D. Nugent, and G. Moore. Xml- bspm: an xml format for storing body surface potential map recordings. *BMC Medical Informatics and Decision Making*, 10:1–26, 2010.

[6] L. De Ambroggi and A. D. Corlan. Clinical use of body surface potential mapping in cardiac arrhythmias. *Anatol J Cardiol*, 7 (1):8–10, 2007.

[7] M. S. Guillem, A. Quesada, V. Donis, A. M. Climent, N. Mihi, J. Millet, and F. Castells. Surface wavefront propagation maps: Non-invasive characterization of atrial flutter circuit. *International Journal of Bioelectromagnetism*, 11 (1):22–26, 2009.

[8] H. S. Oster, B. Taccardi, R. L. Lux, P. R. Ershler, and Y. Rudy. Noninvasive electrocardiographic imaging reconstruction of epicardial potentials, electrograms, and isochrones and localization of single and multiple electrocardiac events. *Circulation*, 96:1012–1024, 1997.

[9] Y. Rudy and R. Plonsey. A comparison of volume conductor and source geometry effects on body surface and epicardial potentials. *Circulation*, 46:283–293, 1980.

[10] M.S. Spach, R.C Barr, C.F. Lanning, and P.C. Tucek. Origin of body surface qrs and t wave potentials from epicardial potential distributions in the intact chimpanzee. *Circulation*, 55:268–278, 1977.

[11] Y. Rudy and BJ. Messinger-Rapport. The inverse problem in electrocardiography: solutions in terms of epicardial potentials. *Crit.Rev.Biomed.Eng*, 16 (3):215–268, 1988.

[12] L.K. Cheng, J.M. Bodley, and A.J.Pullan. Comparison of potential- and activation-based formulations for the inverse problem of electrocardiology. *IEEE Transactionson Biomedical Engineering*, 50 (1):11–21, 2003.

[13] R. M. Gulrajani. The forward and inverse problem of electrocardiography: Gaining a better qualitative and quantitative understanding of the heart's electrical activity. *IEEE Engineering in medicine and biology*, 17:84–122, 1998.

[14] J. Malmivuo and R. Plonsey. *Bioelectromagnetism: Principles and Applications of Bioelectric and Biomagnetic Fields*. Oxford University Press, 1995.

[15] I. Iakovidis and R.M. Gulrajan. Improving tikhonov regularization with linearly constrained optimization: Application to the inverse epicardial potential solution, mathematical biosciences. *Operations Research*, 112:55–88, 1992.

[16] P. C. Hansen. Rank-deficient and discrete ill-posed problems: Numerical aspects of linear inversion. *SIAM Soceity for Industrial And Applied Mathematics*, 110 (4):705–729, 1998.

[17] F.A. Ghandi, D. H. Brooks, and R. S. Macleod. An admissible solution approach to inverse electrocardiography, annals of biomedical engineering. *Annals of Biomedical Engineering*, 26:278–292, 1998.

[18] K. G. Srinidhi. Convex optimization algorithms for inverse electrocardiography with physiologically relevant constraints, 1999. Northeastern University Boston Massachusetts.

[19] G.F. Ahmad, D.H. Brooks, C.A. Jacobson, and R.S. MacLeod. Constraint evaluation in inverse electrocardiography using convex optimization. *IEEE Engineering in Medicine and Biology Society*, 1:30–41, 1995.

[20] Y. Serinagaoglu. Improved performance of bayesian solutions for inverse electrocardiography using multiple information sources. *IEEE TRANSACTIONS ON BIOMEDICAL ENGINEERING*, 53 (10):2024–2034, 2006.

[21] U. Aydin and Y. Serinagaoglu. Use of activation time based kalman filtering in inverse problem of electrocardiography. In *IFMBE Proceedings*, Berlin Heidelberg, 2009. Springer.

[22] K. L. Berrier, D. C. Sorensen, and D. S. Khoury. Solving the inverse problem of electrocardiography using a duncan and horn formulation of the kalman filter. *IEEE Trans Biomed Eng.*, 51 (3):507–515, 2004.

[23] M. Jiang, L. Xia, G. Shou, F. Liu, and S. Crozie. Two hybrid regularization frameworks for solving the electrocardiography inverse problem. *Phys. Med. Biol.*, 53:5151–5164, 2008.

[24] H. S. Oster. The use of temporal information in the regularization of the inverse problem of electrocardiography. *IEEE TRANSACTIONS ON BIOMEDICAL ENGINEERING*, 39 (1):65–75, 1992.

[25] S.O. Howard and Y. Rudy. Regional regularization of the electrocardiographic inverse problem: A model study using spherical geometry. *IEEE Transactions on Biomedical Engineering*, 42 (2):188–199, 1997.

[26] K. M. Lewis and K. A. Handal. *Sensible ECG Analysis*. Delmar Publishers, 2000.

[27] Ziad Issa MD, John M. Miller MD, and Douglas P. Zipes MD. *Clinical Arrhythmology and Electrophysiology: A Companion to Braunwald's Heart Disease*. Saunders, 2009.

[28] Wikipedia. Diagram of the human heart, 2006. http://commons.wikimedia.org/wiki/Media:Diagram_of_the_human_heart_(cropped).svg.

[29] H. T. Shih. Anatomy of the action potential in the heart. *Tex Heart Inst J.*, 21 (1):30–41, 1994.

[30] A. L. Goldberger. *Clinical Electrocardiography: A Simplified Approach*. Mosby, 2006.

[31] R.S. MacLeod and D.H. Brooks. Recent progress in inverse problems in electrocardiology. *IEEE Eng Med Biol Magazine*, 17 (1):73–83, 1998.

[32] D.B. Geselowitz. Multipole representation for an equivalent cardiac generator. *Proc. IRE*, 48:75–79, 1960.

[33] D. T. Trung and P. T. Minh. An analysis of the single moving dipole source for electrocardiography inverse problem. In *2008 IEEE International Conference on Research, Innovation and Vision for the Future in Computing & Communication Technologies*, Vietnam, 2008. IEEE.

[34] D. Lai, C. Liu, M.D. Eggen, P.A.Iaizzo, and B. He. Cardiac source localization by means of a single moving dipole solution during endocardial pacing in an animal model. *Conf Proc IEEE Eng Med Biol Soc.*, 46 (7):1778–1780, 2009.

[35] J.J.M Cuppen and A.van Oosterom. Model studies with the inversely calculated isochrones of ventricular depolarization. *IEEE Trans Biomed Eng*, 31:652–659, 1984.

[36] R. Barr and M. Spach. Inverse calculation of qrs-t epicardial potentials from body surface potential distributions for normal and ectopic beats in the intact dog. *Circulation Research*, 42:661–674, 1978.

[37] M.S. Spach and B.C. Barr. Ventricular intramural and epicardial potential distributions during ventricular activation and repolarization in the intact dog. *Circulation Research*, 37:243–257, 1975.

[38] A. Van Oosterom. Source models in inverse electrocardiography. *International Journal of Bioelectromagnetism*, Sept.:211–214, 2003.

[39] G.J Huiskamp and A. van Oosterom. The depolarization sequence of the human heart surface computed from measured body surface potentials. *IEEE Trans Biomed Eng, YEAR = 1989, volume = 35, pages = 1047-1059,.*

[40] D. B. Geselowitz. On the theory of the electrocardiogram. *Proceeding IEEE*, 77 (6):857–876, 1989.

[41] A. van Oosterom. Genesis of the t wave as based on an equivalent surface source model. *J. Electrocardiology*, 34:217–227, 2001.

[42] D. Farina. Forward and inverse problem of electrocardiography clinical investigations, 2008. Karisruhe Transactions on Biomedical Engineering.

[43] O. Skipa, M. Nalbach, F. Sachse, C. Werner, and O. Dössel. Transmembrane potential reconstruction in anisotropic heart model. *International Journal of Bioelectromagnetism*, 4 (2):17–18, 2002.

[44] A. V. Shahidi and P. Savard. Forward problem of electrocardiography: construction of human torso models and field calculations using finite element method. *Med. & Biol. & Comput*, 32:25–33, 1994.

[45] G. Shou, L. Xia, M. Jiang, F. Liu, and S. Crozier. Forward and inverse solutions of electrocardiography problem using an adaptive bem method. In *Lecture Notes in Computer Science*, Berlin Heidelberg, 2007. Springer.

[46] A. Van Oosterom and G. J. Huiskamp. Implicit and explicit constraints in inverse electrocardiography. *J. Electrocardiol.*, 25:87–92, 1992.

[47] C. G. Xanthis, P. M. Bonovas, and G. A. Kyriacou. Inverse problem of ecg for different equivalent cardiac sources. *Piers Online*, 3 (2):1222–1227, 2007.

[48] G. Huiskampand and F.Greensite. A new method for myocardial activation imaging. *IEEE Transactionson Biomedical Engineering*, 44 (6):433–446, 1997.

[49] S. Boyd and L. Vandenberghe. *Convex Optimization*. Cambridge University Press, 2004.

[50] S.-C. Fang, J. R. Rajasekera, and H.-S. J. Tsao. *Entropy optimization and mathematical programming*. Kluwer Academic Publishers, 1997.

[51] E. T. Jaynes. Information theory and statistical mechanics, 1962. Statistical Physics,Brandeis Summer Institute.

[52] R. M. Gray. *Entropy and Information Theory*. Springer-Verlag, 1990.

[53] C.E. Shannon. A mathematical theory of communication. *Bell System Technical Journal*, 27:379–423, 1948.

[54] S. Guiasu and A. Shenitzer. The principle of maximum entropy. *Mathematical Intelligencer*, 7 (1):42–48, 1985.

[55] R. C. Aster, B. Borchers, and C. H. Thurber. *Parameter Estimation and Inverse Problems*. Elsevier Academic Press, 2004.

[56] E. T. Jaynes. The relation of bayesian and maximum entropy methods. *Mathematical Intelligencer*, 7 (1):42–48, 1985.

[57] E. T. Jaynes. *Probability Theory: The Logic of Science*. Cambridge University Press, 2003.

[58] E. T. Jaynes. Prior probabilities. *IEEE Transactions on Systems Science and Cybernetics*, 4 (3):227–241, 1968.

[59] A. D. Woodbury and T. J. Ulrych. Minimum relative entropy: Forward probabilistic modeling. *Water Resources Res.*, 29 (8):2847–2860, 1993.

[60] A. D. Woodbury. A fortran program to produce minimum relative entropy distributions. *Computers & Geosciences*, 30:131–138, 2004.

[61] A. D. Woodbury and T. J. Ulrych. Minimum relative entropy inversion: Theory and application to recovering the release history of a ground water contaminant. *Water Resources Research*, 32, (9):2671–2681, 1996.

[62] M. Schmelling. The method of reduced cross-entropy a general approach to unfold probability distributions. *Nuclear Instruments and Methods in Physics Research*, 340 (2):400–412, 1994.

[63] Karmeshu. Entropy measures, maximum entropy principle and emerging applications, 2003. Springer.

[64] A. Dukkipati, M. N. Murty, and S. Bhatnagar. Nonextensive triangle equality and other properties of tsallis relative-entropy minimization. *Physica A*, 361:124–138, 2006.

[65] J.E. Shore and R. W. Johnson. Properties of cross-entropy minimization. *Information Theory, IEEE Transactions*, 27 (4):472–482, 1981.

[66] A.S. Cherney and V.P. Maslov. On minimization and maximization of entropy in various disciplines. *Theory Probab. Appl.*, 48 (3):447–464, 2004.

[67] R. M. Neupauerand and B. Borchers. A matlab implementation of the minimum relative entropy method for linear inverse problems. *Computers & Geosciences*, 27 (7):757–762, 2001.

[68] A. D. Woodbury and T. J. Ulrych. Minimum relative entropy and probabilistic inversion in groundwater hydrology. *Stochastic Hydrology and Hydraulics*, 12:317–358, 1998.

[69] R. M. Neupauer, B. Borchers, and J. L. Wilson. Comparison of inverse methods for reconstructing the release history of a groundwater contamination source. *Water Resour. Res.*, 36 (9):2469–2475, 2000.

[70] Pakize Taylan and Gerhard-Wilhelm Weber. Organization in finance prepared by stochastic differential equations with additive and nonlinear models and continuous optimization. *Organizacija*, 41 (5):185–193, 2008.

[71] R. M. Neupauer. A comparison of two methods for recovering the release history of a groundwater contamination source, 1999. M.Sc. Thesis, New Mexico Institute of Mining and Technology.

[72] R.S. MacLeod, R.L. Lux, and B. Taccardi. A possible mechanism for electrocardiographically silent changes in cardiac repolarization. *J. Electrocardiol.*, 30:114–121, 1997.

[73] R. S. MacLeod, R. L. Lux, and B. Tacardi. Electrocardiographic mapping in a realistic torso tank preparation. *Proceedings of IEEE Engineering in Medicine and Biology Society in 17th Annual Conference, IEEE Press*, 1:245–246, 1995.

[74] R. S. MacLeod and C. R. Johnson. Map3d: Interactive scientific visualization for bioengineering data. Proc. Eng. Med. Biol. Soc. 15th Annu. Int. Conf., 1993.